

N73-10470

FINAL REPORT

LABORATORY PROTOTYPE  
FLASH EVAPORATOR

NASA-MSC-07098

VMSC-T157-15

**CASE FILE  
COPY**



**VOUGHT MISSILES  
AND SPACE COMPANY**  
TEXAS DIVISION

P. O. Box 6267

Dallas, Texas 75222

CR-128608

NASA/MSC CONTRACT  
NAS9-12026

FINAL REPORT

LABORATORY PROTOTYPE  
FLASH EVAPORATOR

NASA-MSC-07098  
VMSC-T157-15

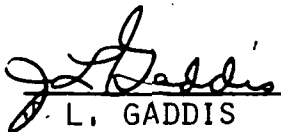
OCTOBER 1972

SUBMITTED BY  
VOUGHT MISSILES AND SPACE COMPANY  
LTV AEROSPACE CORPORATION  
P.O. BOX 6267  
DALLAS, TEXAS 75222

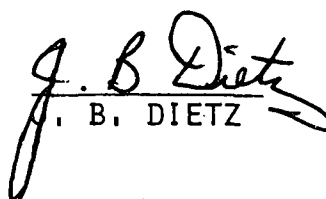
TO

NATIONAL AERONAUTICS & SPACE ADMINISTRATION  
MANNED SPACECRAFT CENTER  
HOUSTON, TEXAS

PREPARED BY

  
J. L. GADDIS

REVIEWED BY

  
J. B. DIETZ

APPROVED BY

  
R. J. FRENCH,  
SUPERVISOR  
EC/LSS GROUP

## A B S T R A C T

A laboratory prototype flash evaporator that is being developed as a candidate for the Space Shuttle Environmental Control System expendable heat sink is described. The single evaporator configuration uses water as an evaporant to accommodate reentry and on-orbit peak heat loads, and Freon 22 for terrestrial flight phases below 120,000 feet altitude. Reported in detail are the design features, fabrication techniques used for the prototype unit, redundancy considerations, and the fluid temperature control arrangement. The results of an extensive test program to determine the evaporator operational characteristics under a wide variety of conditions are presented.

## TABLE OF CONTENTS

1.0	SUMMARY . . . . .	1
2.0	INTRODUCTION . . . . .	2
3.0	EVAPORATOR DESIGN . . . . .	3
3.1	Design Requirements . . . . .	3
3.2	Heat Exchange Core Tradeoffs . . . . .	3
3.2.1	Non Redundant Design . . . . .	3
3.2.2	Redundant Design . . . . .	5
3.3	Detailed Design . . . . .	8
3.3.1	Strip Fin Core Design . . . . .	13
3.3.2	Multiparallel Channel Design . . . . .	13
3.4	Valve and Nozzle Design . . . . .	23
3.5	Structural Considerations . . . . .	31
3.6	Control Analysis . . . . .	32
3.6.1	Temperature Switched Control . . . . .	32
3.6.2	Predictor - Corrector Control . . . . .	43
4.0	EVAPORATOR FABRICATION . . . . .	49
4.1	Fabrication Of First Unit . . . . .	54
4.2	Fabrication of Second Unit . . . . .	56
4.3	Fabrication of the Third Unit . . . . .	58
5.0	EVAPORATOR TESTING	
5.1	Test Chronology and Significant Events . . . . .	59
5.2	Results of Prototype Testing . . . . .	77
5.3	Recommended Design and Engineering Based on Test Outcome . . . . .	100
6.0	REFERENCES . . . . .	101



## LIST OF FIGURES

<u>NO.</u>	<u>TITLE</u>	<u>PAGE</u>
1	CORE CONSTRUCTIONS CONSIDERED . . . . .	4
2	PRESSURE DROP AND AREA FOR VARIOUS NONREDUNDANT CORE DESIGNS.	6
3	SIDE BY SIDE FIN EFFECTIVENESS . . . . .	9
4	SIDE BY SIDE FIN EFFECTIVENESS, $K_f$ . . . . .	10
5	COMPARISON OF REDUNDANT DESIGNS . . . . .	11
6	STRIP FIN CORE DESIGN, ASSEMBLY . . . . .	14
7	STRIP FIN CORE DESIGN . . . . .	15
7A	STRIP FIN CORE DESIGN . . . . .	16
8	STRIP FIN CORE DESIGN EDGE DETAILS . . . . .	17
9	STRIP FIN CORE ORIENTATION . . . . .	18
10	MULTIPARALLEL CHANNEL FORMING TECHNIQUES . . . . .	20
11	MULTIPARALLEL EVAPORATOR ARRANGEMENT . . . . .	21
12	MANIFOLD CUTAWAY . . . . .	22
13	EVAPORATION RATES FOR WATER . . . . .	26
14	TEMPERATURE DISTRIBUTION WITHIN EVAPORATOR . . . . .	33
15	EVAPORATOR NODAL MODEL . . . . .	34
16	DISTRIBUTION OF EVAPORANT SPRAY . . . . .	35
17	TEMPERATURES OF FLUID AND WALL NEAR THE EXHAUST PORT . . . . .	37
18	EFFECT OF PROBE RESPONSE ON OUTLET TEMPERATURE . . . . .	38
19	EFFECT OF HEAT LOAD ON OUTLET TEMPERATURE . . . . .	40
20	FLUID OUTLET TEMPERATURE PREDICTED FROM ANALYTICAL MODEL . . . . .	44
21	RESPONSE OF $\Omega$ FOR VARIOUS PARAMETERS . . . . .	47a
22	EVAPORATOR FABRICATION . . . . .	50
23	EVAPORATOR FABRICATION . . . . .	51
24	FINISHED TUBE WOUND ASSEMBLY . . . . .	52
25	EVAPORATOR WITH BRAZE WIRE ATTACHED . . . . .	53
26	FAILED TUBE AND WEDGE . . . . .	55
27	TUBE TWIST TENDENCY DATA . . . . .	57
28	EVAPORATOR TEST FLUID LOOP SCHEMATIC . . . . .	60
29	DATA OUTPUT FORMAT . . . . .	61

## LIST OF FIGURES (CON'T)

<u>NO.</u>	<u>TITLE</u>	<u>PAGE</u>
30	THERMOCOUPLE SURFACE LOCATIONS . . . . .	63
31	EVAPORATOR TEMPERATURE DISTRIBUTION, ORIGINAL N-8 NOZZLE . .	70
32	EVAPORATOR TEMPERATURE DISTRIBUTION, 0.032 x 0.041 NOZZLE SLOTS . . . . .	71
33	EVAPORATOR TEMPERATURE DISTRIBUTION, 0.032 x 0.044 NOZZLE SLOTS . . . . .	72
34	EVAPORATOR WITH PLEXIGLASS BACK . . . . .	74
35	EVAPORATION AND SUPPLY TIMES FOR WATER . . . . .	75
36	EVAPORATOR TEMPERATURE DISTRIBUTION, DELAVAN NOZZLE . . . .	78
37	EVAPORATOR PERFORMANCE, DELAVAN NOZZLE . . . . .	79
38	EVAPORATOR PERFORMANCE, N-8 NOZZLE . . . . .	80
39	EVAPORATOR TEMPERATURE DISTRIBUTION FOR PRIMARY AND REDUNDANT COMBINATIONS . . . . .	81
40	EVAPORATOR PERFORMANCE WITH VARIOUS REDUNDANCY COMBINATIONS.	83
41	EFFECT OF EVAPORATOR ORIENTATION ON PERFORMANCE . . . . .	84
42	EFFECT OF WATER SUPPLY TEMPERATURE ON PERFORMANCE . . . . .	85
43	EFFECT OF WATER SUPPLY PRESSURE ON PERFORMANCE . . . . .	86
44	EFFECT OF TRANSPORT (R-21) FLOW RATE ON PERFORMANCE . . . .	88
45	EFFECT OF EVAPORATOR ORIENTATION ON PERFORMANCE . . . . .	90
46	EFFECT OF AMBIENT PRESSURE ON PERFORMANCE . . . . .	91
47	EFFECT OF FREON SUPPLY PRESSURE ON PERFORMANCE . . . . .	93
48	EFFECT OF TRANSPORT FLOW RATE ON PERFORMANCE . . . . .	94
49	PERFORMANCE DURING H <sub>2</sub> O TO R-22 EVAPORANT SWITCHOVER . . . .	96
50	PERFORMANCE DURING R-22 TO H <sub>2</sub> O EVAPORANT SWITCHOVER . . . .	97

## LIST OF TABLES

1	Comparison of Nonredundant and Redundant Core Designs . . . .	12
2	Evaporator Test Instrumentation . . . . .	62
3	Evaporator Run Log . . . . .	64
4	Evaporation Enthalpy . . . . .	95

## NOMENCLATURE

$A$	Active surface area, area coordinate
$a_1, a_2, c_1, c_2$	Constants
$c_f$	Fluid specific heat
$c_w$	Wall material specific heat
$F$	Nondimensional fluid temperature
$L$	Fractional heat load
$Q$	Maximum heat load capability
$\dot{Q}$	Heat rejection per length in flow direction
$\ddot{Q}$	Heat rejection per unit surface area
$T_f$	Fluid temperature
$T_{out}$	Fluid outlet temperature
$T_w$	Wall temperature
$\overline{\Delta T}$	Time averaged fluid-to-wall temperature difference
$\Delta T$	Local fluid-to-wall temperature difference
$t$	Time
$U$	Superficial conductance
$U'$	Local product of conductance and active area per unit flow channel length
$W$	Nondimensional wall temperature
$\dot{w}$	Mass flow rate of transport fluid
$w_f$	Fluid mass per unit flow channel length
$w_w$	Wall mass per unit flow channel length
$X$	Temperature
$x$	Flow channel coordinate

## NOMENCLATURE (CONT.)

$\theta$

Nondimensional time

$\tau_f, \tau_s, \tau_w$

Time response characteristics of fluid, system,  
and wall

$\tau_p$

Time response characteristics of sensor probe  
to impressed temperature

## 1.0 SUMMARY

This report documents the second phase of development for a multi-fluid flash evaporator heat sink which vaporizes an expendable fluid to cool a heat transport fluid loop. The device utilizes Freon 21 as the heat transport fluid, and either R22 or water for the expendable evaporant consistent with projected space shuttle orbiter systems and mission operating phases. The evaporants are pulse-sprayed by on-off control onto the walls of a chamber formed by heat transfer surfaces which contain the Freon 21 transport fluid. The vaporized water or R-22 is exhausted to external vacuum or atmospheric surroundings through a fixed size exit. The objectives of this phase of the program were the design, fabrication, and testing of a preliminary laboratory prototype flight configuration evaporator which can meet the space shuttle orbiter performance requirements.

A side-by-side, multi-parallel rectangular transport fluid tube design was selected for the evaporator heat transfer surface. Active and redundant heat transport system tubes are interspersed and brazed together to provide an optimum weight design, and performance which avoids cold spots. The heat transfer surface of 6ft<sup>2</sup> for a nominal 50,000 BTU/hr capability was fabricated in a cylindrical configuration (Figure 11 - page 21) to provide even evaporant spray deposition, and thus maximum evaporant utilization. The evaporant inflow valve/nozzle was designed to prevent freezing on or near the nozzle in the vacuum environment. This was accomplished by minimizing the liquid holdup volume, providing heat from the transport fluid, and providing a smooth surface to which ice cannot adhere.

An on/off temperature switched method of evaporant pulsing for temperature control of the transport fluid was selected over a feedback control method due to simplicity and cost considerations. Extensive thermal analyses were conducted to determine the optimum location of the temperature sensor. A sensor located on the evaporator wall just upstream of the transport fluid exit was selected over a wall mounted or immersion sensor located at the exit since this provides tighter control over fluid temperature, and a common sensor can be utilized by both primary and redundant fluid transport systems. It was also found that different sensor locations are necessary for the water and R-22 evaporants due to differences in spray deposition in the evaporator.

An extensive five week test program was conducted to verify the evaporator design and to demonstrate the capabilities of the device to meet projected shuttle requirements. Thermal control of the transport fluid at 40° ± 5°F by spray pulsing was generally obtained. It was found that the sensor location however, is sensitive to the nozzle spray pattern. Repeated dormant to active operation was demonstrated with no start up constraints. High evaporative efficiencies were obtained during operation: 95% for water and 99% for R-22. The margin on the evaporative side temperature was shown to be larger than previously demonstrated. During previous feasibility testing, (Reference 1), outlet temperatures to 34°F were produced, while in this prototype testing, the outlet temperature was brought deliberately as low as 30°F before any inefficiency was realized.

During early phases of the test program ice was formed near the water nozzle because of insulating surfaces placed adjacent to it. These were installed to prevent possible freezing of the water inflow valve during operation with R-22. It was later determined that they were not required, and no nozzle freezing was observed after removal of insulating surfaces from the evaporator. Frost formation on the walls of the spray chamber was observed with some nozzles due to combinations of large droplets and locally dense spray patterns. Further optimization of nozzle spray patterns and drop size is planned for the next development phase.

Operational characteristics of the evaporator with simulated shuttle heat rejection cycles were also determined. No performance degradation was noted during evaporator operation with: 1) various combinations of active and redundant evaporant and transport systems; 2) different evaporator orientations (up, down, horizontal); 3) variation of evaporant supply pressure; 4) variation of transport fluid flow rate; or 5) variation in ambient pressure (with the R-22 evaporant). Variation in evaporant supply temperature did, however, result in slight changes in performance due to the temperature effects on evaporant properties which changes the spray droplet size and spatial distribution.

The laboratory flash evaporator heat sink designed, fabricated, and tested met the requirements and objectives of the study.

## 2.0 INTRODUCTION

The thermal control system for the shuttle is being projected to include an expendable heat sink to provide primary heat rejection during reentry and atmospheric flight phases, and to augment the radiator system during the orbital operation. For orbital operation, the use of water, generated by the auxiliary power system, is desirable since it does not represent a launch weight penalty to the expendable heat sink. During atmospheric flight a fluorinated hydrocarbon is being considered however, since water evaporates at too high a temperature for use in an environmental heat rejection system.

The Spraying Flash Evaporator is a recent concept for an expendable heat rejection sink. A device of this type directs a sprayed liquid onto a dry heated surface where it is evaporated in single droplet fashion. The latent heat is provided by a circulating transport fluid which flows through the heat exchange surface. The Spraying Flash Evaporator potentially provides (1) a simple design offering high reliability, (2) control by supply rate pulse modulation, (3) low acceleration sensitivity, (4) capability of multifluid evaporation, (5) long life expectancy, and (6) comparatively low weight. Because of these features the evaporator is a candidate for space shuttle use, and its development is being pursued by NASA.

Exploratory tests were conducted in 1970-71 to demonstrate the feasibility of evaporation by direct spray impingement on the heated wall. The objectives of the feasibility tests were (1) to demonstrate the required level of heat fluxes from the evaporating surface, (2) to determine the evaporant liquid utilization efficiency, and (3) to show control during load transients by use of pulse mode evaporant modulation. The tests performed showed: evaporation fluxes of approximately 8000 BTU/hr-ft<sup>2</sup> for H<sub>2</sub>O, NH<sub>3</sub>, and Freon 22 evaporants (with wall temperatures of 28°F for H<sub>2</sub>O); evaporant utilization of 70 percent for NH<sub>3</sub>, 80 percent Freon 22, and 93 percent for H<sub>2</sub>O; outlet circulating fluid temperature control of 35 to 45°F during load transients of zero to 25,000 BTU/hr full load in 4 minutes; and capability for intermittent operation.

Based on the feasibility demonstration tests, it was deemed desirable to pursue the design and testing of a prototype flash evaporator unit which would incorporate the size, construction, flow and temperature conditions expected for the space shuttle application. The following report details the considerations given to the design of the evaporator, selection of a control system, fabrication, and testing of a laboratory prototype evaporator. The work was performed for the NASA-MSC Crew Systems Division, with Mr. Frank Collier the Technical Monitor, by the Vought Missiles and Space Company.

### 3.0 EVAPORATOR DESIGN

#### 3.1 Design Requirements

The Flash Evaporator performance is required to meet the following set of conditions.

Transport Fluid: R-21 ( $\text{CHCl}_2\text{F}$ ) @ 1850 LB/HR  
Heat Load: 0-50,000 BTU/HR  
Outlet Temperature:  $40 \pm 5^\circ\text{F}$   
Evaporants:  $\text{H}_2\text{O}$  and R-22 ( $\text{CHClF}_2$ ) in the appropriate pressure range  
Fail Operational Redundancy  
Aluminum Construction

To implement the design of an evaporator, there are additional considerations concerning the pressure drop of the device, the evaporative side heat transfer coefficient, and the volume of the unit. The testing during the previous program (NAS9-11254) reported in Reference 1 demonstrated heat fluxes of up to 8300 BTU/hr-ft<sup>2</sup>. However, analysis presented in that reference indicates a definite limit in heat flux which theoretically is some 200% above the verified level. In addition, wall temperatures as low as 28°F were realized in testing. The weight and pressure drop of the unit may be traded off using an appropriate weight penalty factor for pressure drop to achieve a minimum total weight penalty. The volume penalty factor is more nebulous. The volume will be naturally proportional to some (positive) power of the weight so that minimization of one insures minimization of the other to a reasonable approximation. The volume is optimum at a condition wherein the pressure drop is somewhat higher than the true minimum for weight/pressure drop considerations alone.

#### 3.2 Heat Exchange Core Tradeoffs

Several standard heat exchanger core sections have been considered for the evaporator surface. The evaporator redundancy requirement has been met using two single-fluid cores or a dual-fluid core. With two cores, a greater number of evaporant supply points is required since each core would require a redundant evaporant supply. One basic difference is not accounted for in the comparison. A dual fluid core is susceptible to damage or certain structural failures which would fail both circuits in one event. This problem is not pertinent for the two evaporator utilization except in the event of some extreme damage or, for example, a colinear meteoroid penetration.

##### 3.2.1 Non-Redundant Design

Figure 1 shows the cores which have been considered for this study. Many of these core designs are intended for gas use and have non-optimum fin thickness. In such cases, increased fin thickness was not found to change the results of the comparison. The cores were evaluated using the assumption of constant heat flux over the active surface and a constant heat transfer



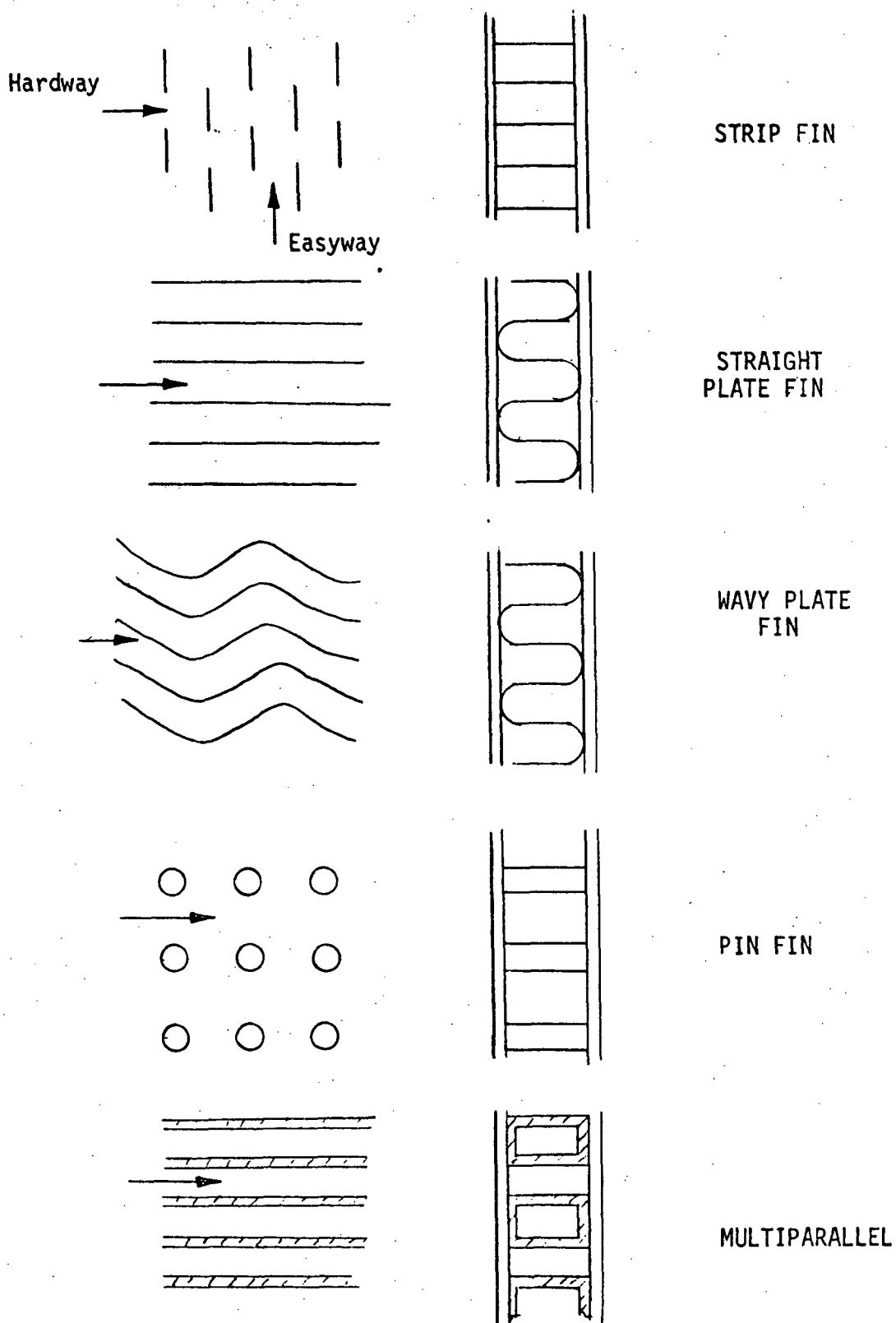


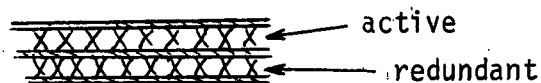
FIGURE. 1 CORE CONSTRUCTIONS CONSIDERED

conductance over the active surface, resulting in a constant value of  $T_f - T_w$ . This value has been chosen as  $10^\circ\text{F}$  for the comparison. The required value of  $UA$  then is  $5000 \text{ BTU/hr-}^\circ\text{F}$ . The transport fluid flow is distributed within a width of heat exchanger core for a length sufficient to achieve the required  $UA$ . As the width is increased, the area generally increases, the length decreases, and the pressure drop decreases. This procedure allows one to compute a pressure drop versus area curve as shown in Figure 2. The area coordinate effectively represents weight since the cores have similar weight per square foot characteristics. Clearly, the hardway short strip fin and multiparallel surfaces are superior, having an area of 3 to  $3.5 \text{ ft}^2$  at a 3psi core pressure drop.

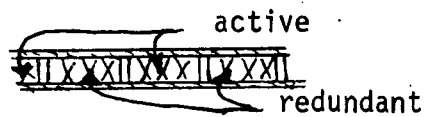
### 3.2.2 Redundant Design

Three basic arrangements of dual fluids within a surface have been considered as shown below.

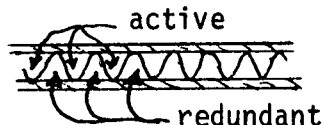
1. Stacked



2. Side-By-Side

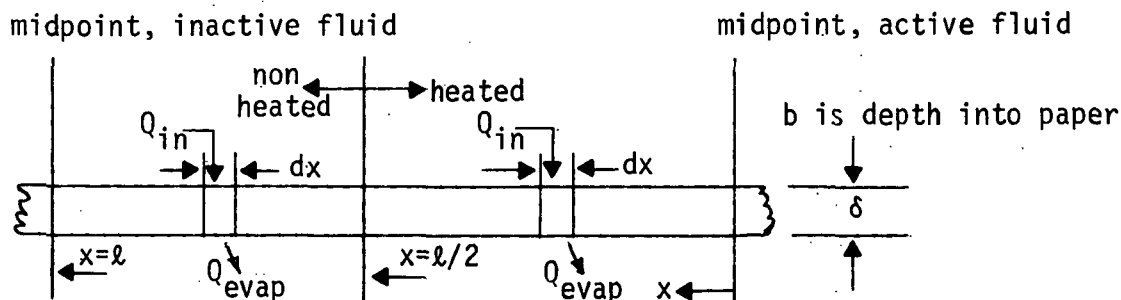


3. Intermingled



The side-by-side and intermingled designs are separated at a condition where the temperature drop from the active mid-point to the inactive mid-point achieves a value roughly equivalent to the temperature difference between the fluid and active mid-point. An analysis of this simple case is presented below.

The side-by-side design must conduct heat from the active channel to each of its neighboring inactive surfaces, since the heat flux is distributed uniformly over each exposed portion. The sketch below illustrates the heat balance for a differential element in each of the inactive and active portions.



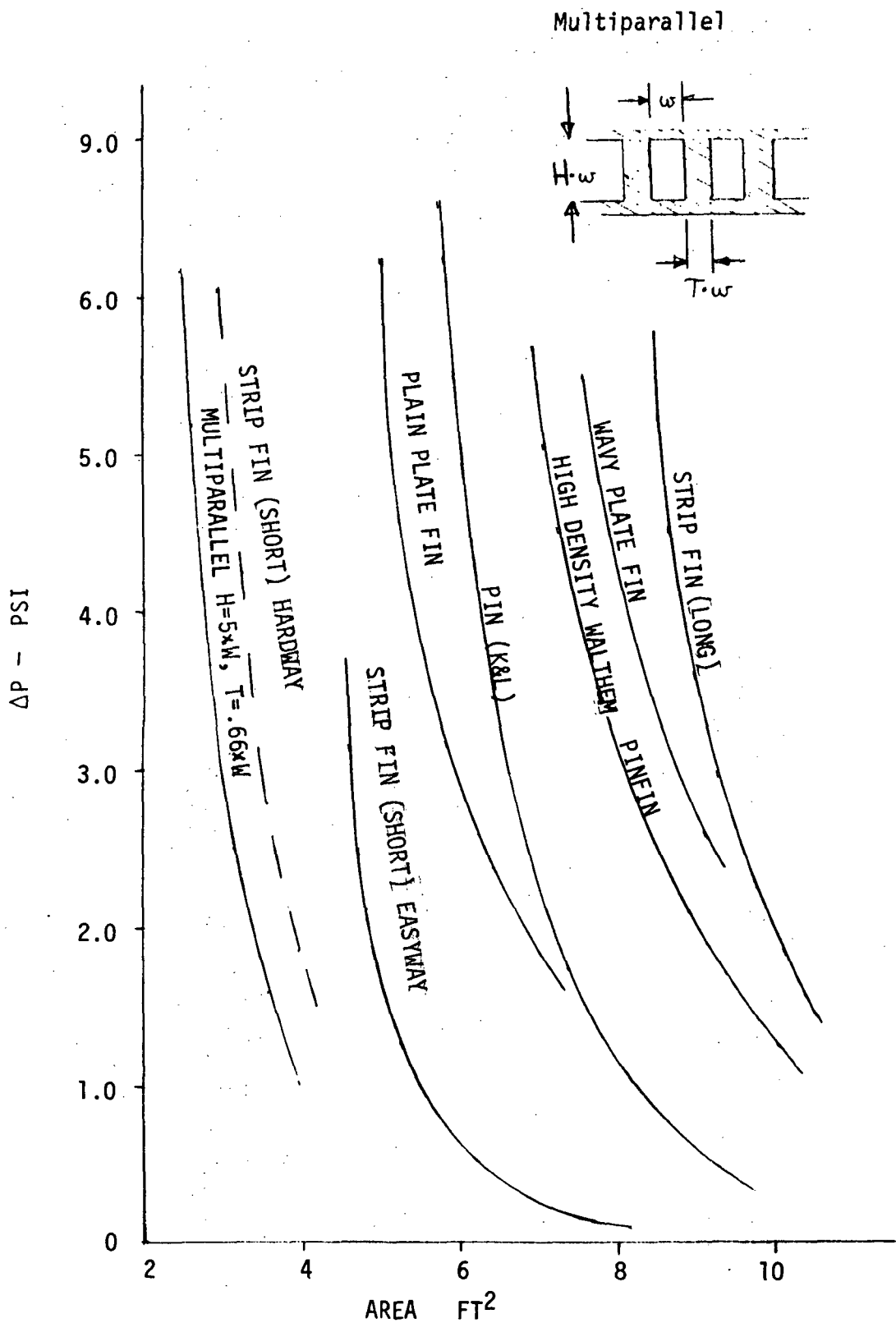


FIGURE 2 PRESSURE DROP AND AREA FOR VARIOUS NON-REDUNDANT CORE DESIGNS

In the heated section,  $Q_{in} = bh\Delta T dx$ , while in the non heated section,  $Q_{in} = 0$ . The evaporation flux is uniform over the surface at value  $Q/A$ , yielding  $Q_{evap} = (Q/A)bdx$ . The heat balance on the element of thickness  $\delta$  and conductivity  $K$  may then be written:

heated portion

$$\frac{d^2T}{dx^2} - \frac{h}{K\delta} (T - T_f) - \frac{Q}{AK\delta} = 0$$

non heated portion:

$$\frac{d^2T}{dx^2} - \frac{Q}{AK\delta} = 0$$

The boundary conditions are:

$$\text{at } x = 0 \quad \frac{dT}{dx} = 0$$

$$\text{at } x = \frac{\ell}{2} \quad \begin{cases} T \text{ is continuous} \\ \frac{dT}{dx} \text{ is continuous} \end{cases}$$

$$\text{at } x = \ell \quad \frac{dT}{dx} = 0$$

The solution for the temperature distribution is as follows:

heated portion:

$$T = T_f - \frac{Q}{Ah} + \frac{Q\ell}{2AK\delta\alpha} \cdot \frac{\exp(\alpha x) + \exp(-\alpha x)}{\exp(\frac{\alpha\ell}{2}) - \exp(-\frac{\alpha\ell}{2})} ; \quad \alpha = \left(\frac{h}{K\delta}\right)^{1/2}$$

unheated portion:

$$T = \frac{Q}{AK\delta} \frac{x^2}{2} - \frac{Q}{AK\delta} \ell x + T_f - \frac{Q}{Ah} + \frac{3}{8} \frac{Q\ell^2}{AK\delta} + \frac{Q}{AK\delta\alpha} \frac{\ell}{2} \coth\left(\frac{\alpha\ell}{2}\right)$$

The temperature at  $x = \ell$  is the lowest temperature and is called  $T_\ell$ . The unheated portion equation may be arranged in the form

$$Q = K_f h A (T_f - T_\ell)$$

$$\text{where } K_f = \frac{1}{1 + 1/2 \left(\frac{\ell}{\alpha}\right)^2 + \frac{\alpha\ell}{2} \coth\left(\frac{\alpha\ell}{2}\right)}$$

In this relation,  $K_f$  is a type of fin effectiveness and is the ratio of the heat transferred to that which would be transferred through a completely active surface at temperature  $T_a$ . Values near 0.5 represent strong fin conduction since the heat transfer coefficient acts on only half the cooled surface. Figure 3 shows the value of  $K_f$  versus the parameter  $\alpha l$ .

For purposes of illustration the fin effectiveness  $K_f$  for a thickness ( $\delta$ ) of 0.02 inches is shown in Figure 4 versus the active passage width  $l$ . From this curve, it is apparent that the span cannot be very large without incurring an excessive temperature drop in the uncooled portion. Thus a side by side redundant design will either have very narrow passages or will tend to be more than twice as large as a non redundant passage. Clearly also, as the passage width decreases, an important omission in the simplified analysis becomes apparent. The web between the active and passive flow passages was assumed to have no contribution, but its effect will become significant as the passage width and the web height tend to be of the same size. Obviously this leads to the third concept of intermingled design.

The short strip fin design (in hardway flow direction) and the multiparallel arrangement with intermingled active and inactive systems are compared for the redundant case. The short strip fin design with side-by-side design requires an active width so narrow (0.2 inch) that it is nearly equivalent to the multiparallel design and thus is not considered further. Figure 5 shows the pressure drop versus area for these surfaces. In the case of the stacked design, the inner side (facing the cooling) has a reduced fin height and increased fin thickness to provide increased conductance from the outer side. The intermingled multiparallel is sensitive to the fin thickness as shown. For the height to width ratio of 5, the 0.66 fin-to-width ratio case is optimum and equal fin and width requires increased area. In reality, the equal fin and width provides a greater strength which is probably required to meet the 900 psi estimated no-fail internal pressure.

A comparison of non-redundant and redundant core design may be made based on Figures 2 and 5. Using a 4 psi pressure drop results in the the comparison of Table 1. On the basis of this evaluation it is clear that the strip fin design could be either redundant or non redundant without a significant weight difference, while the redundant multiparallel design favors the redundant design. With the expected thick fin multiparallel design of 6 ft<sup>2</sup> area, the weight grows to 40 lb., or slightly above the strip fin design. Based on this estimate, the detailed design of the evaporator was sought for the strip-fin redundant design. This decision was partly based on the fact that the evaporative heat flux for the non-redundant design was estimated at 14700 BTU/hr-ft<sup>2</sup>, which is 75% higher than the value demonstrated in feasibility testing.

### 3.3 Detailed Design

Up to this point only the area and pressure drop have been considered, while for the detailed design the configuration must enter the study. Reference 1 testing showed that the cylinder configuration with the nozzle used achieved

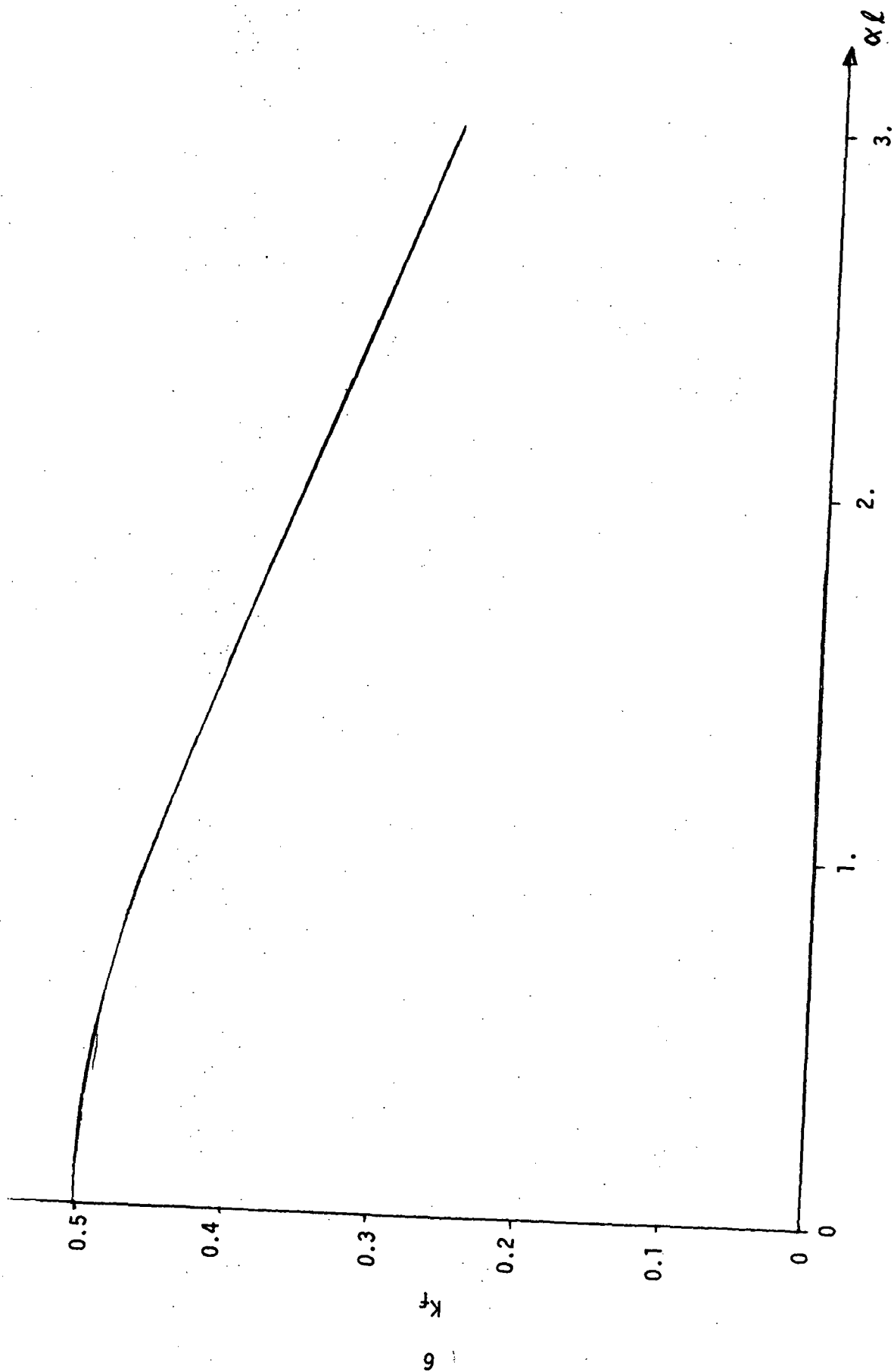


FIGURE 3 SIDE BY SIDE FIN EFFECTIVENESS

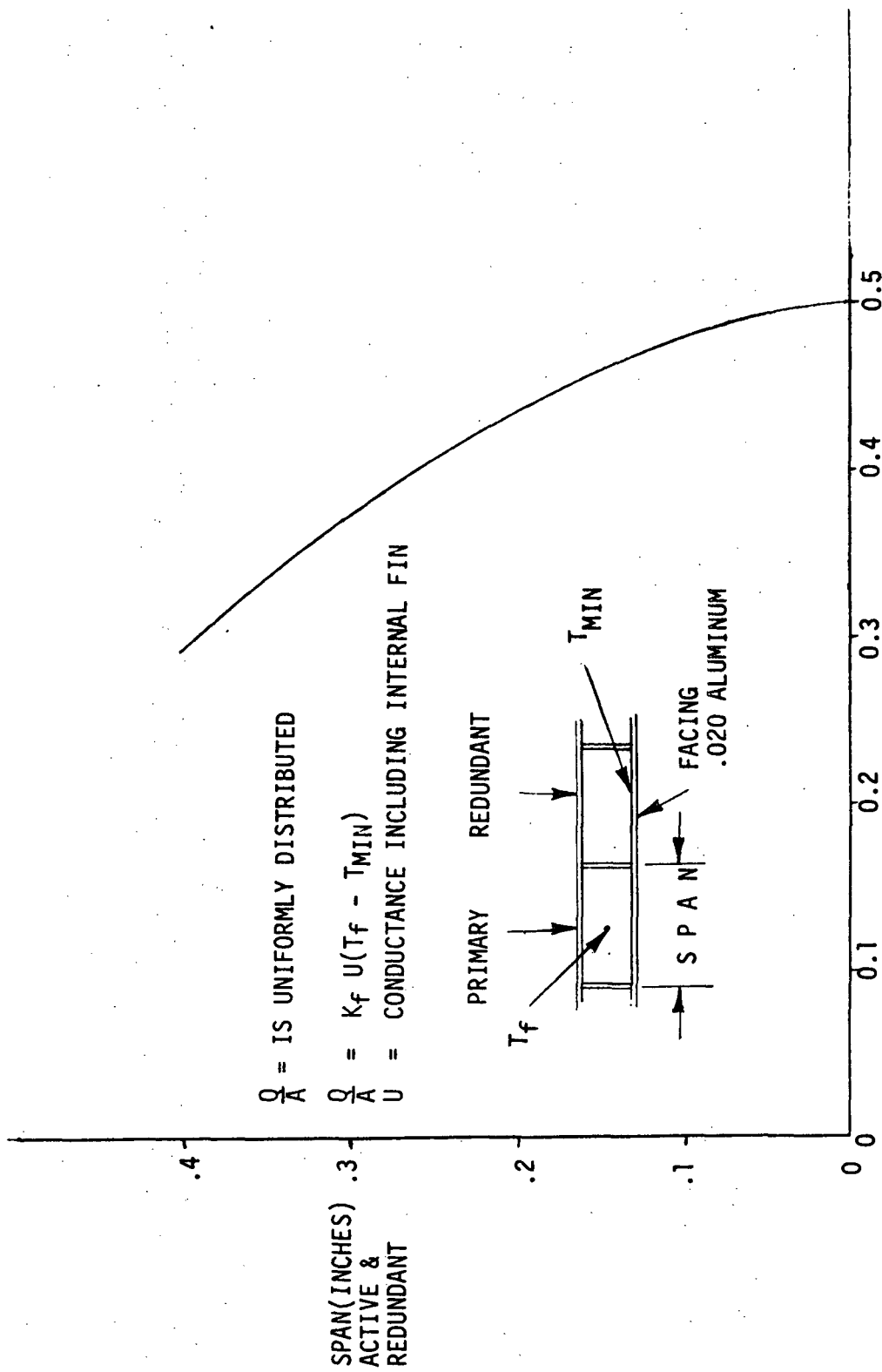


FIGURE 4 SIDE BY SIDE FIN EFFECTIVENESS,  $K_f$

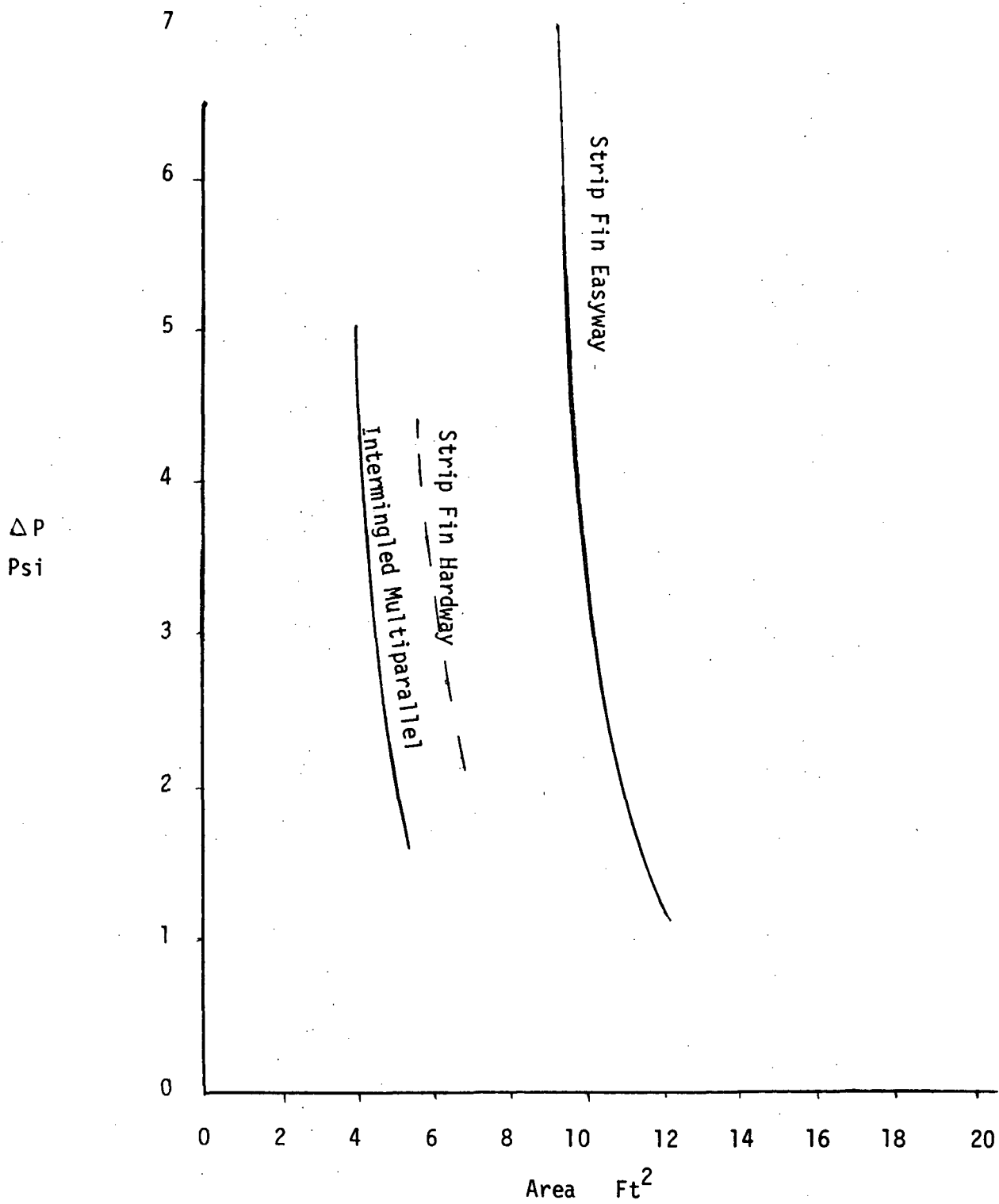


FIGURE 5 COMPARISON OF REDUNDANT DESIGNS



TABLE 1  
COMPARISON OF NONREDUNDANT AND REDUNDANT CORE DESIGNS

	Two Multiparallel Cores H=5, T=.66 Non redundant design	One Multiparallel Core H=5, T=.66 Redundant Design	Two Strip Fin Cores Non Redundant	One Strip Fin Core Redundant Design
Total Active Area FT <sup>2</sup>	5.6	4.2	6.8	6.0
Estimated Weight/ft <sup>2</sup> (wet)	3.8	3.8	1.9	3.3
Estimated Weight Core Only	21.3	15.9	12.9	19.8
Estimated Weight Back Cover(s)	7.6	7	10.2	12
Estimated Weight Valves & Supply Lines	12	6	12	6
Estimated Total Weight	40.9	28.9	35.1	37.8

a considerably more uniform water spray flux than did the plate configuration. Inasmuch as the evaporator heat control mode is by control of the pulse duty cycle, it is desired to obtain a reasonably uniform deposition. A uniform distribution provides the greatest margin against accumulation of frost. At low heat load, during a given pulse, the wall temperature is depressed proportionally to the local value of  $q/U$ . The strong variation of  $q$  in the plate configuration of about 3 to 1 peak to average flux causes a significant reduction in margin against accumulation and to provide  $U$  proportional to  $q$  increases the pressure drop by nearly an order of magnitude. Therefore the cylindrical form of the evaporator was selected with a uniform conductance  $U$  over the active surface.

Local values of spray distribution for Freon were observed at 5 times the average spray distribution. However, in the Freon case the evaporation surface temperature is at or below  $-40^{\circ}\text{F}$ , a temperature the wall can approach without accumulation of evaporant. The value of  $q$  is  $41,600 \text{ BTU/hr-ft}^2$  and  $U$  is  $830 \text{ BTU/hr-ft}^2\text{-}^{\circ}\text{F}$ , so  $T_f - T_w = 50^{\circ}\text{F}$ .  $T_f$  is  $40^{\circ}\text{F}$  at the outlet so the minimum wall temperature is  $-10^{\circ}\text{F}$ , considerably above the lower limit. Therefore the core design is based on water considerations and not on Freon operational requirements.

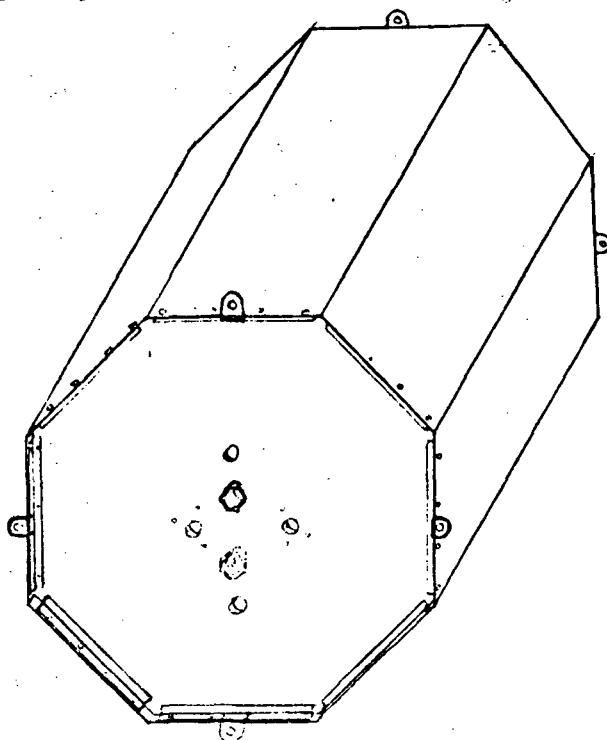
The configuration has been developed to the following general specification. A closed end cylinder with length 0.6 its diameter is expected to be sprayed with a nearly uniform spray flux of water. The area of the cylinder and end plate is required to be about 6 square feet having a superficial conductance  $U$  of  $830 \text{ BTU/hr-ft}^2\text{-}^{\circ}\text{F}$ . The vapor vent size is scaled from the successful feasibility test to a 4-inch diameter. The nozzle position is such that the 50 degree semivertex angle would strike the cylinder at the edge of the active surface. The active surface is required to be devoid of local areas of low conductance to prevent frost accumulation.

### 3.3.1 Strip Fin Core Design

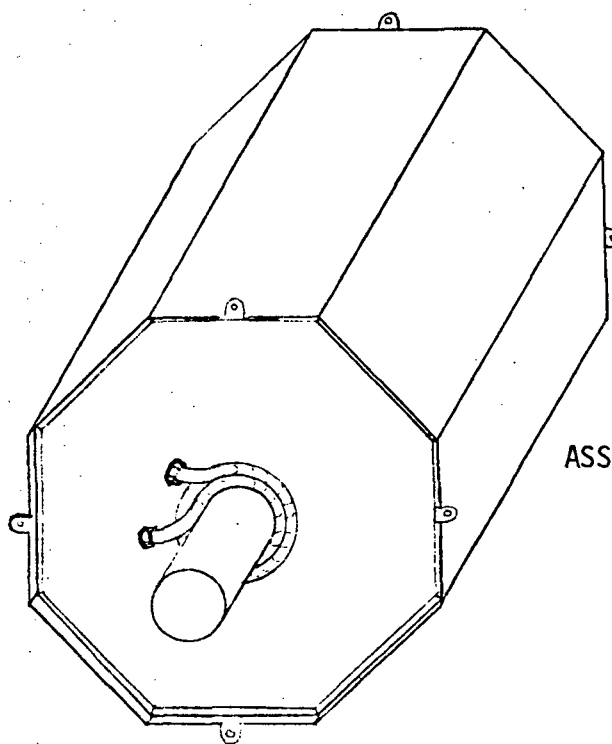
The design of the strip fin heat exchange surface was pursued further to consider the details of its construction. Figures 6 through 9 show the configuration which resulted. The core was configured of stacked sheets having a minimum conductance of  $830 \text{ BTU/hr-ft}^2\text{-}^{\circ}\text{F}$  in non-constricted regions. However, in the joints there is no technique of construction which removes the low conductance edge from the spray. Because these local areas drop by  $\frac{qL^2}{2K\delta} \approx 7^{\circ}\text{F}$  for a maximum value of  $T_f - T_w = 17^{\circ}\text{F}$ , it was anticipated that the risk of local frost formation in the corner areas was significant. In addition, the pressure drop with the  $6 \text{ ft}^2$  active surface was estimated at 16 psi for the final configuration in contrast with the value of 4 psi estimated in the earlier section.

### 3.3.2 Multiparallel Channel Design

Various manufacturing techniques were considered for achieving the multiparallel flow arrangement as shown in Figure 10. The figure also indicates

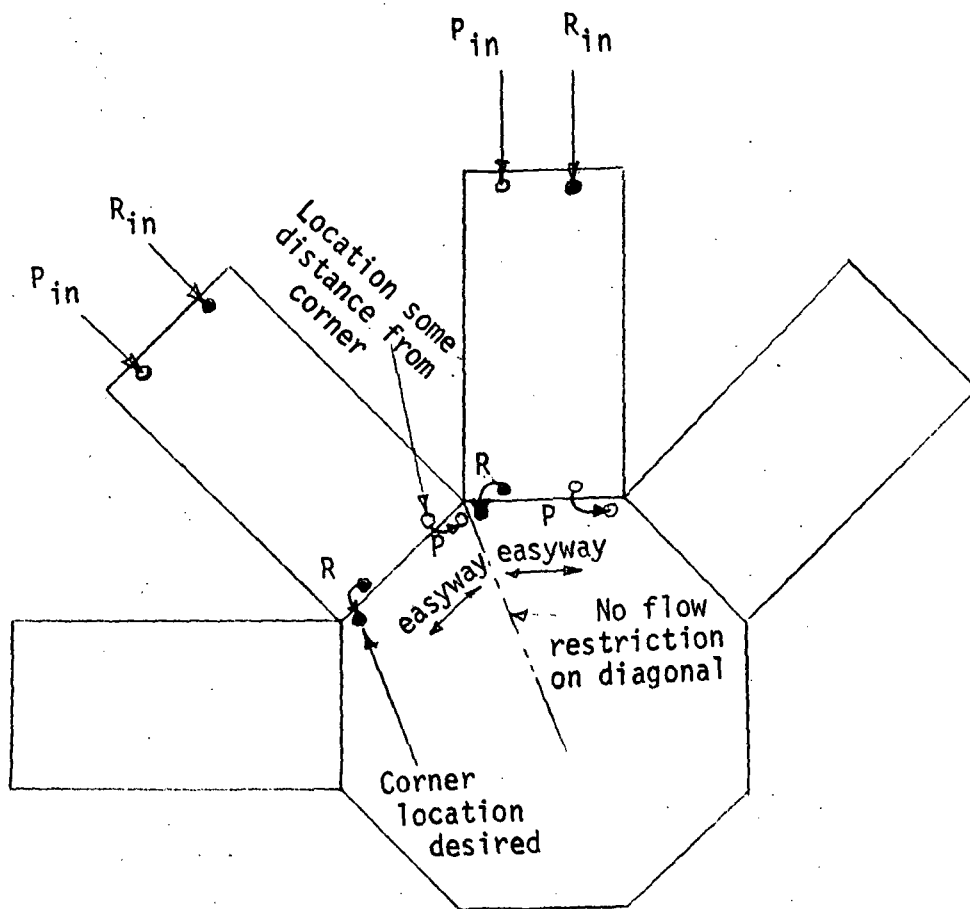


ASSEMBLY, NOZZLE END VIEW



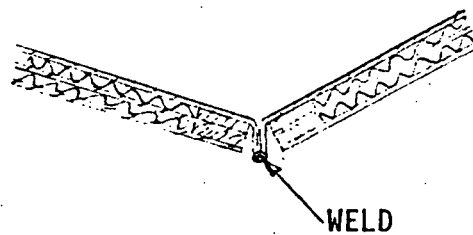
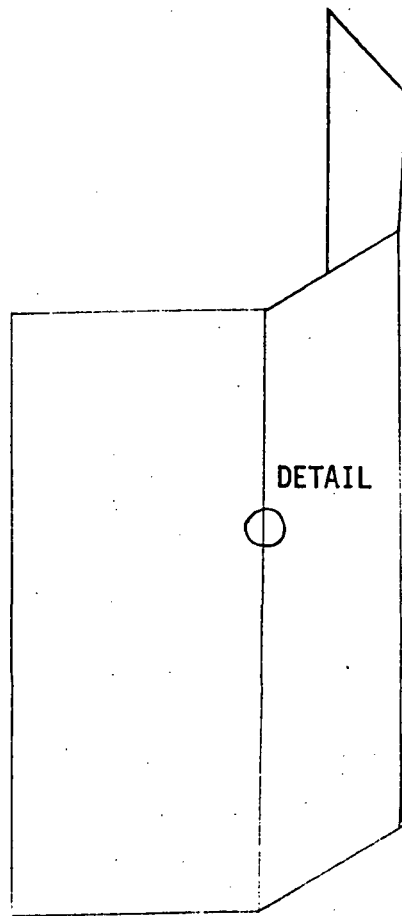
ASSEMBLY, VAPOR EXHAUST END VIEW

FIGURE 6 STRIP FIN CORE DESIGN, ASSEMBLY



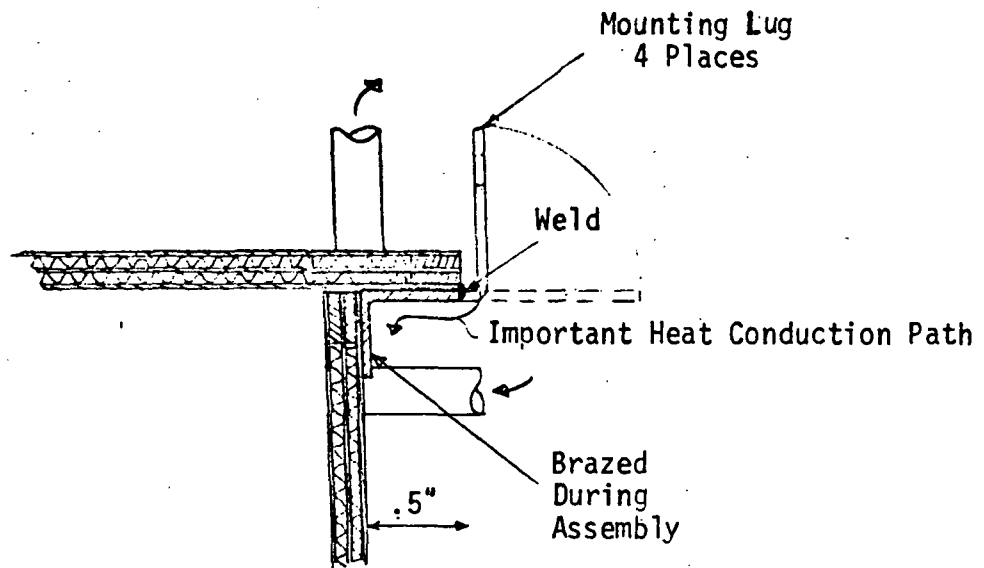
SUGGESTED TRANSFER MANIFOLD LOCATIONS

FIGURE 7. STRIP FIN CORE DESIGN

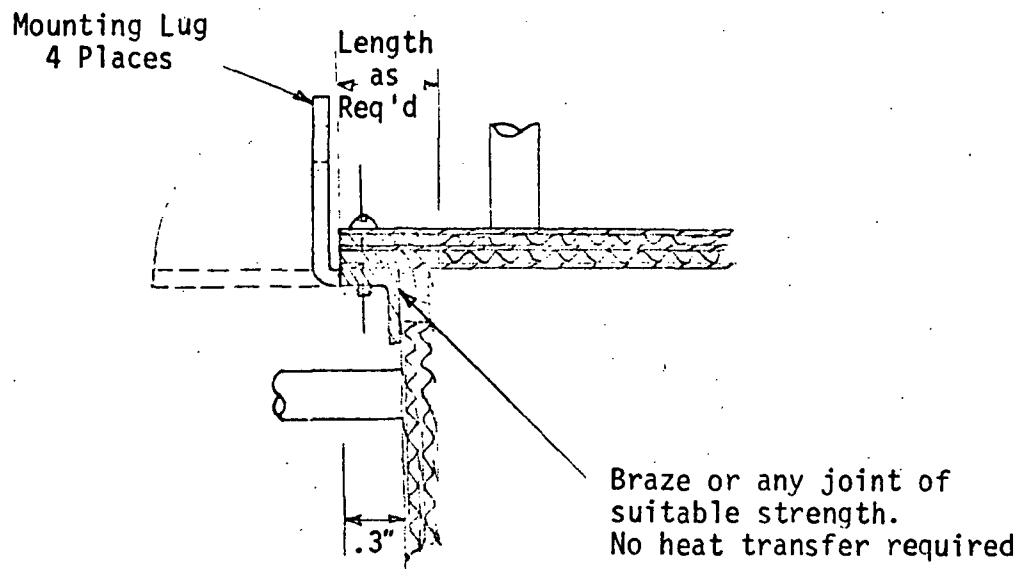


EDGE DETAIL

FIGURE 7A STRIP FIN CORE DESIGN

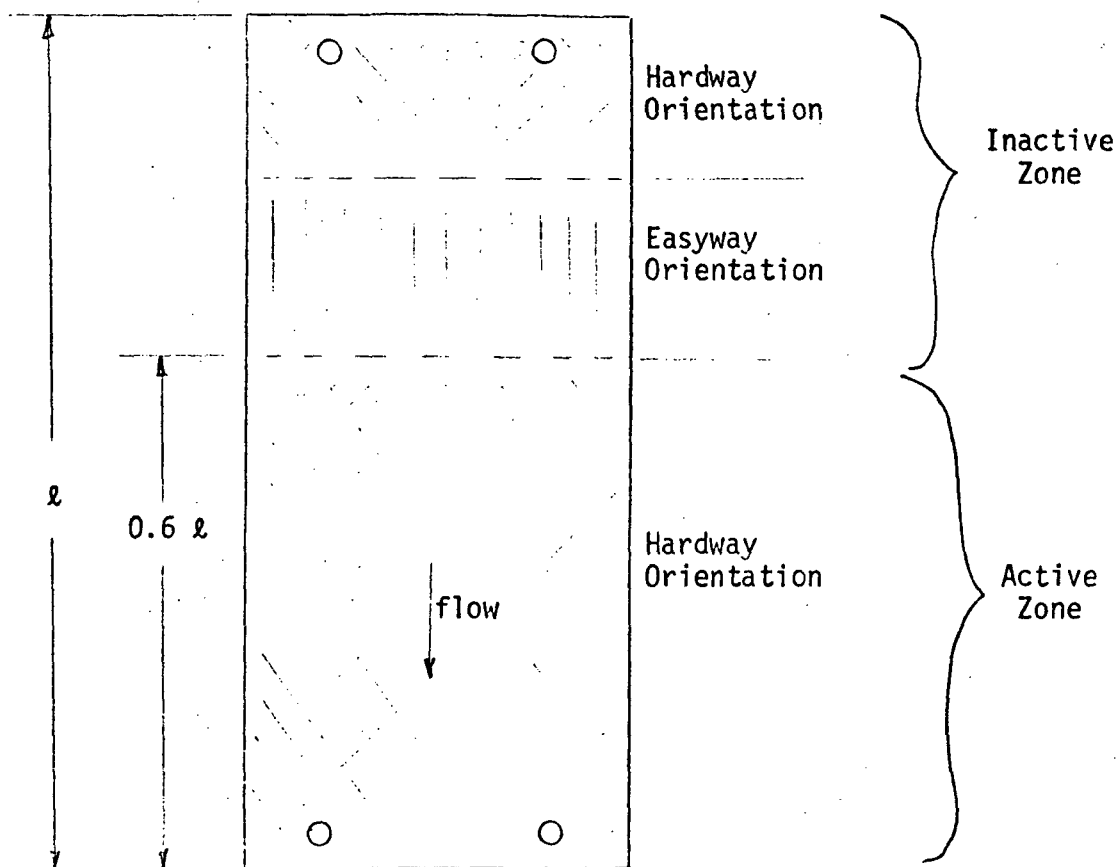


PROSPECTIVE EDGE DETAIL ON END OPPOSITE NOZZLES



PROSPECTIVE EDGE DETAIL ON NOZZLE END

FIGURE 8 STRIP FIN CORE DESIGN EDGE DETAILS



SUGGESTED INCORPORATION OF EASYWAY SECTION  
OUT OF ACTIVE ZONE TO ALLOW RELIEF OF PRESSURE DROP

FIGURE 9 STRIP FIN CORE ORIENTATION

the relative difficulty in achieving the transition from cylinder to end cap, the expected uniformity of flow passage dimensions, and comments concerning the configuration. Of the techniques, the total tube wound (Configuration D) approach appears to offer (1) the least likelihood of system-to-system flow leaks, (2) the least dependence on a high quality brazement, (3) the easiest transition from cylinder to end face, and (4) equivalent manifolding difficulty. A design using the tube wound approach is shown in Figure 11, with a manifold area cutaway sketch shown in Figure 12. This design was considered more promising than the octagonal arrangement primarily because of the lack of areas of low conductance with the multitube continuous wound approach. The weights of the two approaches and pressure drops are re-estimated to include details of the actual design not considered in Table 1.

<u>DESIGN</u>	<u>ACTIVE AREA</u>	<u>WEIGHT</u>	<u><math>\Delta P</math>, PSI</u>
Strip Fin Octagonal Unit	6 ft <sup>2</sup>	32 lb	16 psi
Multitube Unit	6 ft <sup>2</sup>	37 lb	5 psi

Some adjustments could be anticipated to improve the strip fin design to lower the pressure drop and increase the weight somewhat, but the impact is deemed to be minor. For purposes of the trade, a factor of 1.5 lbs per psi pressure drop penalty is estimated from current space shuttle studies.

The weight increase for the multi-tube unit as compared to Table 1 results from increasing the fin thickness to equal the passage width. This increase is deemed necessary from structural and manufacturing consideration and therefore increases the surface area as well as density of the evaporator.



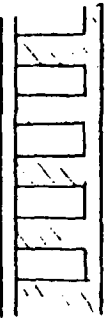
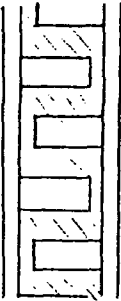
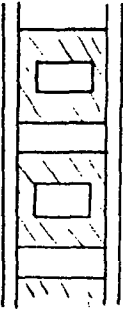

Configuration	Relative Difficulty Transition From Cylinder To Plate	Uniformity Of Flow Passage Dimensions	Comments
 <p>A</p>	Moderate	High	Primary to redundant leaks possible through brazing joint
 <p>B</p>	High	High	
 <p>C</p>	Moderate	Low	
 <p>D</p>	Low	High	Direct heat transfer does not pass through a brazing joint

FIGURE 10 MULTIPARALLEL CHANNEL FORMING TECHNIQUES



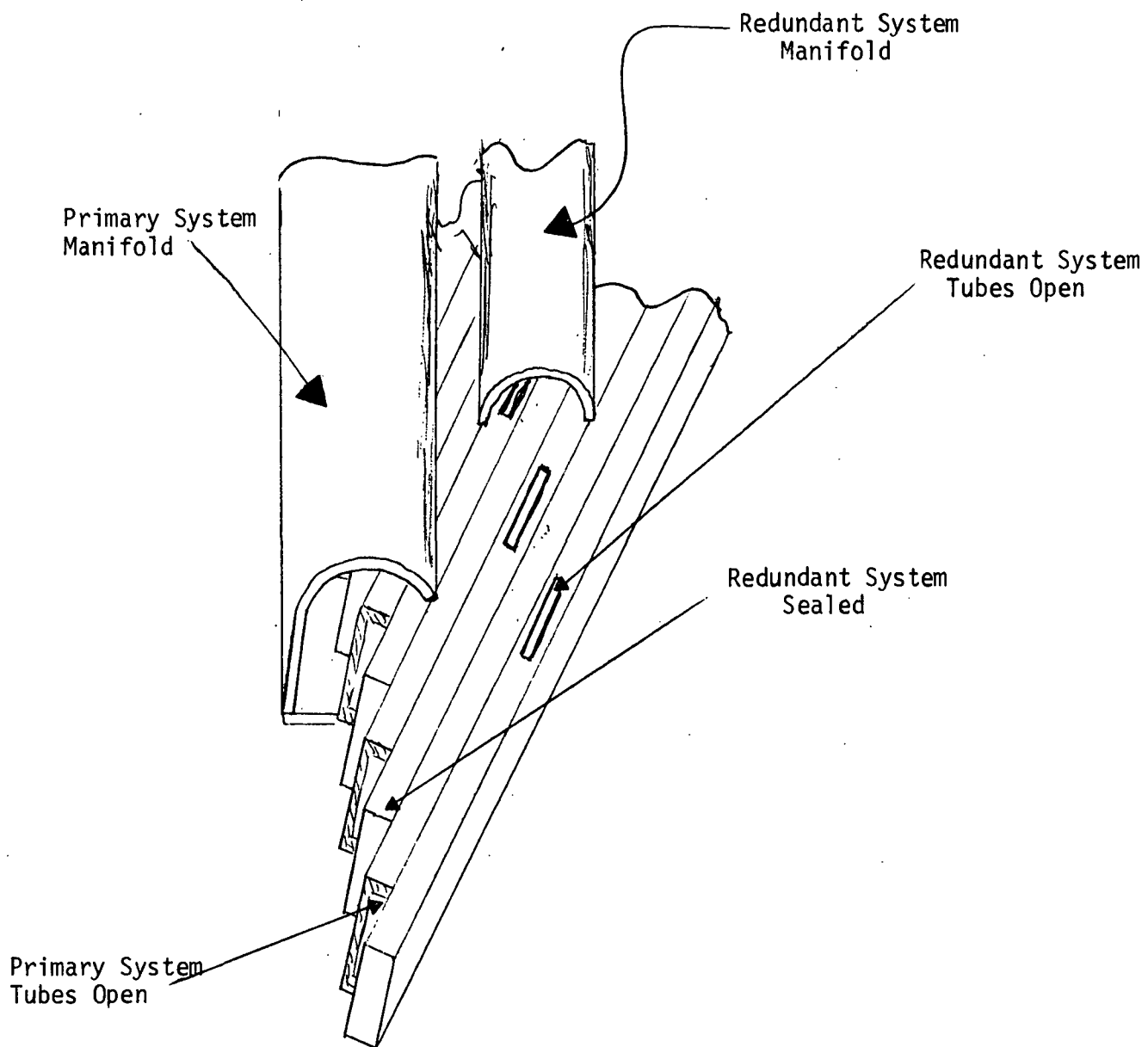
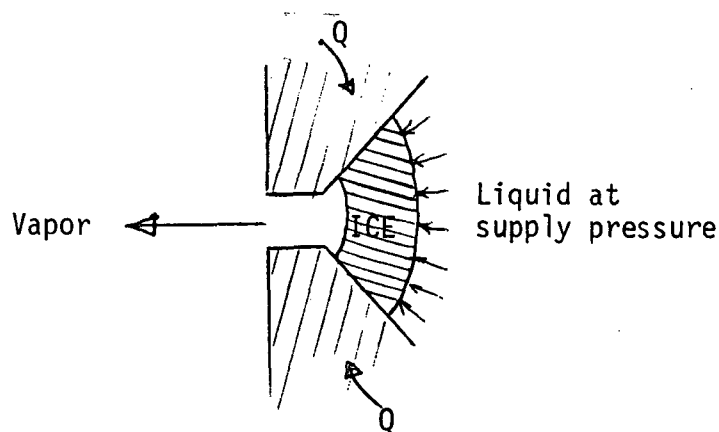


FIGURE 12 · MANIFOLD CUTAWAY

### 3.4 Valve and Nozzle Design

During feasibility testing it was discovered that following the control valve shutoff, the liquid between the valve seat and the nozzle orifice (called "hold up" volume) would dribble out. This hold up volume may have a tendency to freeze onto the nozzle surface resulting in the formation of an ice "tree" which apparently would grow to fill the evaporator void. Inasmuch as such an occurrence represents a failure, action to eliminate this potential freezing was initiated.

The potential for freezing depends upon several factors; the liquid holdup volume, the exit orifice size, the nozzle material properties, the thermal connection of the nozzle to an external heat source, the surface finish of the nozzle, the duty cycle of nozzle pulsing, and the entering evaporant temperature. In general, the critical freezing tendency exists external to the nozzle, but it is conceivable that freezing could occur within the nozzle itself. The nozzle passages are characterized by a surface area and a conduction length for heat flow from an external source to a postulated liquid-vapor interface internal to the nozzle. As liquid is vaporized the conductance increases, so that the boiloff rate is further increased. If the boiloff rate is high enough to choke the exit orifice at a pressure above the triple point, no freezing can occur. For purposes of calculation the hold up volume is estimated as 0.03 cubic inches (0.5cc), with a conduction thickness of approximately 0.03 inch. This produces a conduction area of 0.007 ft<sup>2</sup> for a water film conductance of 0.9 BTU/hr-°F. If the nozzle temperature is held at 10°F above the vaporization temperature, the heat flow rate is 9 BTU/hr representing a vapor flow rate of  $2.5 \times 10^{-6}$  lb/sec. The nozzle exit orifice (0.060 inch dia.) has an area of  $2.83 \times 10^{-3}$  in<sup>2</sup> which at the triple point pressure and 492°R is choked at a flow of  $6 \times 10^{-6}$  lb/sec. At the worst condition, it is conceivable that the pressure internal to the nozzle could drop below the triple point so that freezing internal to the nozzle could be experienced. However, for nozzle temperatures greater than 42°F, conduction paths shorter than 0.03 inch and exit orifice less than 0.060 inch diameter, the possibility is remote. In addition, freezing within the nozzle would be self correcting. For, when flow is initiated, the ice would be flooded with fresh, warm liquid at the supply pressure. At worst, the ice would block the flow passage in such a way that an ice chunk is forced against a heated surface as shown below.



Because of the force balance on the ice, it will continually contact the wall at a pressure of near the supply pressure. This insures sublimation at a rate large enough that all the available heat transfer is consumed in vapor generation. The ice moves in glacier style on the wall and its junction with the wall sustains a temperature depending on the heat transfer from the nozzle and the exit orifice area. At such a condition the rate of growth of the ice/liquid surface may be compared with the rate of recession to determine the stability of the situation. The heat transfer from the 42°F surrounding transport fluid to the nozzle at temperature  $T_n$  is

$$Q = 3(42-T_n) \quad (U = 3)$$

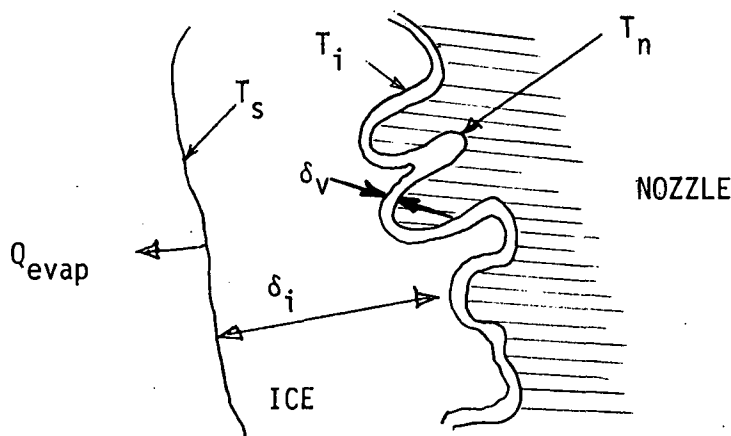
This produces a vapor flow of  $.0025 (42-T_n)$  lb/hr which will raise the choked pressure upstream of the orifice to  $0.28 (42-T_n)$  times the triple point pressure. The situation reaches equilibrium at the condition where  $T_n$  and the choked pressure lie on the vapor phase change saturated condition. Using the values  $P_n$  and  $T_n$  from

$$P_n = (.088)(.28)(42-T_n) \quad (\text{psia})$$

results in an equilibrium achievement at  $T_n \approx 38^\circ\text{F}$  and  $P_n \approx 0.1$  psia which is above the triple point. Therefore any ice blockage cannot persist.

Upon release of the liquid holdup, the nozzle exhibits an initial temperature dependence on the evaporant supply temperature, the transport fluid temperature and conductance to the nozzle, and the aftermath of previous cycles of cooling. In most instances this initial temperature will be an average of the transport fluid temperature and the evaporant supply temperature. Immediately after flow cessation the liquid holdup begins to dribble out of the nozzle, freezing and cooling the nozzle surface. The ice and nozzle may be adherent only if "hooking" of ice and nozzle fingers occurs or if the nozzle temperature is suppressed below  $32^\circ\text{F}$ .

Consider a vapor layer which is thin with respect to the irregularities of the nozzle surface, such that a "hooking" effect could be obtained (see sketch below).



To investigate this proposition, consider the magnitude of heat transfer through the layer of vapor, into the ice, and the sublimation at the surface. In steady state, the heat flux through the vapor layer is

$$\frac{Q}{A} \text{ vapor} = K_V \frac{T_N - T_I}{\delta_V} = K_I \frac{T_I - T_S}{\delta_I} = \frac{Q}{A} \text{ ice}$$

where  $T_N$  is the nozzle temperature,  $T_I$  is the nozzle side ice temperature,  $T_S$  is the vacuum surface ice temperature,  $\delta_V$  is the vapor thickness,  $\delta_I$  is the ice thickness,  $K_V$  and  $K_I$  are vapor and ice conductivities. The maximum value of  $Q/A$  of ice is given by  $1/4 \lambda_{13} \rho \bar{v}$ , where  $\lambda_{13}$  is the sublimation enthalpy,  $\rho$  is ambient vapor density, and  $\bar{v}$  is the average molecular velocity,  $\sqrt{8/\pi RT}$ . The evaporation rate, and this heat transfer rate, is shown in Figure 13 for various surface temperatures. The ratio of vapor to ice thickness is

$$\frac{\delta_V}{\delta_I} = \frac{K_V}{K_I} \frac{T_N - T_I}{T_I - T_S}$$

By assumption,  $T_I \leq 32$  and  $T_N > 32$ , so that if  $T_N - T_I = \epsilon > 0$ , and using  $\frac{K_V}{K_I} \approx \frac{1}{10}$

$$\frac{\delta_V}{\delta_I} = \frac{1}{10} \frac{\epsilon}{T_I - T_S}$$

There is a limit on  $\delta_V$  that it must be much smaller than the scale of roughness ( $\approx 10^{-5}$  ft)

$$\delta_V = \theta (10^{-6} \text{ ft})$$

with  $K_V \approx 0.01 \text{ BTU/hr-ft-}^\circ\text{F}$

$$\frac{Q}{A} > \frac{.01}{10^{-6}} \cdot \epsilon = 10^4 \epsilon$$

This implies  $T_S$  must be above about 400 R ( $-60^\circ\text{F}$ ) for reasonable  $\epsilon$  (i.e., 1 to 10) so that the ratio of thickness is

$$\frac{\delta_V}{\delta_I} = \theta \left( \frac{1}{10} \cdot \frac{\epsilon}{100} \right) = \theta (10^{-4} \epsilon)$$

This would permit  $\delta_I$  to be perhaps as large as 0.01 ft. if  $\epsilon \longrightarrow 1$  ( $T_N \longrightarrow 33^\circ\text{F}$ ), but no larger. Thus only a thickness of 1/8 inch of ice could "hook" itself to a rough nozzle surface. Thicker ice layers would incur lower heat fluxes resulting in vaporization of the tiny ice fingers.

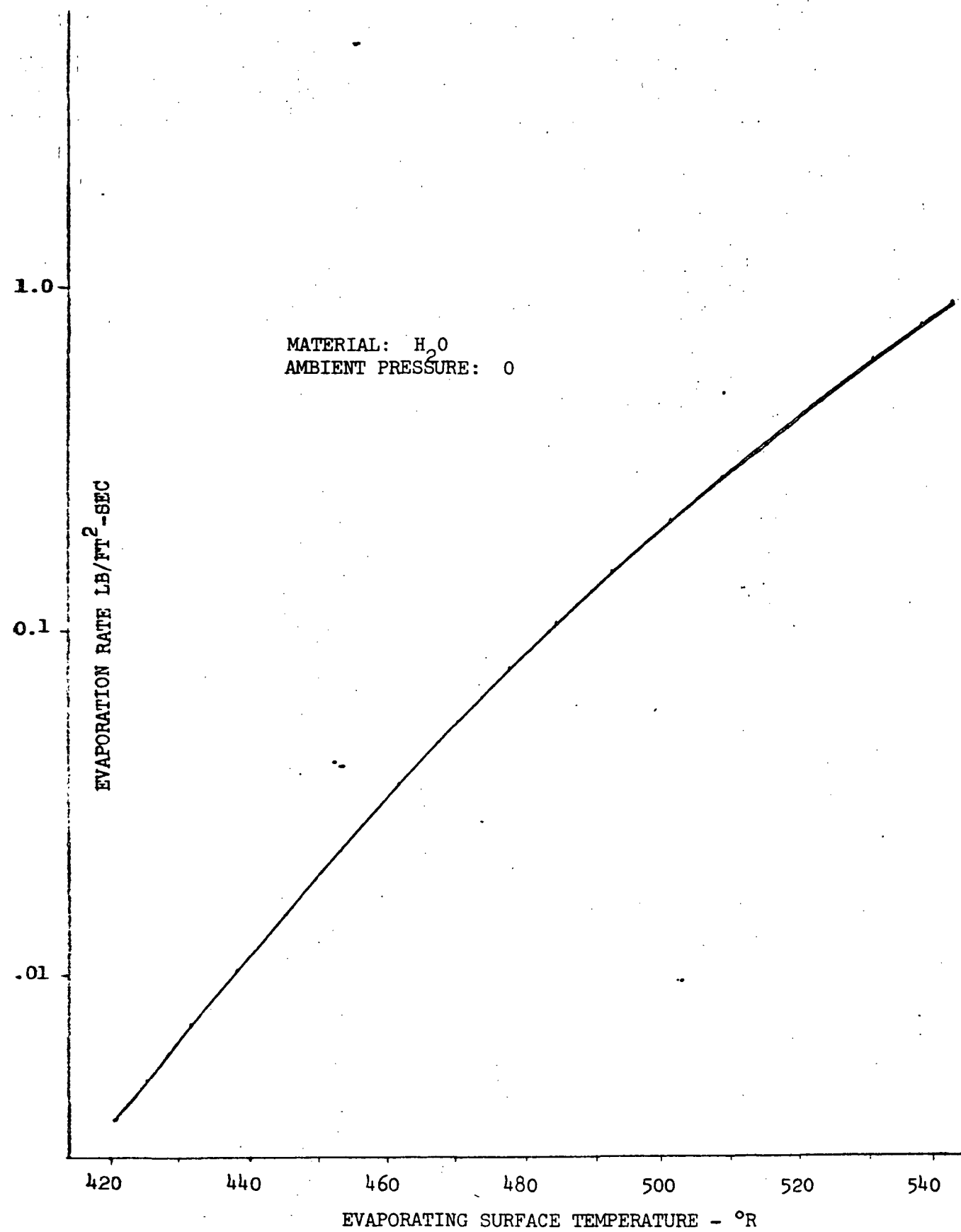


FIGURE 13 EVAPORATION RATES FOR WATER

It has been argued that adhesion to a solid surface above freezing temperature can occur by small thicknesses which cling to the rough surface by an interlocking arrangement. These small thicknesses, it has also been shown, must sublime at a rate of about 10 lb/ft<sup>2</sup>/hr if the roughness is less than 10<sup>-5</sup> ft (100 μ inches). The persistence of such a layer is readily estimated by calculating the time to total evaporation of a 0.01 ft. thickness at 10 lb/ft<sup>2</sup>/hr. A layer 0.01 ft thick represents 0.6 lb/ft<sup>2</sup> and would persist 0.06 hour. Clearly some combination of smoother surface or high nozzle temperature must be provided to avoid this lengthy persistence. The persistence of any ice formation must be less than the cycle time of the evaporator function (order .002 hour). The evaporation flux is proportional to  $\epsilon/\delta_R$  while the maximum ice thickness is proportional to  $\delta_R/\epsilon$ , where  $\delta_R$  is the roughness and  $\epsilon$  is the nozzle temperature above freezing. The persistence time is proportional to  $(\epsilon/\delta_R)^2$  so that an increase in  $\epsilon/\delta_R$  of a factor of six will allow extinction of any accumulation within 0.002 hour. A surface finish of 16μ inches or nozzle temperature in excess of 38°F will accomplish the desired result.

An additional mode of attachment of ice to a solid surface with temperature above 32°F can be postulated. If the metal surface has filaments or whiskers of significant length to diameter ratio, the ice could attach to the end of the filament. This contact could be maintained at a temperature below 32°F even though the base of the filament is above 32°F. In such a case, the ice could be firmly attached to the solid surface. The whiskered surface is not considered a probable occurrence.

If the surface of the nozzle is lowered to below 32°F, ice adhesion is possible without a vapor interface. Overall conductances are generally the same as those with a vapor interface, and the thicknesses of ice possible to be maintained would be similar. There are three items crucial to the determination of whether the nozzle surface could be lowered to below 32°F. These are the quantity of liquid holdup, the mode of fluid outflow, and the availability of heat from the nozzle and its intimate surroundings to the cooled locations.

As a droplet is formed on the nozzle surface the rapid heat transfer will exhaust the heat capacity of the nozzle to evaporate the drop. Within the short lifetime of the liquid, the affected portion of the nozzle may be quite small. The question arises "Does the nozzle temperature drop below 32°F during the droplet lifetime?" To answer this, postulate that the nozzle is semi-infinite at temperature  $T_i$ , and that it is suddenly lowered in temperature at the surface to 32°F. The classic solution for the temperature distribution is:

$$T(x,t) = T_i + (32 - T_i) \operatorname{erf} \left( \frac{x}{2\sqrt{\alpha t}} \right)$$

where  $\alpha$  is the diffusivity. The heat flux at the surface ( $x=0$ ) is

$$Q/A = -K \frac{\partial T}{\partial x} \quad \text{or} \quad Q/A = -(32 - T_i) \frac{1}{\sqrt{\pi}} \frac{K}{\sqrt{\alpha t}}$$



The energy flowing through the surface through time  $\tau$  is

$$E = \sqrt{\frac{2}{\pi}} (T_i - 32) \int_0^{\tau} \frac{K}{2\sqrt{\alpha t}} dt = \sqrt{\frac{2}{\pi}} (T_i - 32) K \sqrt{\frac{\tau}{\alpha}}$$

The droplet evaporative energy is  $\lambda_{23} \rho \delta$  per unit area, where  $\delta$  is the initial thickness. Equating these yields

$$\sqrt{\frac{2}{\pi}} (T_i - 32) K \sqrt{\frac{\tau}{\alpha}} = \lambda_{23} \rho \delta$$

This equation may be solved for  $\tau$  as

$$\sqrt{\tau} = \frac{\sqrt{\pi \alpha} \lambda_{23} \rho \delta}{2 K (T_i - 32)}$$

The heat flux at this time is

$$Q/A = 2 \frac{(T_i - 32)^2 K^2}{\pi \alpha \lambda_{23} \rho \delta}$$

By calculating the heat flux at the last instant of evaporation of the droplet, one may compare its value with that required to evaporate the droplet at a temperature of 32°F. If the calculated value exceeds the required value, subfreezing nozzle temperatures are not expected, and vice versa. For argument, set  $T_i$  to 42,  $\rho = 62.5$ ,  $\lambda_{23} = 1070$ , and  $\delta = .002$  ft.,

$$Q/A = 47.5 K \rho \delta c = 47.5 \frac{K^2}{\alpha}$$

For aluminum,  $Q/A$  calculates to  $1.67 \times 10^5$ ; for brass,  $1.39 \times 10^5$ ; and for stainless steel,  $0.43 \times 10^5$  BTU/hr-ft<sup>2</sup>. Heat fluxes of  $10^5$  are approximately required for evaporation, so that the stainless steel surface could well dip below 32°F. These calculations indicate what would occur with a single sheet of liquid 0.002 ft thick. The total amount of liquid held up is of some interest since thicker sheets are more restrictive and multiple repeated sheet applications would occur if sufficient liquid were available.

The simplest statement of the effect of holdup volume is by a time-independent heat balance equating the evaporation energy of the holdup volume and the stored energy change of the nozzle material. The volume of liquid is designated  $V_l$ , of nozzle  $V_n$ ; thermal properties are density  $\rho$ , specific heat  $c_p$ ; and vaporization enthalpy  $\lambda$ . The heat balance may be written

$$\rho_N c_{PN} V_N \Delta T_N = \rho_l V_l \lambda$$

$$\Delta T_N = \frac{\rho_l V_l \lambda}{\rho_N c_{PN} V_N}$$

The value of  $\lambda$  is about 1000 BTU/lb,  $\rho = 62.4 \text{ lb/ft}^3$ , and  $\rho_N c_{pN}$  for most solid materials is about 35 to 50 BTU/ft<sup>3</sup>-°R. Using 35 as typical (actual for aluminum) yields

$$\Delta T_N = 1780 \frac{V_\ell}{V_N}$$

If the nozzle is to be prohibited from attaining sub-freezing temperatures, and initially has temperature 42°F, the volume ratio must be less than  $V_\ell/V_N < .0056$ . The value of  $V_\ell$  has been estimated at 0.028 cu inches so that  $V_N$  must be greater than 5 cu inches. Clearly this volume is larger than the anticipated nozzle volume, so a portion of nozzle surroundings must be involved.

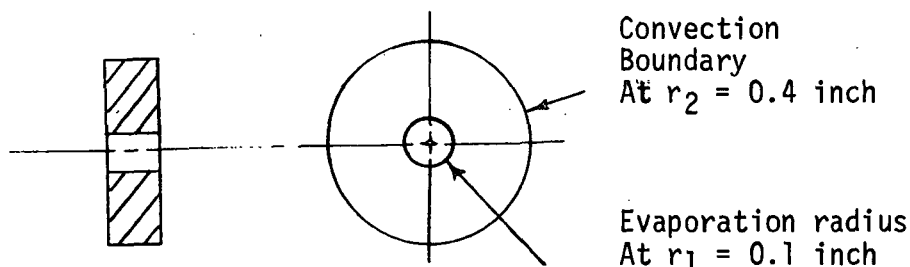
One shortcoming of the foregoing analysis is that it was assumed all of the fluid was vaporized. Certainly some small solid formation could be tolerated without incurring a problem, but the amount is difficult to judge. The other shortcoming lies in the time dependent nature of the assumptions and the premise that only stored energy was available to the nozzle. The time required to exude the fluid from the nozzle may also be longer than the time between evaporator pulses.

The cooling effect from a sudden cooling propagates to a distance  $x$  in time  $t$  given by

$$x \approx 2\sqrt{\alpha t}$$

This distance represents the location of first impulse while the distances about half as great incur significant heat fluxes. Stated another way, elements located at a distance  $\sqrt{\alpha t}$  from the cooling can contribute significantly to the heat flux at the cooling location. If the time in the relation is half the time between turn off and turn on of the evaporant, or about 5 seconds, the effective location of cooling may be estimated. For aluminum  $\alpha \approx .001 \text{ sq ft per second}$  and  $x = \sqrt{\alpha t} = .07 \text{ ft}$ . A tube of coolant located around the nozzle area at a radius of 0.4 inches can be fairly effective in heating the nozzle face. In such a case, the minimum heat flux supplied to the nozzle would be the steady state value, while initial transient values would be higher.

Consider the simplified steady state model shown below



$$K 2\pi r \frac{dt}{dr} = Q$$

$$T_2 - T_1 = \frac{Q}{2\pi K} \log \frac{r_2}{r_1}$$

$$Q = \frac{K}{\log\left(\frac{r_2}{r_1}\right)} (T_2 - T_1)$$

The convective heat transfer coefficient is  $h$  and yields

$$Q = 2 \pi r_2 h (T_f - T_2)$$

The overall conductance of the convective and conductive components is  $\kappa$  so that  $Q = \kappa (T_f - T_i)$

$$\kappa = \frac{1}{\frac{1}{2\pi r_2 h} + \frac{\log(r_2/r_1)}{2\pi K}}$$

For  $h = 200 \text{ BTU/hr-ft}^2\text{-}^\circ\text{F}$ , and  $K = 100 \text{ BTU/hr-ft-}^\circ\text{F}$ ,  $r_2 = 0.4 \text{ inch}$ , and  $r_1 = 0.1 \text{ inch}$ ,  $K = 38.5 \text{ BTU/hr-}^\circ\text{F}$ . Almost all the resistance is associated with the convection heat transfer. Within the 10 seconds between pulses the amount of heat which could be transferred from a  $42^\circ\text{F}$  fluid to a  $32^\circ\text{F}$  centrally cooled area is slightly over 1 BTU, or

$$Q = (38.5 \text{ BTU/hr-}^\circ\text{F}) (10^\circ\text{F}) (10 \text{ sec}) \left(\frac{1}{3600} \frac{\text{hr}}{\text{sec}}\right) \\ = 1.03 \text{ BTU}$$

The amount of fluid evaporated by 1 BTU is .001 lb which represents a hold up volume of 0.0267 cu inches. Thus, conservatively, the nozzle surface may be raised to above  $32^\circ\text{F}$  at the end of a 10 second complete evaporation of the expected 0.028 cu inches of holdup fluid. The surface temperature may drop to near or below  $32^\circ\text{F}$  in the 10 second period, but will be quickly restored to normal levels.

In summary, the valve/nozzle was designed to prevent the possible freezing of the water evaporant by: (1) minimizing the valve-to-nozzle volume for minimum liquid holdup. A holdup volume of 0.028 cubic inches (0.46 cc) should be small enough when accompanied by the other recommended items. (2) Providing liquid transport flow to the vicinity of the nozzle at temperatures  $10^\circ$  above freezing. Heat transfer coefficients of about  $200 \text{ BTU/hr-ft}^2\text{-}^\circ\text{R}$  at distances accessible to the nozzle are adequate. A consideration of the distance which is acceptable leads to the selection of a material with high thermal diffusivity. Aluminum is nearly twice as "close" as brass, and far surpasses stainless steel, while avoiding material electrochemical difficulties with the aluminum evaporator; it is thus preferred. (3) machining the nozzle face to a  $16 \mu$  inches roughness to preclude the possibility of ice formation on a warm nozzle exposed to the evaporant by an interlocking process.

### 3.5 Structural Considerations

The evaporator tubes have been analyzed to determine the stresses produced in various configurations. First, a single tube with internal pressure 600 psi produces stresses of 24,500 psi and 31,400 psi at the tube corner and midpoint of long side, respectively. A tube within a group which is perfectly brazed and with pressure of 600 psi applied to alternate tubes results in stresses of 14,900 psi and 10,550 psi at the tube corner and long side midpoint respectively. With both systems at 600 psi pressure the stresses are 4200 psi at the corner and less at other locations. Within the braze the tension stress reaches 3000 psi, shear stress reaches 2480 psi for the both systems pressurized case.

In the manifold regions, at 600 psi pressurization in both systems, the direct tension in the manifold joint reaches 3750 psi, while the tension induced by bending of the tube group reaches 14,850 psi. With one system under pressure the latter stress rises to 26,750 psi.

The effect of pressure internal to the evaporator chamber tends to "balloon" the evaporator resulting in high stresses near the shoulder or at the exit manifold depending on the constraint of the assembly. The stresses are less when the vapor exit duct is not rigidly fixed, i.e., is mounted by a slider or bellows arrangement. Internal pressurization of 1 psi produces limit stresses of about 30,000 psi according to an approximate analysis. This stress adds to stresses already present from tube pressurization.

The above values are based on analysis which is preliminary in nature, but which should be representative. Actual tubes in the annealed condition (yield point  $\approx$  9000 psi) were pressurized individually, and of the five yielded, the lowest yield pressure was 700 psi. The evaporator assembly (non heat treated) was pressurized to 300 psi without incident prior to testing.

### 3.6 Control Analysis

Two types of control logic have been considered for spray pulse tailoring. The first is a common system where a temperature representative of the fluid outlet is used to initiate spraying above a certain temperature and to cease spraying below a lower temperature. In the second, a logic, which predicts the duty cycle based on inlet temperature and corrects the duty cycle based on outlet temperature, may be employed. Of these, the former is simpler and was selected to avoid development of the latter system.

#### 3.6.1 Temperature Switched Control

With pulse mode control, it is desired to relate the fluid outlet temperature excursion to the wall temperature excursion. This may be performed by approximate analytical means or by numerical modeling. The former is capable of faster estimation of quasi-static load cases and is useful for parametric study, while the latter accounts for more of the details, such as non-uniformity and allows computation of transient effects. Both models have been developed; the numerical model results are presented first with the approximate analytical model discussed later. The basic function of the control is best described in terms of the temperature distribution in the evaporator. Figure 14 shows the instantaneous temperature distribution within an idealized evaporator. The fluid and wall temperature execute transient variations relative to the temperatures shown as sketched in the inset of Figure 14. At each point (except for longitudinal conduction which has a small effect), the temperatures undergo the same relative variations. Two overall observations are pertinent concerning Figure 14. First,  $\partial T_f / \partial A = -QL / \dot{w} c_f A$  so that the temperature slopes (fluid and wall) through the evaporator are proportional to the load. Also, the mean (time averaged) temperature difference between fluid and wall is  $\overline{\Delta T} = LQ / UA$ , and is thus also proportional to the load. A wall-mounted temperature sensor in the cooled region,  $\Delta A$  upstream of the last cooled location, has a temperature related to the outlet temperature expressed by:

$$T_s = T_{out} - \frac{\partial T}{\partial A} \Delta A - \overline{\Delta T}$$

$$T_s = T_{out} + \frac{QL}{A} \left( \frac{\Delta A}{\dot{w} c_f} - \frac{1}{U} \right)$$

The mean sensor-to-outlet temperature difference is independent of heat load,  $LQ$ , and is only slightly dependent upon flow rate,  $\dot{w}$ , since  $U$  is nearly proportional to flow rate. The sensor can then be used to control the outlet temperature from a position on the wall upstream of the outlet. Also, of course, the sensor could be located in the outlet line. There are two advantages to the upstream position of the sensor. First, the cooled wall executes a larger temperature excursion than the fluid, where the wall temperature simply lags the fluid temperature at the outlet position. This leads to a tighter

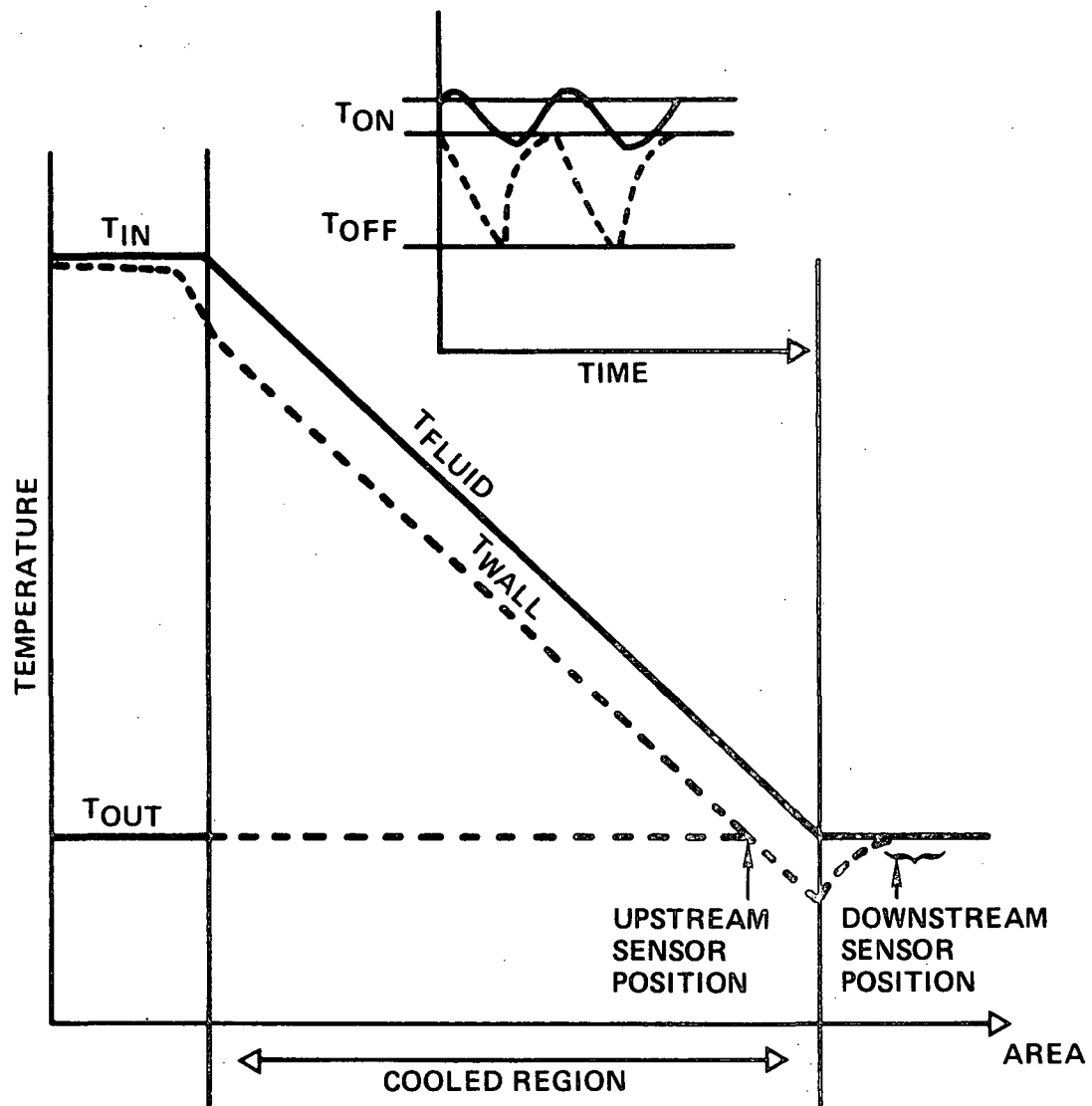


FIGURE 14 TEMPERATURE DISTRIBUTION WITHIN EVAPORATOR

control over fluid temperature. Second, the sensor in the upstream position participates with both primary and redundant fluid systems without switching sensors. It may be possible to use a sensor positioned on the wall in the downstream position also, depending on the relative position of the edge of the sprayed zone and the manifolding.

The flash evaporator design has been subjected to a thermal analysis to analyze its prospective response and to aid in sensor positioning. A nodal model has been constructed as shown in Figure 15. In region 1 of the model, the model is characterized as a single tube encapsulating a fluid node. Nine of these nodes, comprising 90 percent of the active area are arranged in physical sequence. Following these nodes, there are eight segments representing the remaining 10 percent active area. Each of the segments represents the fluid as a single node and the tube by a composite of six sections as shown in the inset. The sensor is a single node which may be thermally connected to any of the nodes in the model in such a way as to simulate the response of the sensor. A major simplification has been made in constructing the model, in that despite the eccentricity of the spray ports, rotational symmetry is assumed which implies also that the flow in each tube is assumed equal.

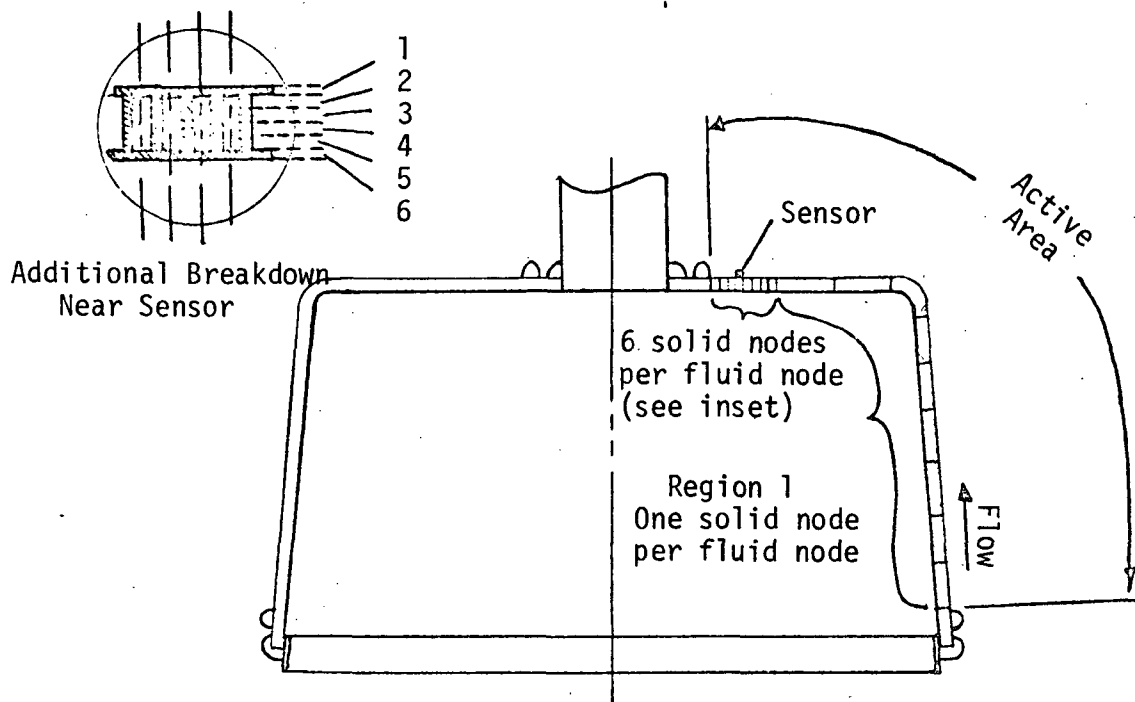


FIGURE 15 EVAPORATOR NODAL MODEL

The evaporant spray distribution was extracted from the feasibility test results. The increase in heat load, hence flow rate, in the present design results in a small change in the spray angles according to manufacturer's data. Accounting for this effect, the spray distribution has been estimated as

shown in Figure 16 for water and Freon

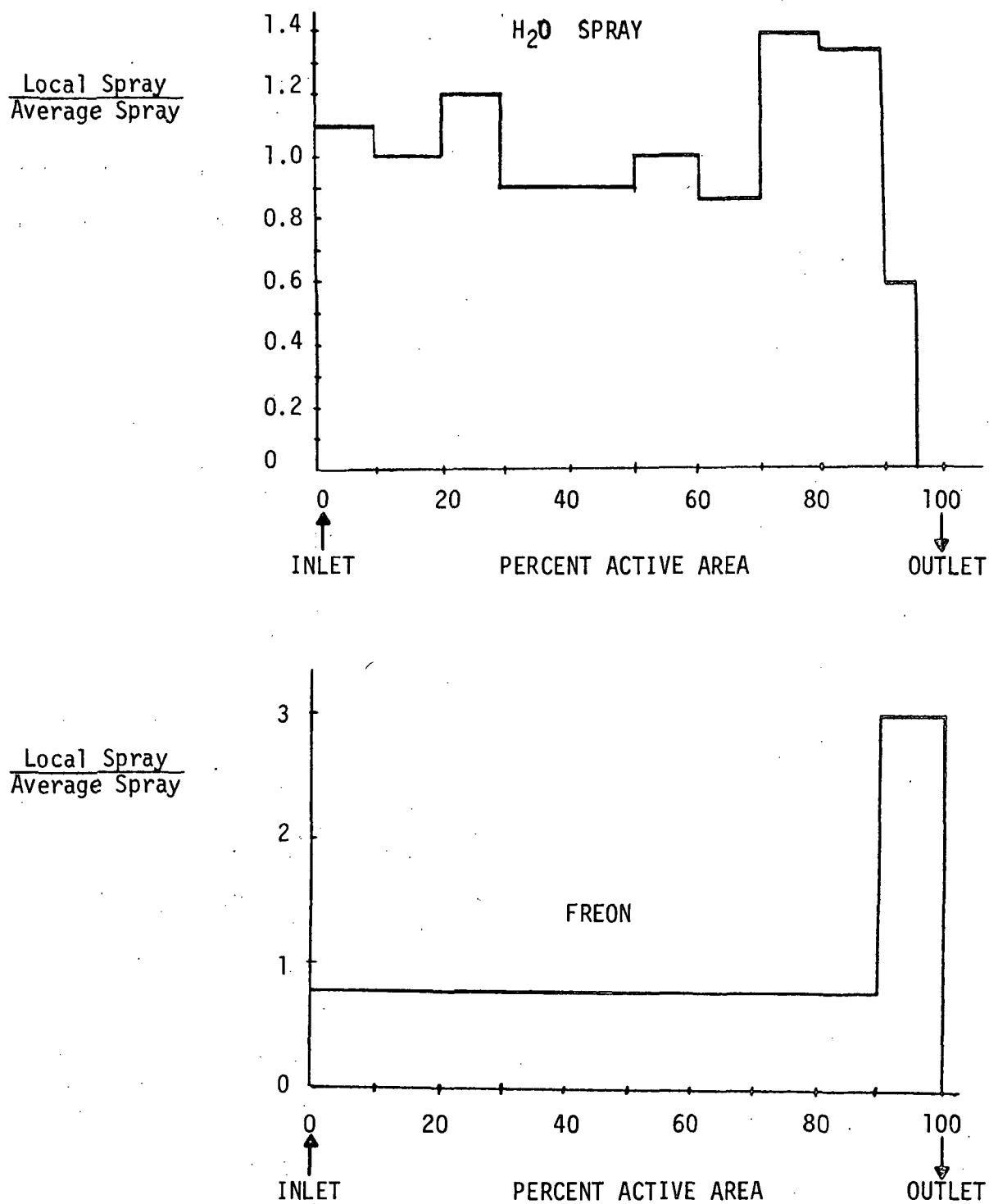


FIGURE 16 DISTRIBUTION OF EVAPORANT SPRAY



The resulting surface and fluid temperature distribution in the vicinity of the vapor and fluid outlet at steady state full load conditions is shown in Figure 17.

The Freon spray distribution is much more dense in the vicinity of the exit so that the corresponding temperature gradient in Figure 17 is much higher. This causes the surface temperatures to cross each other at a reasonably well defined location. The wall temperature with Freon spray is depressed significantly below the fluid while with water it is not. This causes the control cycle to be different as explained in a later paragraph. The steady state map can be used to locate the sensor for nearly full load operation. At the steady condition, locating the sensor at positions near the fluid outlet results in the achievement of the "off" temperature, even though the fluid outlet is at or above the desired level. Thus, with a 39°F (3.8°C) sensor "off" temperature, the sensor must be located at a radius greater than a determinable amount. A similar situation exists for the nearly full load operation and the "off" sensor temperature. That is if all temperatures are reduced by 10°F in Figure 17 the sensor must turn the spray off to avoid an under-temperature condition. Simple relations may be written for these two limits. Define  $T(r)$  as the temperature of a sensor mounted at position  $r$ . This sensor controls the spray such that  $T > T_{\text{"on"}}$  initiates spraying which continues until  $T < T_{\text{"off"}}$ . Assume  $T_{\text{"on"}} = 42.5^\circ\text{F}$  ( $5.8^\circ\text{C}$ ) and  $T_{\text{"off"}} = 39^\circ\text{F}$  ( $3.8^\circ\text{C}$ ).  $T_{\text{max}}$  and  $T_{\text{min}}$  define the control band upper and lower limits, respectively of 45 and 35°F.  $T_{\text{out}} - T(r)$  must not exceed  $T_{\text{max}} - T_{\text{"off"}}$  or the device would turn off without achieving the required outlet temperature band.

$$T_{\text{out}} - T(r) < T_{\text{max}} - T_{\text{"off"}} = 45 - 39 = 6^\circ\text{F}$$

Reference to Figure 17 shows that this is satisfied for both evaporants if  $r > 5.0$  inches. Similarly, another inequality may be derived from the condition that the device must turn off before the outlet drops below the minimum allowed temperature.

$$T(r) - T_{\text{out}} < T_{\text{off}} - T_{\text{min}} = 39 - 35 = 4^\circ\text{F}$$

This condition is satisfied at positions  $r < 5.75$  inches. These conditions then require  $5.0 < r_{\text{sensor}} < 5.75$  if one sensor is to control both evaporants.

This condition is necessary, but not sufficient. It is anticipated that the inequalities must be satisfied with some margin if the transient behavior is to be satisfactory. Also shown on Figure 17 are the upstream and downstream positions for the sensor with water operation. The downstream Freon position conflicts with the manifold and is not included.

Results of computer analysis to determine sensor lag effects were obtained for both the upstream and downstream positions of the sensor. The control points were 42.5 F (5.8c) switch-on temperature and 39F (3.9c) switch-off temperature. Figure 18 shows the effect of probe response on the outlet temperature at low (5 percent of full) load operation with both the upstream and downstream sensor position. The transport fluid flow rate for these runs

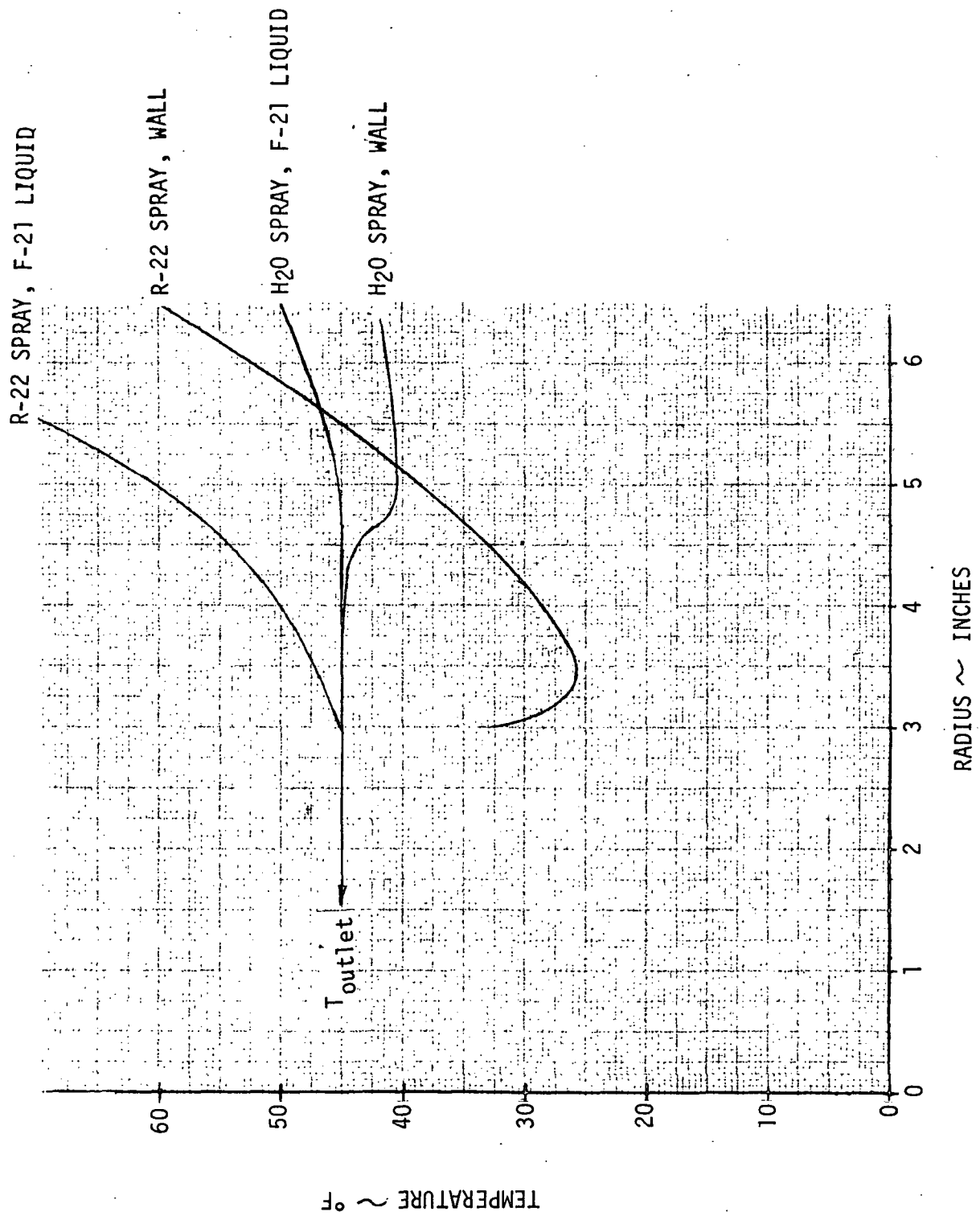


FIGURE 17 TEMPERATURES OF FLUID AND WALL NEAR THE EXHAUST PORT

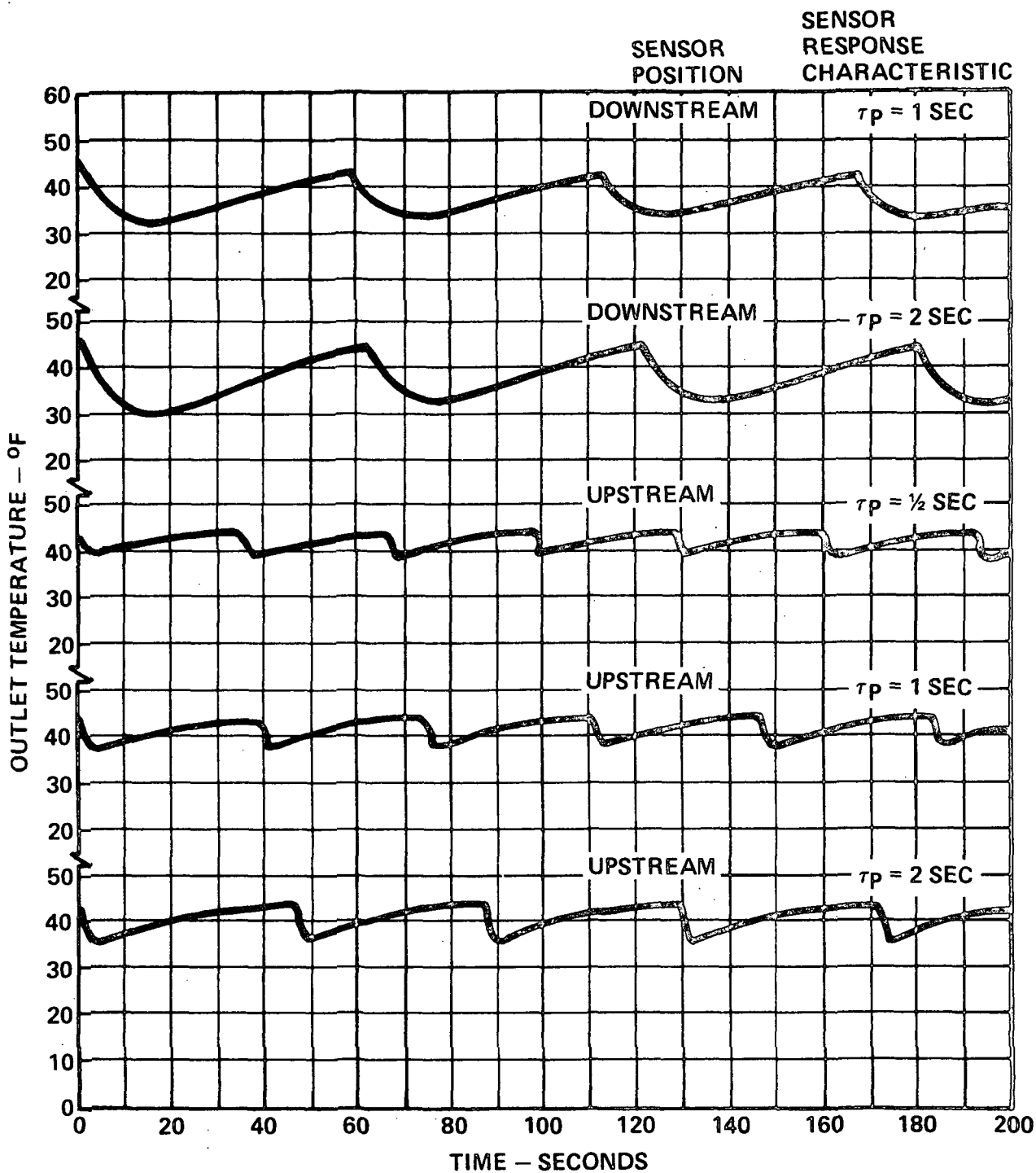


FIGURE 18 EFFECT OF PROBE RESPONSE ON OUTLET TEMPERATURE

was 90 percent of the nominal rate, at which the temperature overshoot tendency is greatest. Similar results are obtained at near maximum load for the device, while moderate loads are more tolerant of probe lag. From this result, it was deemed desirable to employ a sensor with less than one second characteristic response time. It is also obvious that the downstream sensor position allows a greater temperature excursion.

The effect of heat load on the outlet temperature is predicted in Figure 19 with nominal transport fluid flow rate. At low heat loads, a quick cooling pulse, which causes spray cutoff, is followed by a longer warmup time to spray initiation. The rise and fall rates are similar at midload range which produces the shortest cycling time and least temperature excursion. Near maximum load, the cooling pulse lengthens while the heating phase decreases in length. There is a load-sensitive shift in the average outlet temperature with the downstream sensor location which is negligible with the upstream position. The shift is in the direction of the highest temperature change rate and is due to the lag of the wall temperature behind the fluid temperature. In addition to the mean temperature shift, the maximum-to-minimum temperature excursion varies with the load and is greater for the downstream sensor position. For this reason, the upstream position is favored.

The following section describes an approximate analytical solution for the transient temperature of the evaporator wall and transport fluid. The analysis depends on assumptions that both the local wall and fluid may be characterized by mean temperatures, that the heat transfer between wall and fluid is characterized by a time-invariant conductance, that the thermal mass of fluid and wall are invariant, and that the heat absorbed from the wall occurs in square wave pulses of constant magnitude over the entire cooled region. The differential equations for the evaporator wall and fluid are:

$$w_f c_f \frac{\partial T_f}{\partial t} + \dot{w} c_f \frac{\partial T_f}{\partial x} = -U (T_f - T_w) + \text{conduction terms} \quad (1)$$

$$w_w c_w \frac{\partial T_w}{\partial t} = U (T_w - T_f) - Q \cdot l(t) + \text{conduction terms} \quad (2)$$

The symbol,  $l(t)$ , implies a cyclic step function of value 0 and 1. Only cyclical situations representing steady-state evaporator heat loading will be investigated herein, in which case both the fluid and wall temperatures assume solutions of the form

$$T_w(x, t) = X(x) + \Delta T \cdot W(t) \quad (3)$$

$$T_f(x, t) = X(x) + \Delta T \cdot F(t) \quad (4)$$

In particular,  $dX/dx = \text{constant}$  is implied, a characteristic which is forced to occur by the cyclic cooling and is aided by conduction effects. Whenever the load transients wane and equations (3) and (4) emerge as solutions,

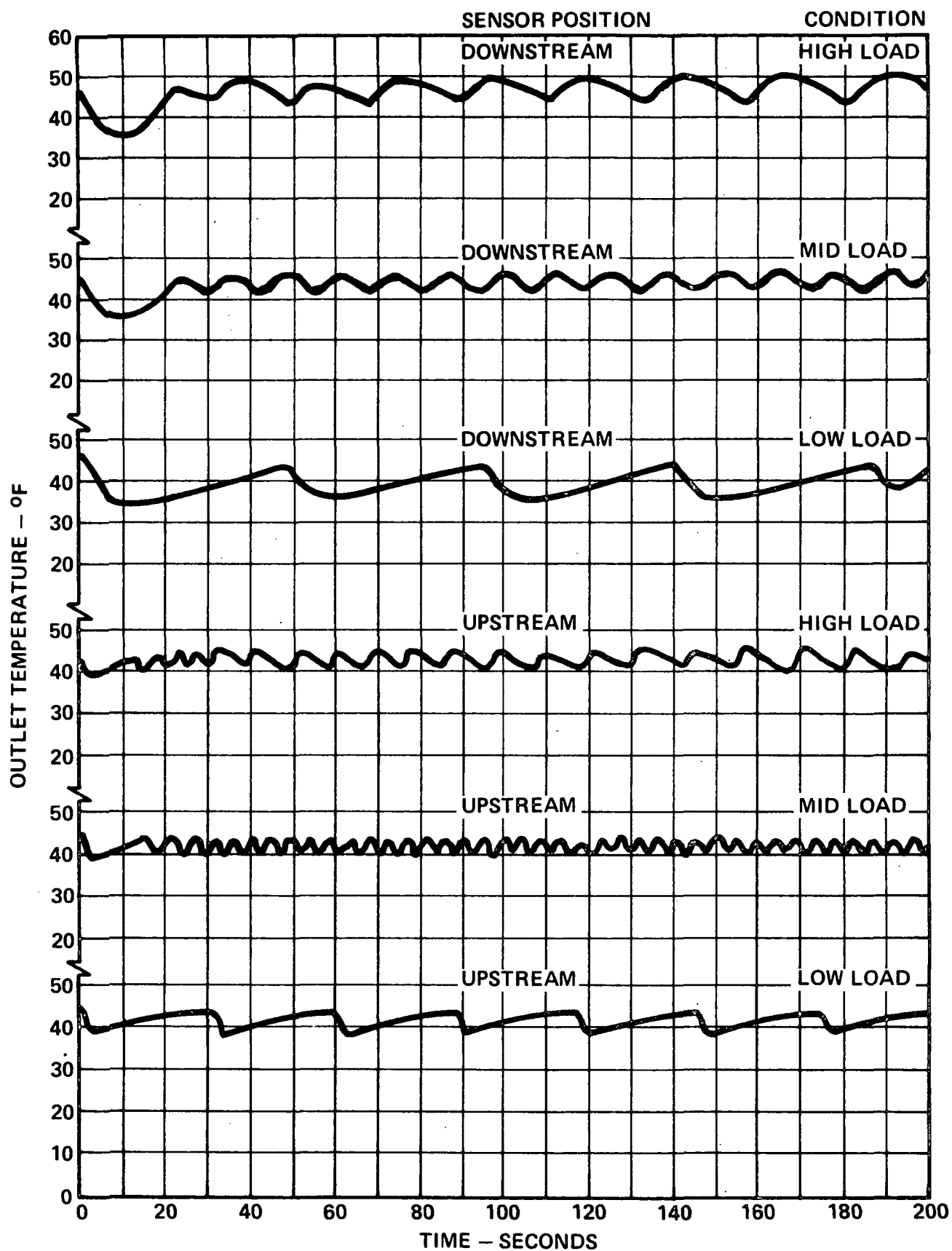


FIGURE 19 EFFECT OF HEAT LOAD ON OUTLET TEMPERATURE

the conduction terms in equations (1) and (2) tend to zero. At true steady state, equations (1) and (2) combine to yield

$$\dot{w}c_f \frac{\partial T_f}{\partial x} = \dot{Q}$$

The value of  $\partial T_f / \partial x$  must be proportional to the load  $L$ , so

$$\dot{w}c_f \frac{\partial T_f}{\partial x} = \dot{Q}L \quad (5)$$

Equations (1) and (2), incorporating equations (3), (4), and (5), and using the definitions

$$\tau_w = \frac{w_w c_w}{\dot{U}}$$

$$\tau_f = \frac{w_f c_f}{\dot{U}}$$

$$\tau_s = \frac{\tau_f \tau_w}{\tau_f + \tau_w}$$

$$\theta = t / \tau_s$$

$$\Delta T = \dot{Q} / \dot{U}$$

produce the following equations

$$\frac{\tau_f}{\tau_s} \frac{dF}{d\theta} - L + F - W = 0$$

$$\frac{\tau_w}{\tau_s} \frac{dW}{d\theta} - F + W = -1(\theta)$$

This set of equations may be solved by any of several existing techniques. The solution of the equation during phase 1 has the cooling active [ $l(\theta) = 1$ ] from  $\theta = 0$  to  $\theta = \theta_1$ , and during phase 2 is not cooled [ $l(\theta) = 0$ ] from  $\theta = \theta_1$ , to  $\theta = \theta_2$ . These solutions are:

$$F_1 = a_1 \exp(-\theta_1) + [L-1] \left[ \frac{\tau_s}{\tau_f + \tau_w} \right] \theta + c_1 \quad 0 \leq \theta \leq \theta_1$$

$$W_1 = a_1 \frac{\tau_f}{\tau_w} \exp(-\theta_1) + [L-1] \left[ \frac{\tau_s}{\tau_f + \tau_w} \right] \left[ \theta + \frac{\tau_f}{\tau_s} \right] + c_1 - L$$

$$F_2 = a_2 \exp(-(\theta - \theta_1)) + L \left[ \frac{\tau_s}{\tau_f + \tau_w} \right] (\theta - \theta_1) + c_2$$

$$\theta_1 \leq \theta \leq \theta_2$$

$$W_2 = -a_2 \frac{\tau_f}{\tau_w} \exp(-(\theta - \theta_1)) + L \left[ \frac{\tau_s}{\tau_f + \tau_w} \right] \left[ \theta - \theta_1 + \frac{\tau_f}{\tau_s} \right] + c_2 - L$$

The relationship between  $a_1$ ,  $a_2$ ,  $c_1$ ,  $c_2$ ,  $\theta_1$ , and  $\theta_2$  may be determined from continuity,  $F_2(\theta_2) = F_1(0)$ ,  $F_1(\theta_1) = F_2(\theta_1)$ ,  $W_2(\theta_2) = W_1(0)$ , and  $W_1(\theta_1) = W_2(\theta_1)$ . These relations are:

$$\theta_1 = L\theta_2$$

$$a_1 = - \frac{\tau_f \tau_w}{(\tau_f + \tau_w)^2} \frac{1 - \exp[-\theta_2(1-L)]}{1 - \exp[-\theta_2]}$$

$$a_2 = a_1 \exp[-L\theta_2] + \frac{\tau_f \tau_w}{(\tau_f + \tau_w)^2}$$

$$c_2 = c_1 + a_1 \exp[-L\theta_2] + (L-1) \left[ \frac{\tau_f \tau_w}{(\tau_f + \tau_w)^2} \right] \theta_1 - a_2$$

The constant,  $c_1$ , is an arbitrary constant added to each solution, and the value of  $\theta_2$  is related to the magnitude of the temperature excursion during the cycle. In the case of present interest, when the wall temperature undergoes a temperature excursion,  $W_1(0) - W_1(\theta_1)$ , equivalent to a fixed control dead band, the value of  $\theta_2$  may be evaluated. In general, plots of  $W_1(0) - W_1(\theta_1)$  may be obtained versus  $\theta_2$  with parameter,  $L$ . This plot is dependent on the ratio,  $\tau_f/\tau_w$ , also, which, for the evaporator, has a value of 0.73. From such a plot, the anticipated dead band of the controller may be used to determine the value of  $\theta_2$  corresponding to each value of  $L$ . For the present case, with  $W_1(0) - W_1(\theta_1) = 0.48$ , the solutions for the fluid temperature ( $F$ ) have been generated. The value of  $W_1(0)$  is fixed by adjusting  $c_1$  for each value of  $L$ . The fluid outlet temperature may be projected from the fluid temperature at the sensor by the equation.

$$F_{\text{outlet}} = F_{\text{sensor}} - A \cdot L$$

The value of A has been selected by forcing  $[W_1(0)+W_1(\theta_1)]/2$  to equal

$$\int_0^{\theta_2} F(\theta) d\theta$$

at  $L = 0.5$ . The solution for the fluid outlet temperature for several load values is shown in Figure 20. In all cases, the fluid temperature excursion is within the dead band, and there is a small load-sensitive mean temperature shift as indicated in the following table.

LOAD	$\int_0^{\theta_2} F d\theta$	$F_{\max} - F_{\min}$
.05	-.180	0.3
.25	-.212	0.205
.50	-.245	0.182
.75	-.272	0.208
.95	-.293	0.286

For reference purposes, these values may be multiplied by  $\Delta T (\approx 10)$  for application to the actual evaporator test article.

The foregoing analysis is not applicable to a sensor positioned downstream of the cooled section, and does not account for the lag effect of the sensor. Simple extensions using the same solutions for fluid and wall temperature are available for these cases. In the sensor lag effect analysis, a third differential equation must be added which is first order and not coupled to the other equations. Most of the effort is computational in producing each of these solutions and is not presented here.

### 3.6.2 Predictor - Corrector Control

A second control scheme is based on a predictor-corrector technique wherein the duty cycle is estimated based on the inlet temperature and corrected based on outlet temperature. For nominal conditions, the inlet temperature to set point difference is proportional to the duty cycle required, i.e., the fraction of  $\phi$  is given by

$$\phi = \frac{T_{in} - T_{set}}{T_{max} - T_{set}} \quad (6)$$



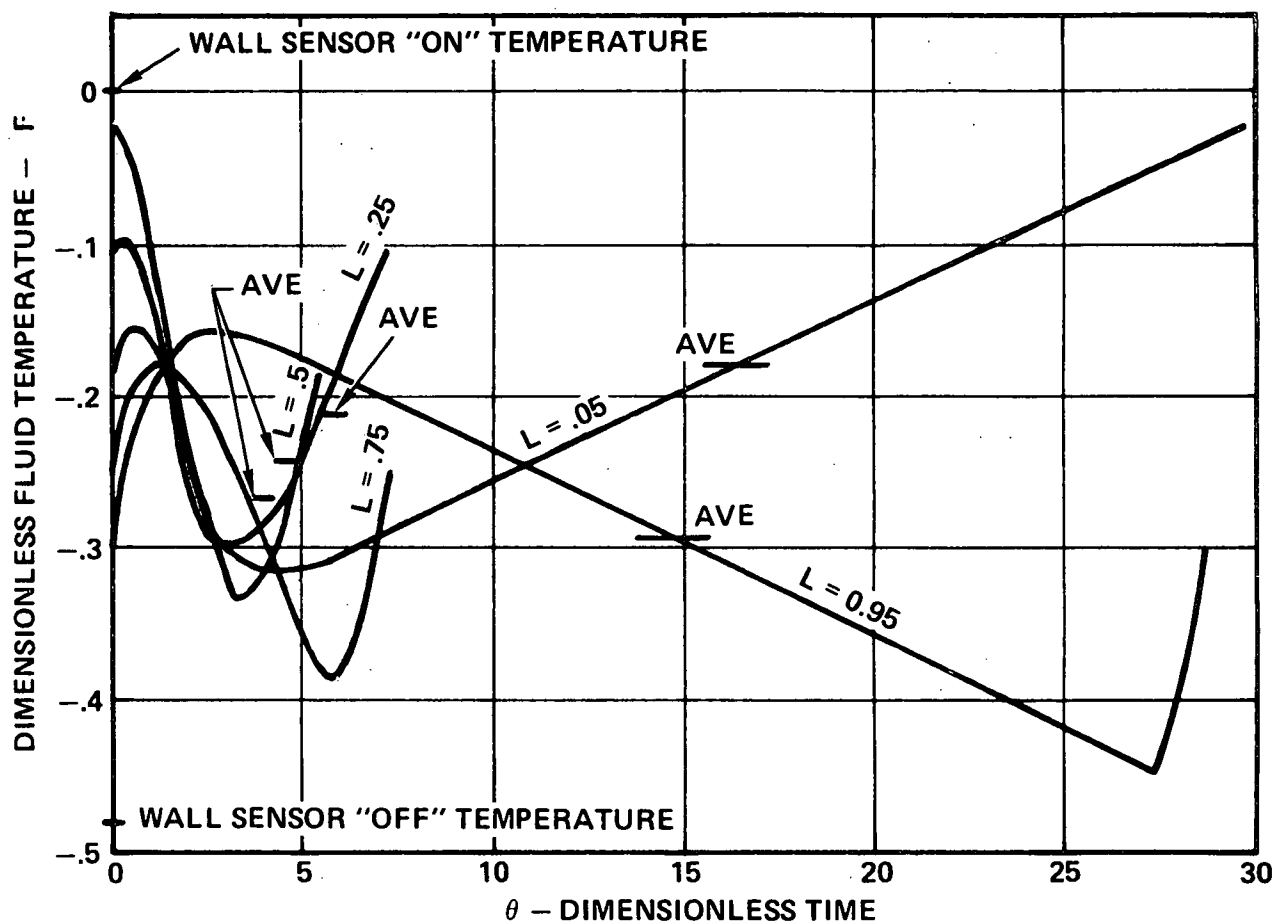


FIGURE 20 FLUID OUTLET TEMPERATURE PREDICTED FROM ANALYTICAL MODEL

Here  $T_{\max} = 150^{\circ}\text{F}$  and  $T_{\text{set}} = 40^{\circ}\text{F}$  yield a nominal 50,000 BTU/hr heat rejection with an R-21 flow rate of 1850 lb/hr. There is a lag between the sensor and device outlet caused by the time required to flow from one point to the other. The last cooled location in the evaporator is assumed to be removed a time  $\tau_u$  from the inlet temperature sensor. The inlet temperature signal may be delayed (electronically or thermally) from the actual fluid temperature according to the characteristic of the following differential equation

$$\frac{dT_{\text{signal}}}{dt} = -\frac{1}{\tau_s} (T_{\text{signal}} - T_{\text{in}} + T_{\text{set}})$$

This equation has the solution

$$T_{\text{signal}} = e^{-t/\tau_s} \frac{1}{\tau_s} \int_{-\infty}^t (T_{\text{in}} - T_{\text{set}}) e^{t'/\tau_s} dt' \quad (7)$$

The evaporator yields an outlet temperature which is according to

$$T_{\text{out}}(t) = T_{\text{in}}(t - \tau_u) - \phi \Delta T \quad (8)$$

Integrating equation (7) for a linear inlet temperature ramp yields

$$T_{\text{in}} = \begin{cases} T_{\text{set}} & t < 0 \\ T_{\text{set}} + mt' & t > 0 \end{cases}$$

$$T_{\text{signal}} = e^{-t/\tau_s} \left[ m\tau_s e^{t/\tau_s} \left( \frac{t}{\tau_s} - 1 \right) + m\tau_s \right]$$

$$T_{\text{signal}} = m\tau_s \left( \frac{t}{\tau_s} - 1 \right) + m\tau_s e^{-t/\tau_s}$$

$$\phi = \frac{m(t - \tau_s) + m\tau_s e^{-t/\tau_s}}{\Delta T}$$

And thus the outlet temperature predicted from (8) is

$$\left. \begin{aligned} T_{\text{out}}(t) &= T_{\text{set}} - \left[ m(t - \tau_s) + m\tau_s e^{-t/\tau_s} \right] & t < \tau_u \\ T_{\text{out}}(t) &= T_{\text{set}} + m(t - \tau_u) - \left[ m(t - \tau_s) + m\tau_s e^{-t/\tau_s} \right] & t \geq \tau_u \end{aligned} \right\} \quad (9)$$

There is a tendency for the value of  $T_{out}$  to stray from the intended value ( $T_{set}$ ) during transients as indicated in equation (9). The use of  $\tau_s = \tau_u$  produces a maximum deviation at  $t = \tau_u$  of  $T_{out} - T_{set} \max = m\tau_u e^{-1}$ . The evaporator most severe ramp is anticipated to be  $0.5^\circ\text{F}/\text{sec}$  and the time constant  $\tau_u$  is expected to be approximately 20 seconds, so that the maximum deviation should be less than  $4^\circ\text{F}$ , for the predictor portion of the control system.

In addition to the predictor type function, it is desired to provide a corrector function. This corrector is designed to compensate for (1) variations in transport fluid flow rate, (2) variations in evaporant flow rate and enthalpy, (3) non-linearity in the predictor phase electronics, and (4) some correction for the error induced by the lag during transients. This corrector function modifies equation (6) as follows:

$$\phi = \frac{T_{\text{signal}} - T_{\text{set}}}{T_{\text{max}} - T_{\text{set}}} + A(t),$$

where A results from

$$\frac{dA}{dt} = R(T_{out} - T_{set}) \quad A_{\min} \leq A \leq A_{\max}$$

The corrector phase must be examined for its tendency to be unstable, a condition induced by lag of the outlet temperature measurement and the magnitude of the value R. The stability criteria may be derived independent of the predictor function. The outlet temperature responds following a corrector-induced duty cycle change as follows

$$T_{out}(t) = T' (t - \tau_d)$$

This accounts for the lag ( $\tau_d$ ) between the last cooled point (designated prime) and the outlet sensor. The effect of the corrector function (A) on the duty cycle  $\phi$  is

$$\frac{d\phi}{dA} = 1$$

The outlet temperature effect due to the corrector function is

$$\frac{dT'}{dF} = -\Delta T$$

Combining the above equations yields

$$\frac{dT'}{dt} = -R \Delta T [T'(t - \tau_d) - T_{set}] \quad (10)$$

During any given time interval ( $\tau_d$ ) the right hand side is a known function which generates  $T'$  for the ensuing time interval. The situation is stable whenever the effect of an initial perturbation is not amplified.

Equation (10) may be transformed using the following changes

$$\Omega = T' - T_{\text{set}}$$

$$t/\tau_d = \theta$$

$$R\Delta T\tau_d = a$$

There results

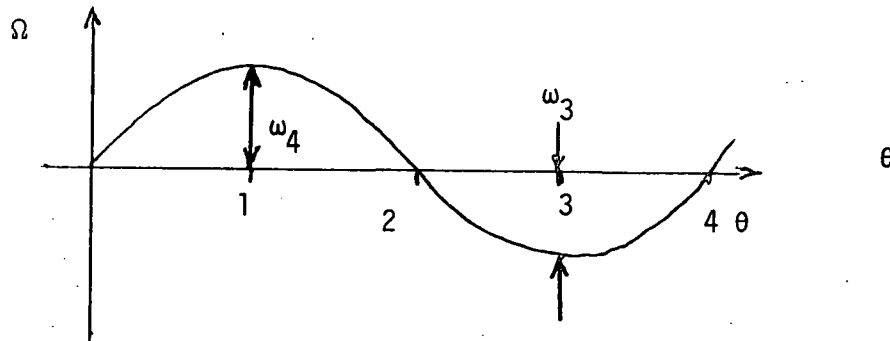
$$\frac{d\Omega}{d\theta} = -a\Omega(\theta-1) \quad (11)$$

For the case where  $\Omega=b$  for  $-1 < \theta < 0$ , the solution to equation (11) is

$$\Omega = b \left\{ 1 - a\theta + \frac{a^2(\theta-1)^2}{2!} + \dots + \frac{(-a)^{n+1}(\theta-n)^{n+1}}{(n+1)!} \right\} \quad (12)$$

for  $n < \theta < n+1$ .

This solution yields the response of the outlet temperature excursion which results from a perturbation of magnitude  $b$ . Figure 21 shows the early response of  $\Omega$  for three values of the parameter  $a$ . It is apparent that for  $a = 1/2$  or  $1$  that the perturbation is damped while for  $a = 2$  it is amplified, so that  $a \approx 1$  represents a stability limit for the corrector. It should be obvious that convergence is necessary but not sufficient for a system having a continued finite perturbation. An additional criteria is that the amplitudes of successive cycles must be monotonically diminishing with increasing  $\theta$ . Particularly this should be strengthened since the representation shown here does not include the cyclic temperature perturbations resulting from the predictor-required pulsing. This latter cyclic perturbation can conceivably tend to excite the corrector activity in a type of resonant manner. It is apparent that the "natural frequency" of the system has a period of 4 (i.e.  $4 \tau_d$ ) as sketched below.



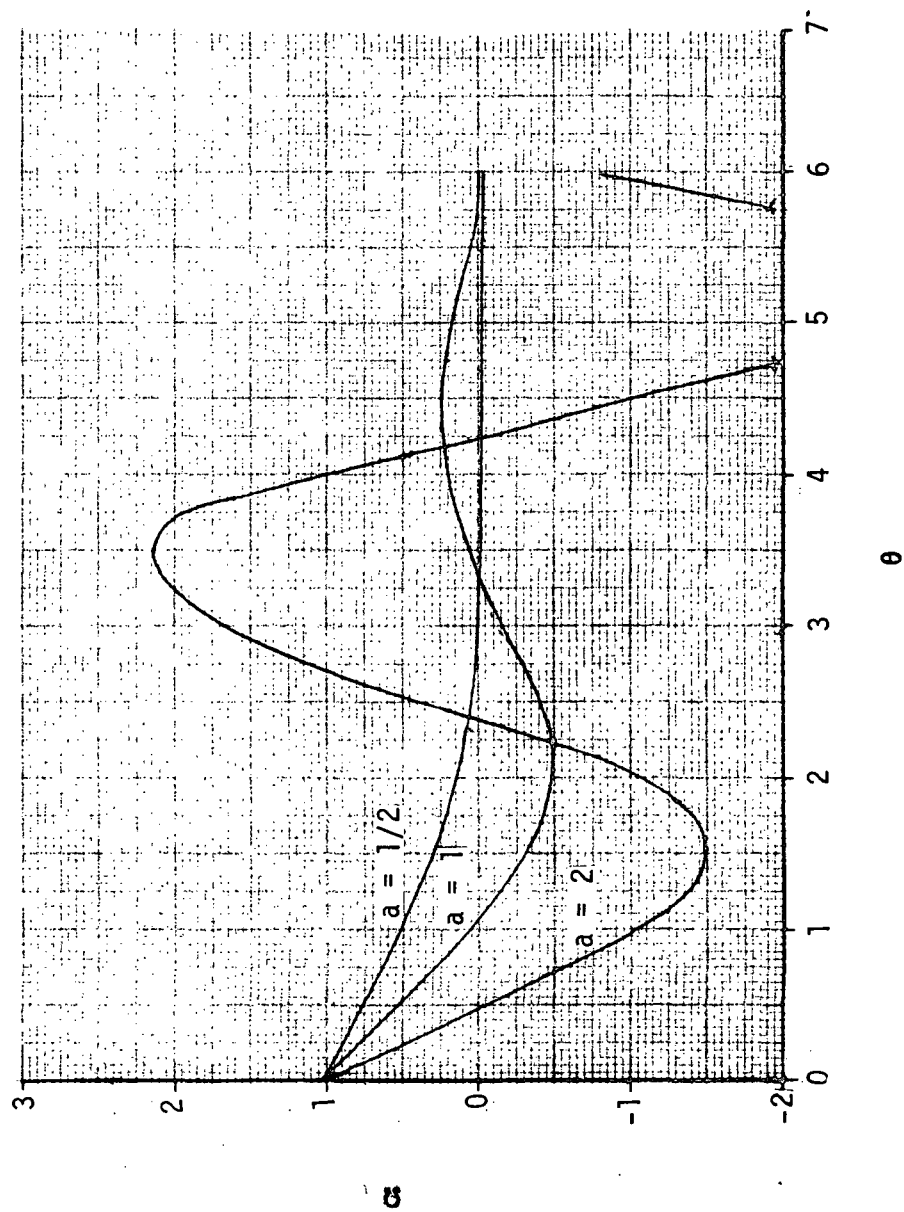


FIGURE 21 RESPONSE OF  $\Omega$  FOR VARIOUS PARAMETERS

No other choice of period can satisfy the differential equation (11) and be even approximately repetitive. Integrating equation (11) from  $\theta = 1$  to 2 and from 2 to 3 and combining yields

$$\Omega - \Omega \Big|_2 = a^2 \int_0^{\theta} \int_0^{\theta^2} \Omega d\theta d\theta,$$

and in particular,

$$\omega_3 = a^2 \int_0^1 \int_0^1 \Omega d\theta d\theta$$

If  $\omega_3 \leq \Omega_{\max}$  over  $(0,1)$  the convergence is insured for the cyclic type of function considered. This leads to

$$a \leq \sqrt{\frac{2}{2}}$$

Practically speaking, the value of  $(a)$  could be higher and achieve convergences, but for certain perturbations, the value may be required to be smaller to eliminate both the function and the perturbation. The value of  $a \approx 0.7$  should lead to stability with confidence. Using  $a = 0.7$  leads to a value of  $R$  of

$$R = \frac{0.7}{\Delta T \tau_d}$$

The value of the maximum correction  $(A)$  must be somewhat aided by judgement, but should be at least as large as

$$B = \frac{1}{100} \left\{ \sum E_i \right\}$$

The  $E_i$ 's indicated here are the predictor errors for which the corrector must compensate in percentages. These include percent error in (1) transport fluid flow, (2) evaporant flow, (3) non-linearity in specific heat of transport fluid, (4) non-linearity in inlet temperature measurement, and (5) variation in evaporant enthalpy. It is anticipated that  $A_{\max}$  will approximate 30 percent so that

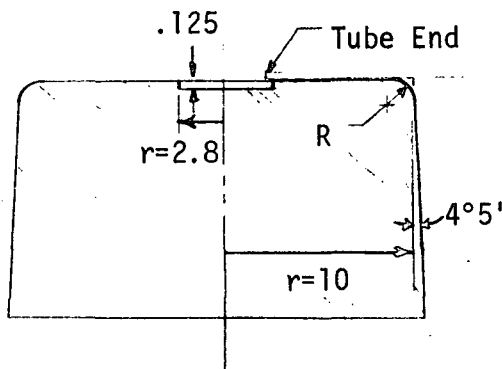
$$F = \frac{T_{\text{signal}} - T_{\text{set}}}{T_{\text{max}} - T_{\text{set}}} + A(t)$$

$$\frac{dA}{dt} = \frac{0.7}{\tau_d} \frac{T_{\text{out}} - T_{\text{set}}}{T_{\text{max}} - T_{\text{set}}}$$

$$|A| < A_{\max} \approx 0.3$$

#### 4.0 EVAPORATOR FABRICATION

The evaporator shell design of multiparallel flow within rectangular tubes brazed together into a unit was introduced in Section 3.3. A VMSC sponsored program was initiated to determine whether a group of tubes could be wound side-by-side representing the first unit described herein. The general fabrication technique followed the sequence of steps outlined with refinements added in three attempts. First a male mandrel was built of wood to the desired contour. The center of the face was recessed as shown in the sketch below.



The 0.120"x 0.36"O.D. rectangular tubes were precleaned to remove grease and oxide. The starting end of each tube was welded closed. A starter plate was formed, to which the end of each tube was welded at an angle such that the tubes were initially positioned for windup. The tubes were then formed simultaneously to lie adjacent to each other and contact the mandrel. As the shoulder position was reached, each tube acquired an increasing twist so that the short side of the tube always contacted the mandrel surface. Tack welds were used progressively to hold the tubes together during the wind-up process. Photographs of the work in progress are shown in Figures 22 and 23. The ends of the tube were allowed to extend past the assembly as vent tubes for air during brazing which was performed in a salt bath. The finished tube wound assembly is shown in Figure 24. To this assembly a skirt piece was tacked in preparation for the skirt manifold junction. The skirt sheet overlapped about four tubes and extended a little over an inch.

Preparation for brazing involved cleaning of the assembly and attachment of brazing filler. For dip brazing the use of filler in wire form was selected over sheet and flux/powdered filler slurry. This selection was made primarily upon experience of personnel associated with the braze operation. The use of mechanically attached filler often leads to loss of material to the convection currents in the flux bath. The weld tack sites used during assembly were used to attach eutectic braze alloy wire by welding. Filler wire .032 inch diameter was tacked on 3 to 5 inch spans at approximately .375 inch spacing over the cylindrical and shoulder portions of the assembly as shown in Figure 25. A group of wires was formed into rings and spokes, and was laid into the bottom of the basket. The unit was again cleaned and

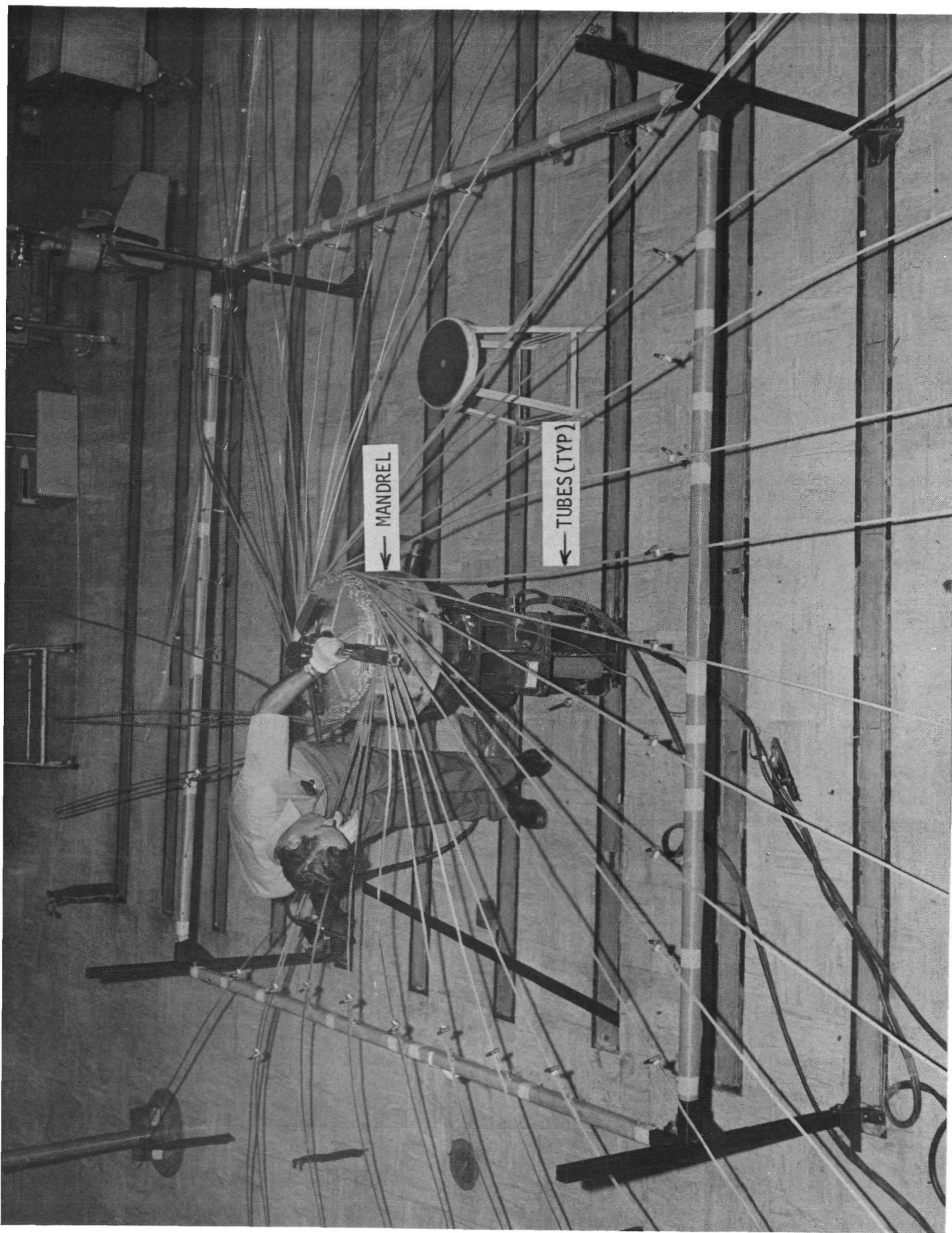


FIGURE 22 EVAPORATOR FABRICATION



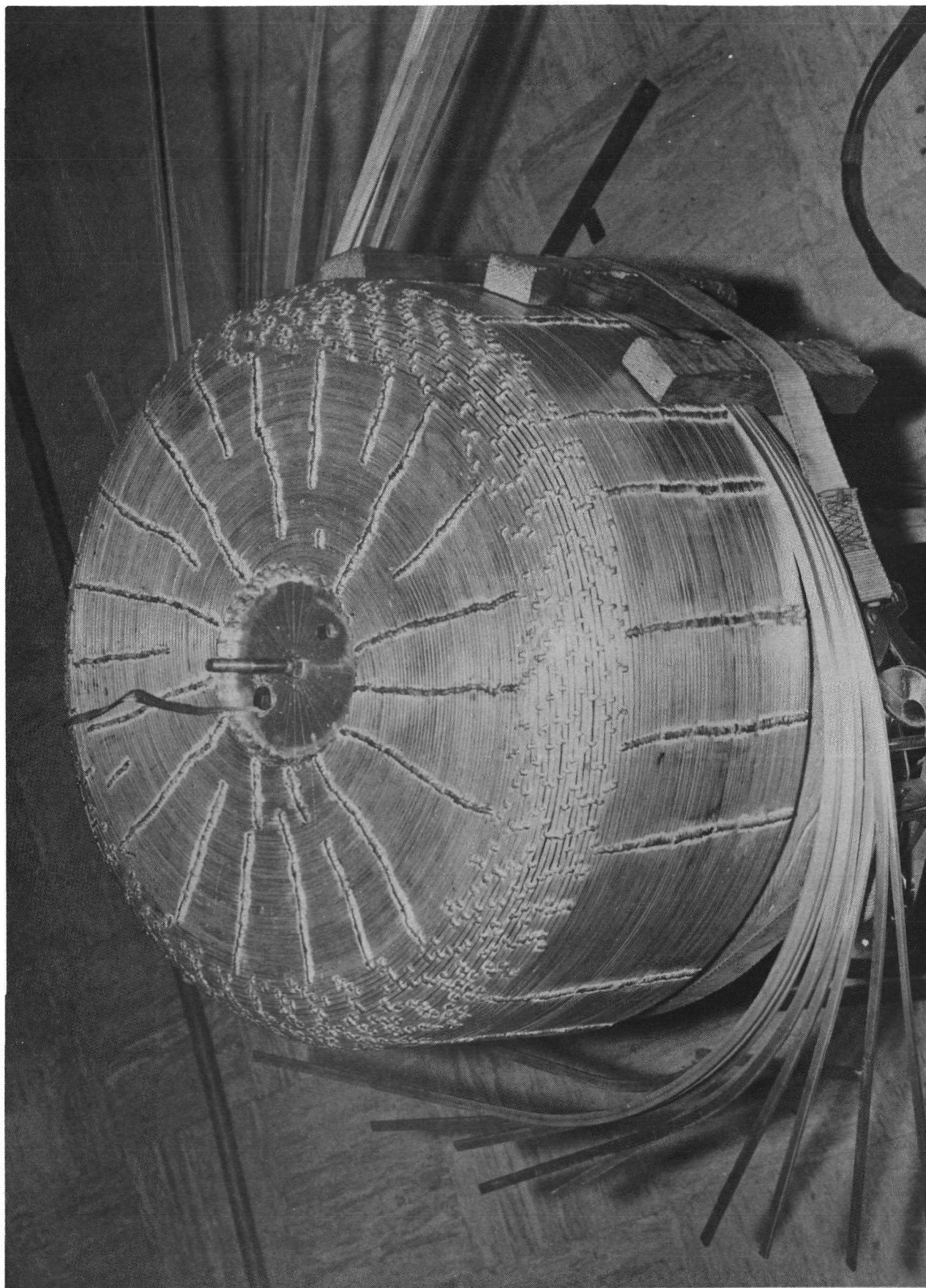


FIGURE 23 EVAPORATOR FABRICATION

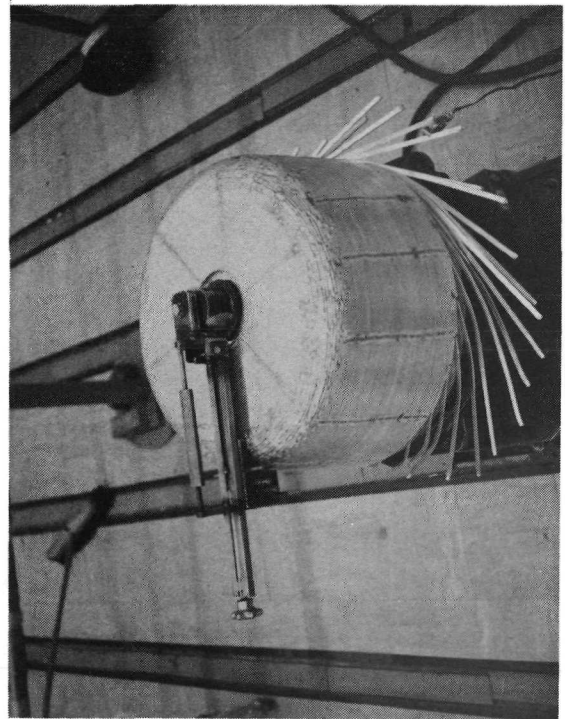
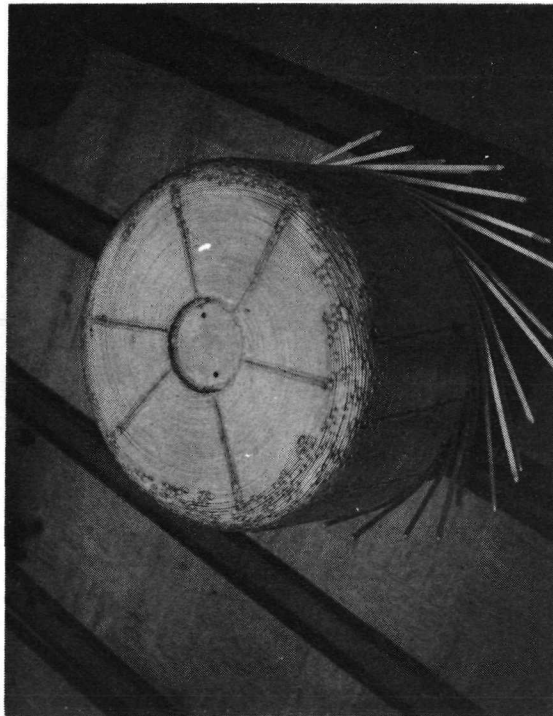
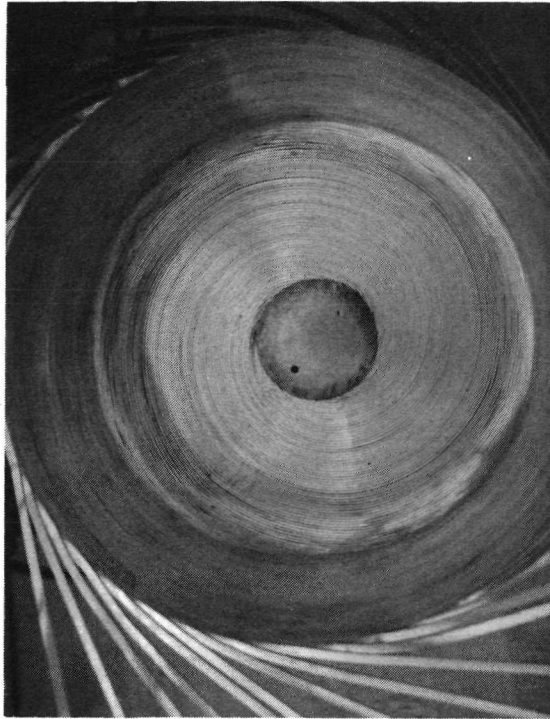


FIGURE 24 FINISHED TUBE WOUND ASSEMBLY



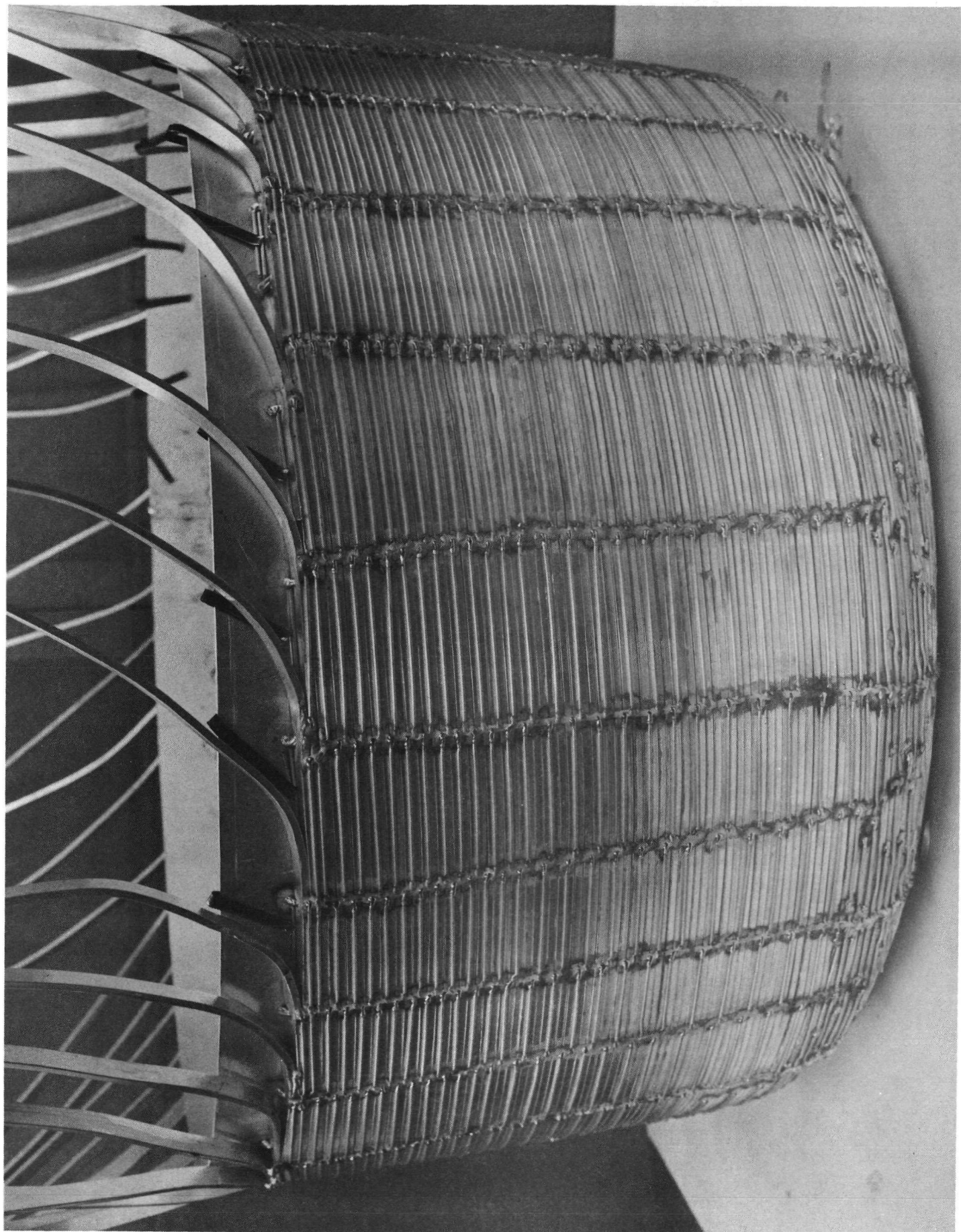


FIGURE 25 EVAPORATOR WITH BRAZE WIRE ATTACHED

a flux/filler powder slurry added to the tacked regions. The unit was preheated to 1000°F for 20 minutes and then dipped into the brazing salt bath at 1100°F for approximately one minute. After removal from the bath it was allowed to cool in air for several minutes and was then introduced to a vat of boiling water. Post cleaning to remove the smut and about four hours exposure to boiling water removed the residual flux.

The integral manifolds were formed on the face end by machining from stock. On the skirt end, tubing was rolled to slightly oversized diameter, welded to form a hoop, and cut on a band saw to remove the inside of the hoop. The manifolds were then cut and fit to the basket. Tube ends and side walls were alternately opened to allow flow into the appropriate manifold. A flow check was run on each tube to preclude flow blockage. The ends of all tubes at the skirt were cut off and alternate tubes were blocked at the end and opened under the secondary manifold position. Manifolds were attached by welding. (See Figure 12)

The aft cone and nozzle plate were formed in a comparatively straightforward manner. Tubing was rolled to a spiral helix and tack welded to a preformed cone. The helix was formed by controlling manually the radius of bend as the winding progressed and manually pulling the wound portion away from the rolling plane. The soft aluminum used could readily be hand forced to a reasonable displacement during assembly. This back cone was also dip brazed. The nozzle plate was formed of two plates diffusion bonded together. One of the plates was milled to form a passage through which a warm fluid could be diverted in the assembled article.

#### 4.1 Fabrication of First Unit

The initial fabrication was unsuccessful due to penetration of salt through the tube wall and longitudinal failure of two tubes. The penetration of salt occurred when an area of the normal tube had been welded using a lower melting point alloy. The eutectic alloy positioning onto the tack welds was preferred so that the crater of eutectic-filled material would not penetrate the entire wall. In some instances, however, the wire was melted short of the weld area and was carelessly welded to the tube. The crater thus formed melted in the braze pot allowing flux penetration. Also the rod used to perform tack welding was of an alloy having a solidus temperature below 1100°F so that the original tack welds could also have been penetrated. This fact was only realized after brazing of the second unit since the tacks were first ground off and then replaced on the first unit. The longitudinal splitting of the tube observed in two tubes results from the extrusion of the tube wherein the material must part and reform in the extrusion die. Contamination and slight temperature variations during the extrusion lead to a fault in the direction of the extrusion which can subsequently fail. Tests to eliminate bad tubes were applied on the following articles. These tests included die penetrant (ZYGL0) and pressurization to 0.66 yield point, neither of which disclosed faults. Also used was a simple wedge test where a tapered drill rod was driven into the tube end producing a failure in weakly joined tubes (see Figure 26). The first unit was scrapped due to the tube splitting.

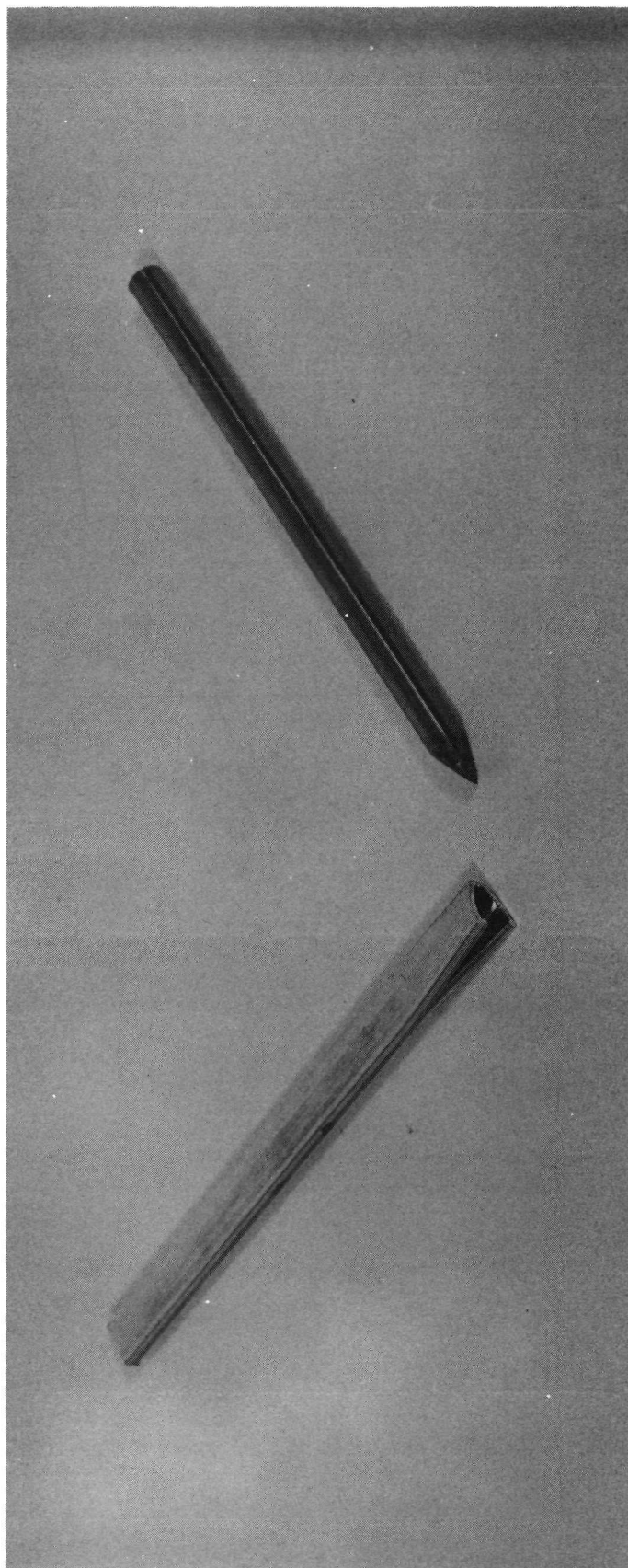
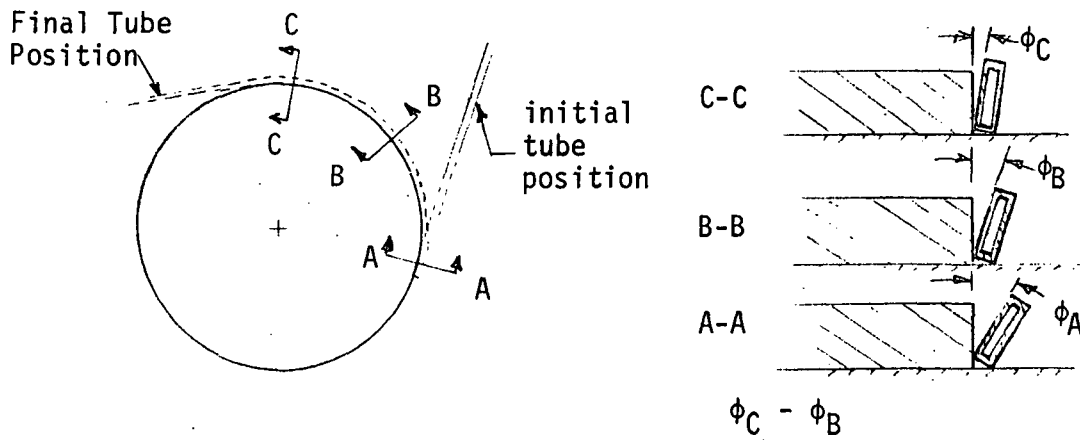


FIGURE 26 FATLED TUBE AND WEDGE

## 4.2 Fabrication of Second Unit

The second unit was fabricated like the first with several differences. Based on the first unit, some tooling was fabricated in the form of individual tensioners on each tube, a rotating foundation for the mandrel, and a tool which fit the external shape of the evaporator on the shoulder. In addition it was observed that the "righting" tendency of the tube undergoing transition from front face to cylinder could be compensated by pretwisting the tubes before assembly. The amount of "righting" tendency was measured as follows: A plate of radius 10 inches was placed on a table with the tube fixed thereto at an initial angle. The tube was then formed to the plate radius and the relative angle of plate and tube measured at several locations (see sketch)



The derivative of the twist is approximately  $\frac{\phi_C - \phi_B}{\Delta X_{BC}}$ , where  $\Delta X_{BC}$  denotes the arc length between B and C. The data obtained was prepared thusly to produce the curve of Figure 27. As the tube makes the transition from flat to cylindrical surface, a total angle of 85.5 degrees transition occurs linearly distributed over the length in which the tube makes the transition. For a shoulder radius of 1.85 inches used in the first and second units, the length is approximately 35 inches. The twist angle measured from the initiation of the shoulder region is found from the equation

$$\phi = \left( \frac{85.5}{35} \right) x + \int_0^x \frac{d\phi}{dx} \left( \phi = \left( \frac{85.5}{35} \right) x \right) dx$$

Using the data from Figure 27 for  $\frac{d\phi}{dx}$  this equation integrates readily to the required twist function. In reality it proved difficult to precisely twist the tube closer than five degrees with the tooling available. The spacing between adjacent tubes was only three degrees and a five degree error at an early section produced a magnified error at a later section. For this reason some tubes had been twisted in excess and others deficiently so that the uniform wedge between tubes did not appear. These discrepancies were corrected by gently twisting a local area of individual tubes. However, this twisting resulted in an inevitable gap between tubes proportional to the correction applied. This second unit was eventually completed and brazed.

Tube Sample No.

1  
2  
3  
4

○  
◇  
△  
×

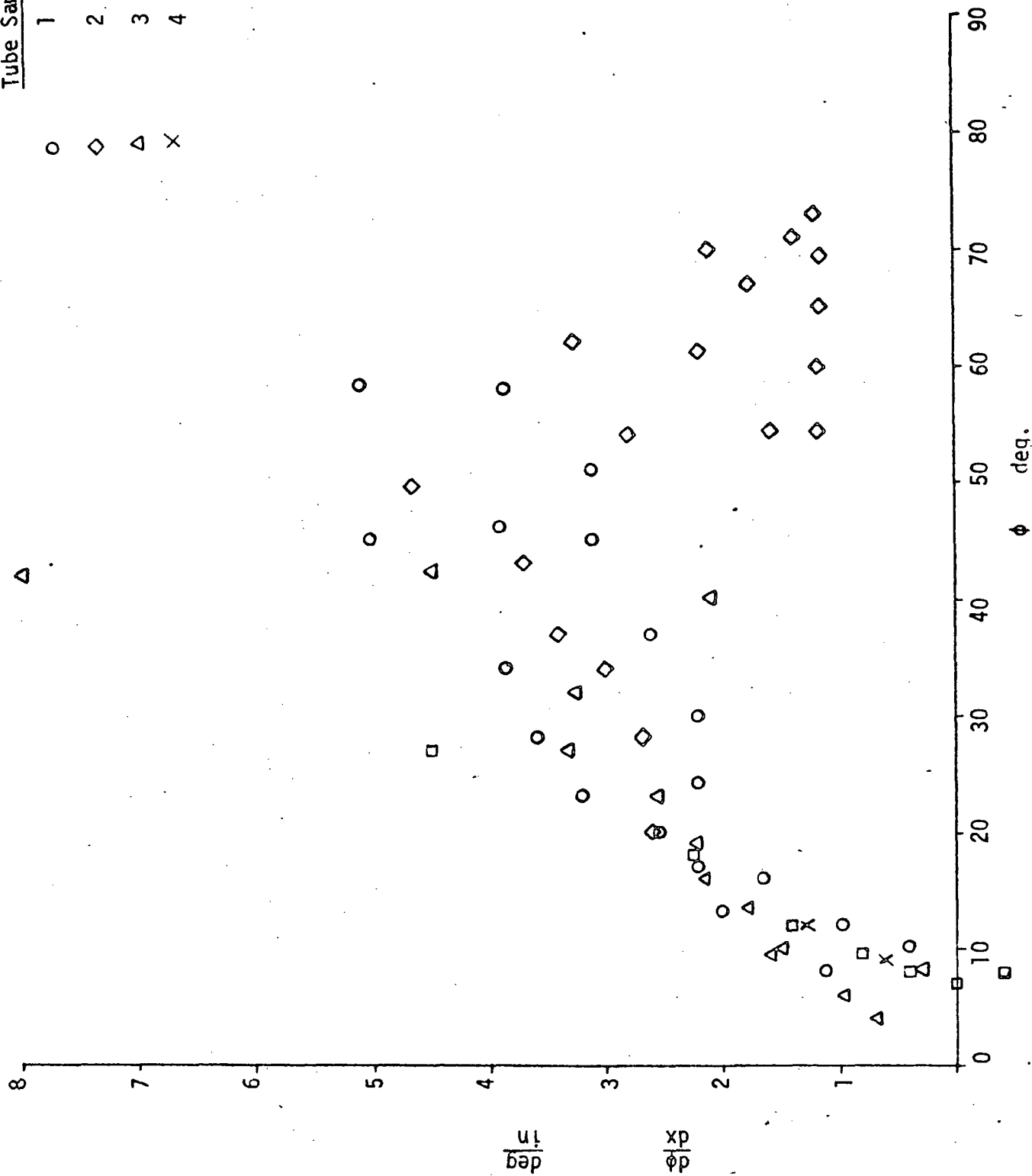


FIGURE 27 TUBE TWIST TENDENCY DATA

The weld rod used for tacking was 5% silicon having solidus below 1100°F. This was recognized before brazing and high melting point pure aluminum rod tacks were added on the cylindrical section. During brazing, some of the tacks on the bottom face were broken and the tubes offset. To remedy this the unit was rebrazed with a weight on top of the flat section. The unit was realigned during the operation but the tube ends which had been sealed with 5% silicon rod softened to penetration of salt. Attempts to remove the salt proved futile so a third unit was fabricated.

#### 4.3 Fabrication of the Third Unit

Having the experience gained in the first two attempts, it was decided to modify the shoulder radius to 0.85 inches. At this radius the tube-to-tube angle is about eight degrees and the twist error estimate reduced to four degrees. The twist also would be accomplished in a length of 17 inches. This benefit was only obtained with the sacrifice that the braze would fill only a portion of the gap. The only other modification was that pure aluminum rod would be exclusively used for tacking the assembly.

During fabrication some modification of the tube position was required after winding the shoulder, but a significant improvement was noted. A considerable number of shrink cracks resulted due to the change from 5% silicon weld rod to pure aluminum. Also the starting ring was found to leak profusely. The tube ends were severed from the starting ring and each welded closed individually before the leakage problem was solved. Even after the unit had been leak checked, small cracks continued to occur.

Brazing of the unit was routine with the best quality of the three attempts achieved. The gaps of .1 inch on the shoulder were nearly brazed completely. In three locations, shrink cracks formed which admitted small amounts of salt and aluminum. These deposits were readily removed although the side wall was opened to relieve the aluminum. The skirt end manifolds were welded on without incident, but the flat end manifolds caused differential shrinkage when welded. This shrinkage caused the braze to fail in several locations between the tubes. In those areas filler was added to insure heat conductance between tubes and to eliminate vapor leakage. The filler was also applied to the large gaps on the shoulder portion. Filler material was mixed from 240 mesh aluminum powder 95 percent and 5 percent "flake" aluminum which is very fine like that used for paint pigment. This mixture was suspended in the minimum amount (about 1%) of sodium silicate (water glass) solution and trowelled into the desired locations. A crude thermal diffusivity test showed that the conductivity of the material was about 20 BTU/hr-ft-°F. Most of the filler failed to bond to the shoulder area completely but apparently filled the small cracks well.



## 5.0 EVAPORATOR TESTING

The prototype unit was prepared for testing. The object of the program was manifold with the overall objective to demonstrate the capability of the evaporator to meet the projected space shuttle requirements. Items in this requirement were (1) to show the absence of nozzle freezing problems, (2) to demonstrate complete evaporation for all test conditions, (3) for demonstrate all redundancy modes, (4) to test controller action, (5) to check for exhaust tube frost tendencies, and (6) to evaluate sensitivity to off-nominal conditions.

The test item was installed in the space environment testing chamber as shown in the schematic diagram of Figure 28. Transport flow was measured in the 40°F section of the loop between the auxiliary cooler and the heaters. The heaters were 10kw helical-passage electrical units arranged in parallel for pressure drop minimization. Valves in each leg were adjusted to provide equal flow with the flow through each leg monitored to indicate instability. The pressure in the loop was maintained by a pump-suction-side accumulator pre-ssurized by heating to insure the existence of subcooled Freon 21 in the entire loop. Two pumps were flowed in series to achieve the pressure drop of about 75 psi through the cooler, filters and heater.

The evaporator was instrumented to reflect all flow rates and thermodynamic conditions pertinent to the evaporator function. Figure 29 is the data output format as produced by the on-line data system, while Table 2 gives a description of the instruments used for each channel. The thermocouples were arranged as shown in Figure 30 on the external surface of the evaporator. The full data scan shown in Figure 29 was collected at one minute intervals. An abridged data scan comprising the first 31 channels was collected at 12 second intervals and was generally used during transient runs. Also an on-line data plot of channels 2, 3, 13, 14, 15 was produced on request. A single channel temperature recorder was also used primarily for outlet temperature monitoring, but was also used for nozzle temperature determination. Flow bench, heater control, and cryopump information was displayed for the test operator's surveillance.

### 5.1 Test Chronology and Significant Events

Table 3 presents the run log in two sections. The first section describes the run, description of conditions, events of significance and corrective action taken due to the events of the run. The second section begins at the point where modifications were effectively complete and simply designates the runs which occurred in chronological order.

Nozzle spontaneous freezing and under-temperature achievement from R-22 exposure proved to be of some concern initially. Early runs in which R-22 was sprayed from a point on the nozzle plate cooled the nozzle plate as low as -23°F. The routing of more warm fluid through the plate was not effective

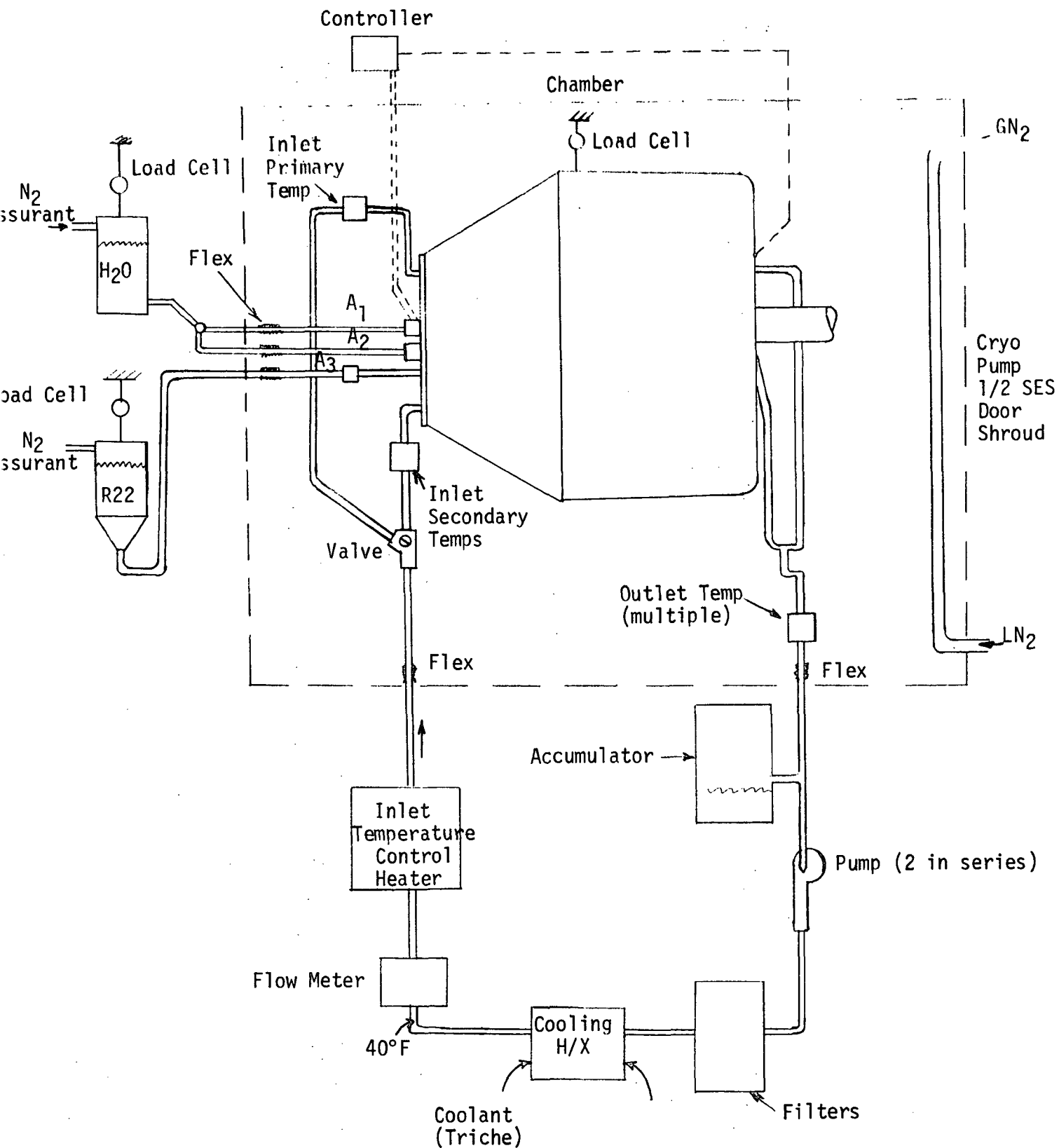


FIGURE 28: EVAPORATOR TEST FLUID LOOP SCHEMATIC

DAY 016 TIME 010:40:00

RECORD 0019

CH 001 + 80.3	LBS TOTAL WT	CH 002 + 97.5	LBS R22 WT	CH 003 + 35.5	LBS WATER WT	CH 004 + 172.0	PSIG R22 SUPPLY
CH 005 + 0	PSIG WATER	CH 006 + 1.0	MPST EVAP-CHER	CH 007 + 391.2	MPST CHAMBER	CH 008 + 7.5	PSIG R01 SUPPLY
CH 009 + 8	PSIG SEC XPORT	CH 010 + 185.2	WHR R21 XPORT	CH 011 + 0	WHR R22 SVAP	CH 012 + 244.0	WHR WATER SUPPLY
CH 013 + 42.2	DEGF PT INLET	CH 014 + 71.3	DEGF ST INLET	CH 015 + 23.9	DEGF OUTLET	CH 016 + 140.0	WHR DELTA BY
CH 017 + 760.0	WICV DELTA ST	CH 018 + 190.0		CH 019 + 27.2	DEGF WATER PSI	CH 020 + 34.1	DEGF WATER PSI
CH 021 + 66.0	DEGF R22 SUPPLY	CH 022 + 40.0	DEGF P5	CH 023 + 40.0	DEGF P7	CH 024 + 40.0	DEGF P9
CH 025 + 40.9	DEGF R10	CH 026 + 40.9	DEGF X7	CH 027 + 40.9	DEGF X5	CH 028 + 41.5	DEGF X1
CH 029 + 41.4	DEGF X1	CH 030 + 48.5	DEGF NOZL PLY	CH 031 + 24.2	DEGF EXHAUST DUCT		
CH 032 + 40.0	DEGF	CH 033 + 40.0	DEGF	CH 034 + 40.0	DEGF	CH 035 + 40.0	DEGF
CH 036 + 40.4	DEGF	CH 037 + 40.4	DEGF	CH 038 + 40.4	DEGF	CH 039 + 40.4	DEGF
CH 040 + 40.0	DEGF	CH 041 + 40.4	DEGF	CH 042 + 40.4	DEGF	CH 043 + 40.4	DEGF
CH 044 + 40.4	DEGF	CH 045 + 40.0	DEGF	CH 046 + 40.4	DEGF	CH 047 + 40.4	DEGF
CH 048 + 40.4	DEGF	CH 049 + 40.4	DEGF	CH 050 + 40.9	DEGF	CH 051 + 40.9	DEGF
CH 052 + 40.4	DEGF	CH 053 + 40.4	DEGF	CH 054 + 40.4	DEGF	CH 055 + 42.2	DEGF
CH 056 + 40.4	DEGF	CH 057 + 40.9	DEGF	CH 058 + 40.9	DEGF	CH 059 + 40.4	DEGF
CH 060 + 40.9	DEGF	CH 061 + 40.9	DEGF	CH 062 + 40.9	DEGF	CH 063 + 40.9	DEGF
CH 064 + 40.9	DEGF	CH 065 + 41.4	DEGF	CH 066 + 40.9	DEGF	CH 067 + 40.9	DEGF
CH 068 + 40.9	DEGF	CH 069 + 40.9	DEGF	CH 070 + 40.9	DEGF	CH 071 + 40.9	DEGF
CH 072 + 40.9	DEGF	CH 073 + 41.4	DEGF	CH 074 + 41.4	DEGF	CH 075 + 40.9	DEGF
CH 076 + 41.4	DEGF	CH 077 + 41.4	DEGF	CH 078 + 41.4	DEGF	CH 079 + 41.4	DEGF
CH 080 + 41.4	DEGF	CH 081 + 40.9	DEGF	CH 082 + 41.9	DEGF	CH 083 + 41.4	DEGF
CH 084 + 41.4	DEGF	CH 085 + 258.4	DEGF	CH 086 + 41.4	DEGF	CH 087 + 41.4	DEGF
CH 088 + 41.9	DEGF	CH 089 + 41.9	DEGF	CH 090 + 41.9	DEGF	CH 091 + 41.9	DEGF
CH 092 + 41.9	DEGF	CH 093 + 42.3	DEGF	CH 094 + 41.9	DEGF	CH 095 + 42.2	DEGF
CH 096 + 41.9	DEGF	CH 097 + 42.3	DEGF	CH 098 + 42.3	DEGF	CH 099 + 42.2	DEGF
CH 100 + 42.0	DEGF	CH 101 + 42.3	DEGF	CH 102 + 42.3	DEGF	CH 103 + 42.2	DEGF
CH 104 + 41.9	DEGF	CH 105 + 41.9	DEGF	CH 106 + 42.0	DEGF	CH 107 + 40.4	DEGF
CH 108 + 40.9	DEGF	CH 109 + 42.3	DEGF	CH 110 + 41.9	DEGF	CH 111 + 40.9	DEGF
CH 112 + 39.0	DEGF	CH 113 + 40.4	DEGF	CH 114 + 41.9	DEGF	CH 115 + 41.4	DEGF
CH 116 + 40.4	DEGF	CH 117 + 40.4	DEGF	CH 118 + 39.5	DEGF	CH 119 + 40.9	DEGF
CH 120 + 831.3	DEGF	CH 121 + 40.9	DEGF	CH 122 + 39.0	DEGF	CH 123 + 391.2	DEGF
CH 124 + 40.9	DEGF	CH 125 + 40.4	DEGF	CH 126 + 28.5	DEGF	CH 127 + 27.1	DEGF
CH 128 + 35.6	DEGF	CH 129 + 37.5	DEGF	CH 130 + 29.0	DEGF	CH 131 + 40.4	DEGF
CH 132 + 38.0	DEGF	CH 133 + 36.1	DEGF	CH 134 + 26.2	DEGF	CH 135 + 27.1	DEGF
CH 136 + 41.9	DEGF	CH 137 + 40.4	DEGF	CH 138 + 41.4	DEGF	CH 139 + 39.0	DEGF
CH 140 + 37.1	DEGF	CH 141 + 36.1	DEGF	CH 142 + 41.9	DEGF	CH 143 + 41.9	DEGF
CH 144 + 41.9	DEGF	CH 145 + 41.9	DEGF	CH 146 + 40.0	DEGF	CH 147 + 30.9	DEGF
CH 148 + 41.4	DEGF	CH 149 + 41.9	DEGF	CH 150 + 42.0	DEGF	CH 151 + 30.0	DEGF
CH 152 + 43.2	DEGF	CH 153 + 40.9	DEGF	CH 154 + 41.9	DEGF	CH 155 + 42.2	DEGF
CH 156 + 42.3	DEGF	CH 157 + 436.7	DEGF	CH 158 + 45.2	DEGF	CH 159 + 42.2	DEGF
CH 160 + 43.8	DEGF	CH 161 + 40.4	DEGF	CH 162 + 46.6	DEGF	CH 163 + 42.5	DEGF
CH 164 + 47.6	DEGF	CH 165 + 101.6	DEGF				

FIGURE 29 DATA OUTPUT FORMAT

TABLE 2  
EVAPORATOR TEST INSTRUMENTATION

MEASUREMENT #	MEASUREMENT	RANGE (ACCURACY)	INSTRUMENT
1	Evaporator Weight	0-60 lbs ( $\pm .02$ Lbs)	SN-101 0-200 lbs Load Cell
2	Evaporant R22 Weight	0-300 lbs ( $\pm .3$ lbs)	SN-129 0-500 lbs Load Cell
3	Evaporant H <sub>2</sub> O Weight	0-50 lbs ( $\pm .02$ lbs)	SN-111 0-100 lbs Load Cell
4	R22 Supply Pressure	150-300 psia ( $\pm 5$ psi)	Teledyne 0-300 psia S/G SN671199
5	H <sub>2</sub> O Supply Pressure	20-50 psia ( $\pm 5$ psi)	Teledyne 0-100 psia S/G SN2160
6	Evaporator Int. Pressure	0-.1 psia ( $\pm .02$ psi)	Dynisco $\pm .25$ psid SN18058
7	Chamber Pressure	0-500 mm (1%)	Magnevac GNA-140
8	Primary Transport	5-25 psid (0.1%)	CEC S/G 16142
9	Secondary Transport	5-25 psid (0.1%)	Dynisco S/G 2449
10	(R-21) Transport Flow Rate	1500-2100 lb/hr (1%)	Cox AN-8 S/N 8432
11	R22 Flow Rate	700-1000 lb/hr ( $\pm 10$ lb/hr)	Cox LF6-0 5N 3258
12	H <sub>2</sub> O Flow Rate	40-65 lb/hr ( $\pm .5$ lb/hr)	Cox AN8-45
13	Primary Transport Inlet Temp.	+ 40°F - +180°F ( $\pm .5$ °F)	Thermistor #1
14	Primary Transport Outlet Temp.	$\approx + 40$ °F ( $\pm .5$ °F)	Thermistor #6
15	Secondary Transport Inlet Temp.	+ 40°F - +180°F ( $\pm .5$ °F)	Thermistor #5
16	Secondary Transport Outlet Temp.	$\approx + 40$ °F ( $\pm .5$ °F)	Thermistor #8
17 to 165	Evaporator Temperatures	( $\pm .5$ °F)	Thermocouples

rays 4,5,6 have  
T/C at r = 4.5  
5.  
5.5  
6.0  
6.5  
7.0  
8.0  
9.0

T/C's on each ray  
between manifolds and  
at  $x = 0, 1, 2, 3, 4, 5, 6, 7, 8, 9$

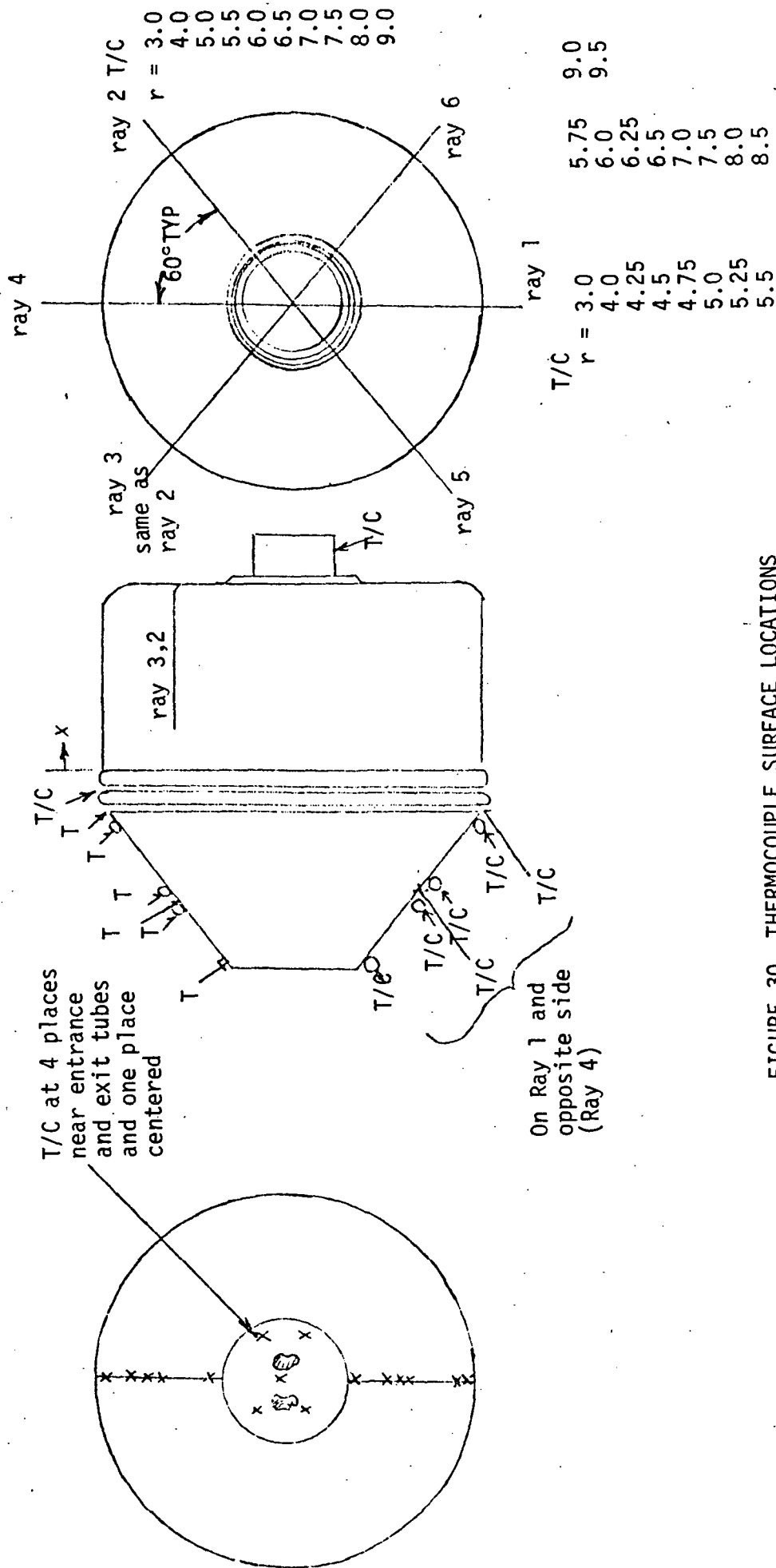


FIGURE 30 THERMOCOUPLE SURFACE LOCATIONS

TABLE 3 EVAPORATOR RUN LOG

<u>RUN</u>	<u>DESCRIPTION</u>	<u>MODIFICATION</u>
A-1	14.7 psi, nominal full load, position 1 Freon. Overcooled nozzle mounting plate resulted	Increase flow rate to nozzle mounting plate
A-2	Nominal full load, Freon, atmos, position 2: plate too cold still	Install insulation sheet on nozzle mounting plate
A-2 Repeat	Nominal full load, Freon, Atmos, Position 2	
A-3	H <sub>2</sub> O pri, nozzle freeze up	
A-3 Repeat	Watch freeze up on insulation	Cut out nozzle insulation holes
A-5	Freon, 1 psi	
A-6 (A-3 repeat)	Froze up again	put 1/8" teflon insulation 2" nozzle spacer
A-7 (A-3 repeat)	H <sub>2</sub> O, 10 psi supply, ice accumulation	Put in another 1" spacer Mod nozzle to larger slots
	Run off/on cycles, observing nozzle temps. Froze an inlet water line	insulate water line
Mockrun 1	120°F inlet, 0 psig supply	Mod nozzle to larger slots
Mockrun 2	120°F inlet, 0 psig supply	
A-8	Full load, 10 psi, H <sub>2</sub> O; iced up in middle of run	
A-9	Switch to sec. nozzle, observed leaks around threads	Fix leaks; add another spacer 1"; Controller setup
A-10	Controller active - froze nozzle	
A-11	Repeat A-10	
A-12	Secondary supply, froze nozzle	

TABLE 3 (CON'T)

<u>RUN</u>	<u>DESCRIPTION</u>	<u>MODIFICATION</u>
A-13	Freon 1 psi, 900 lb/hr  Attempt to measure ice formation deposit on freezing surface. Futile.	Remove teflon insulator
A-14	R-22 (-60°F) @ atmosphere	
C-1	Control run, H <sub>2</sub> O, frost accumulation evident	
C-2	Control run, H <sub>2</sub> O, frost increased	
C-3	Secondary nozzle 4 psi, frost increased, froze up	Remove glue from nozzle plate
C-4	Repeat C-3, SES chamber @ 1 mm frost formed	Build plexiglas back to view frost formation
C-5	H <sub>2</sub> O, primary (full load)  → secondary → primary	Put in brass nozzle (NN4)
A-15	R-21 @ 95° inlet (half load) A-OK @ 25 lb/hr Frost with 28 lb/hr water flow at 6 to 9" radius uniform. Lower H <sub>2</sub> O flow to 25 lb/hr & lower inlet to 90, to 80; frost again.	Install 4 slot Al nozzle in pri 2 slot Al nozzle in sec
A-16	Trial of 2 nozzles - no good	Replace Al cone extending spray of NN-4 nozzle, NN4 in secondary } 2 in. spacers Delavan in primary
A-17	Run secondary (NN4) Frost in duct and fails heat load. Primary looks better-must be repositioned	Replace NN4 with another Delavan nozzle, 4" total spacers  Put Freon nozzle in lower cone section

END OF MAJOR MODIFICATIONS

TABLE 3 (CON'T)

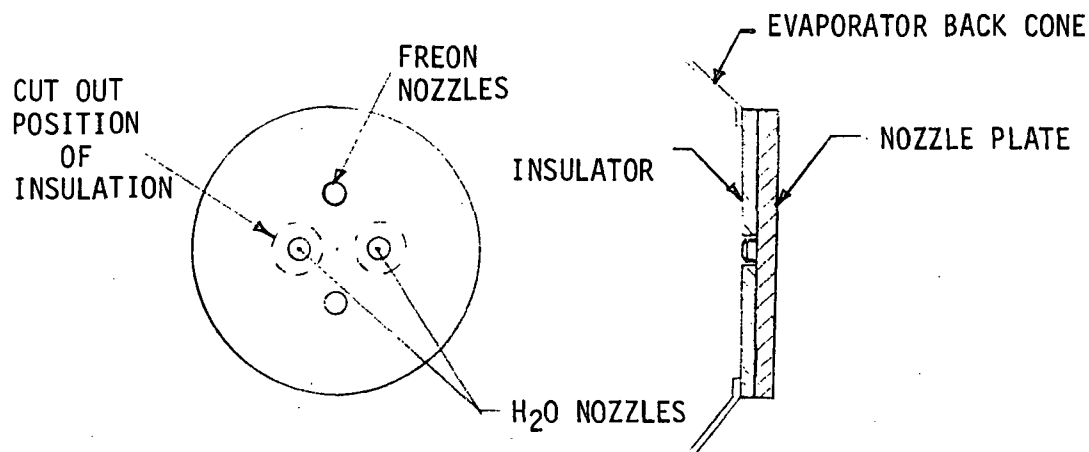
<u>RUN</u>	<u>EVAPORANT</u>	<u>DESCRIPTION</u>
A-18	H <sub>2</sub> O	Full load, transport and supply redundancies exercised
A-19	R22	Full load, atmospheric run. Alignment of R22 flow judged poor and changed
A-20	R22	Full load, atmospheric run
C-6,7,8,9	H <sub>2</sub> O	Control run. Sensor on ray 3, set point 8C; all transport and supply redundancies exercised
E-3	H <sub>2</sub> O	High supply pressure
E-4	H <sub>2</sub> O	Low supply pressure
A-21	R22	Full load (1 psia), run bad - Freon 22 leak
A-22	R22	Full load (Atmos) repeat A19 after nozzle changes
A-23	R22	Full load (1 psia)
B-13	H <sub>2</sub> O	1 hour at 50°F inlet (10 percent load)
C-10	R22	Control run on heat load profile @ atmos
C-11	R22	Control run on heat load profile @ atmos
C-12	R22	Control run on heat load profile @ 1 psia
E-9	H <sub>2</sub> O	Cooled water supply - profile run
E-5	H <sub>2</sub> O	Transport flow 1600 lb/hr profile run
E-10	H <sub>2</sub> O	Heated water supply - profile run. Leak in nozzle
C-13	H <sub>2</sub> O	Spray downward, profile run
E-8	H <sub>2</sub> O	Spray downward, transport flow 2100 lb/hr, maximum load in profile - 60,000 BTU/hr
E-6	H <sub>2</sub> O	Spray downward, transport flow 2100 lb/hr Profile run to 50,000 BTU/hr
E-1	H <sub>2</sub> O → R22	Spray downward, 50,000 BTU/hr switchover run
C-14	H <sub>2</sub> O	Primary H <sub>2</sub> O spray up
C-15	H <sub>2</sub> O	Sec H <sub>2</sub> O spray up
E-7	H <sub>2</sub> O	Load 60,000 BTU/hr, $T_{in} = 192^{\circ}\text{F}$ , Transport flow 1600 lb/hr. Spray up
E-14	H <sub>2</sub> O	Load 60,000 BTU/hr, $T_{in} = 172^{\circ}\text{F}$ , Transport flow 1850 lb/hr. Spray up
C-16	R22	Atmos pressure spray up
C-17	R22	1 psia spray up
E-15	R22 → H <sub>2</sub> O	Switchover run at unknown pressure
C-18	H <sub>2</sub> O	Installed horizontal with plexiglas back plate. Combination of dropped inlet temperature & increased flow used to attempt frost formation. Outlet temperature decrease below 32°F encouraged frost formation in exit duct.
C-19	R22	@ atmos (increase R22 flow)



TABLE 3 (CON'T)

<u>RUN</u>	<u>EVAPORANT</u>	<u>DESCRIPTION</u>
C-20	R22	@ atmos (increase R22 flow)
C-21	R22	@ atmos (increase R22 flow)
C-22	R22	@ atmos (decrease R22 flow from level of C-21)
C-23	R22	@ 1 psig supply pressure as in C-21
C-24	R22	@ 3 psig supply pressure as in C-21
E-7A	R22	@ 10 psia low transport flow 1600 lb/hr
E-8A	R22	@ 10 psia high transport flow 1960 lb/hr
E-1	R22	@ 10 psia, supply pressure high

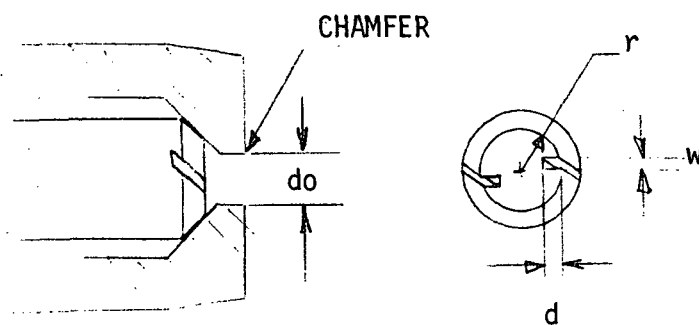
in maintaining the temperature above 32°F due to the large area being cooled. An insulator was added (see figure below) which was effective in precluding excessive cooling, but this insulator gave rise to a new problem.



The first insulator added was thick enough that the insulator and water nozzles were in the same plane. The dribble volume formed at each shut-off froze readily to the insulator and ultimately caused build up of ice over the nozzle. To remedy this, the insulation was removed for about one inch surrounding the nozzles. Further testing showed that occasional droplets sprayed directly on the lip of the insulator and froze. Even removal of the original 1/4 inch rubber insulation sheet and replacement with a 1/8 inch sheet of teflon failed to remedy the problem. Upon complete removal of the insulation, one other ice build up was noted on a section having residual glue about an inch below and slightly aside of the nozzle. After removal of all the glue, no further problems of freezing occurred. All of the testing after run C-5 was free of any nozzle freezing problem. Other incidents during the program of insulation changes included freezing on a thermocouple wire attached to the nozzle and freezing of fluid leaking past the seal and around the threaded nozzle. This leaking aggravated freezing in the presence of the insulation sheets but had no effect on a later run with a bare plate. A later configuration in which the Freon spray was issued from a position farther from the water supply showed that the nozzle plate cooling was no longer great enough to require the insulation anyway. Stemming from this experience it is recommended that no insulative materials exist within the evaporator chamber.

Some difficulty was obtained in achieving the spray distribution which was anticipated. It was known that the spray tended to expand in vacuum more than at atmospheric pressure due to the relatively lower effect of vapor entrainment. This expansion was larger than anticipated, requiring

the nozzle to be relocated closer to the shell. The nozzle position was successively advanced until the entire spray fell on the evaporator surface which is active with both transport circuits. Even with this advancement the area coverage was less than predicted. The sketch below shows the dimensions of the prototype nozzles and the old nozzles used for pattern predictions.



NOZZLE	$d_0$	$d$	$w$	$r$	CHAMFER
Prototype Spraying Systems N-8	.060	.025	.037	.07	$\approx .01$
Feasibility Test Spraying Systems N-4	.042	.020	.031	.07	$\approx 0$
Geometrically Scaled N-4	.0595	.0283	.044	.099	$\approx 0$

Comparison of the prototype centerbody dimensions and the geometrically scaled dimensions indicated that some nozzle modifications were in order. Under the assumption that the ratio of slot area to orifice area could be a significant parameter, the slots were increased to .032 x .041 dimension. This change produced the correct tendency but a greater effect was desired. Figures 31 and 32 show the temperature pattern produced by the original N-8 design and that with enlarged slots. Further modification of slot dimensions to .032 x .044 produced the temperature pattern shown in Figure 33. The spray pattern appears to be reasonably acceptable from a spray distribution standpoint, since it produces a more uniform temperature drop with evaporator area (due to more uniform spray deposition) than the previous two nozzles.

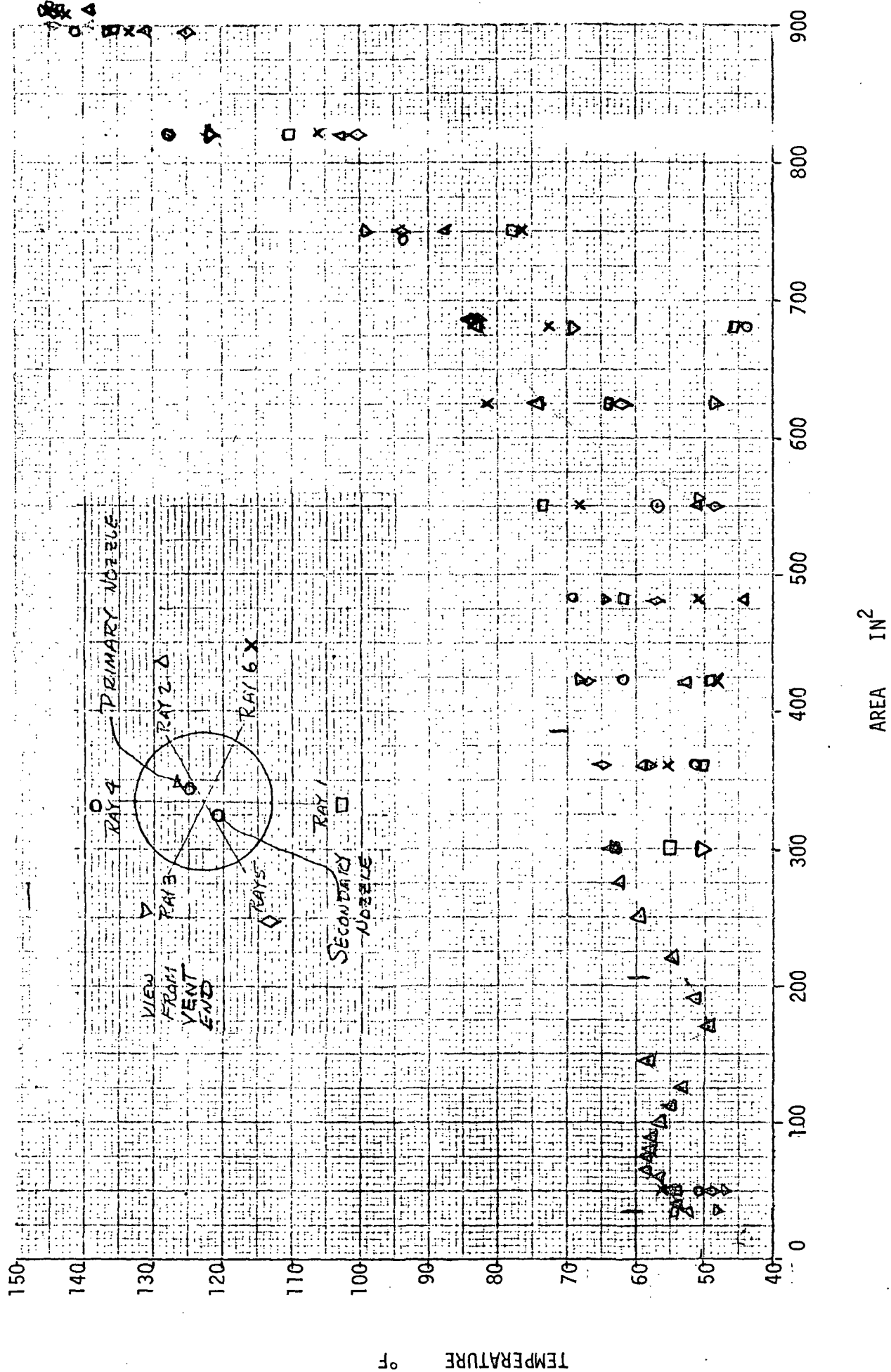


FIGURE 31 EVAPORATOR TEMPERATURE DISTRIBUTION, ORIGINAL N-8 NOZZLE

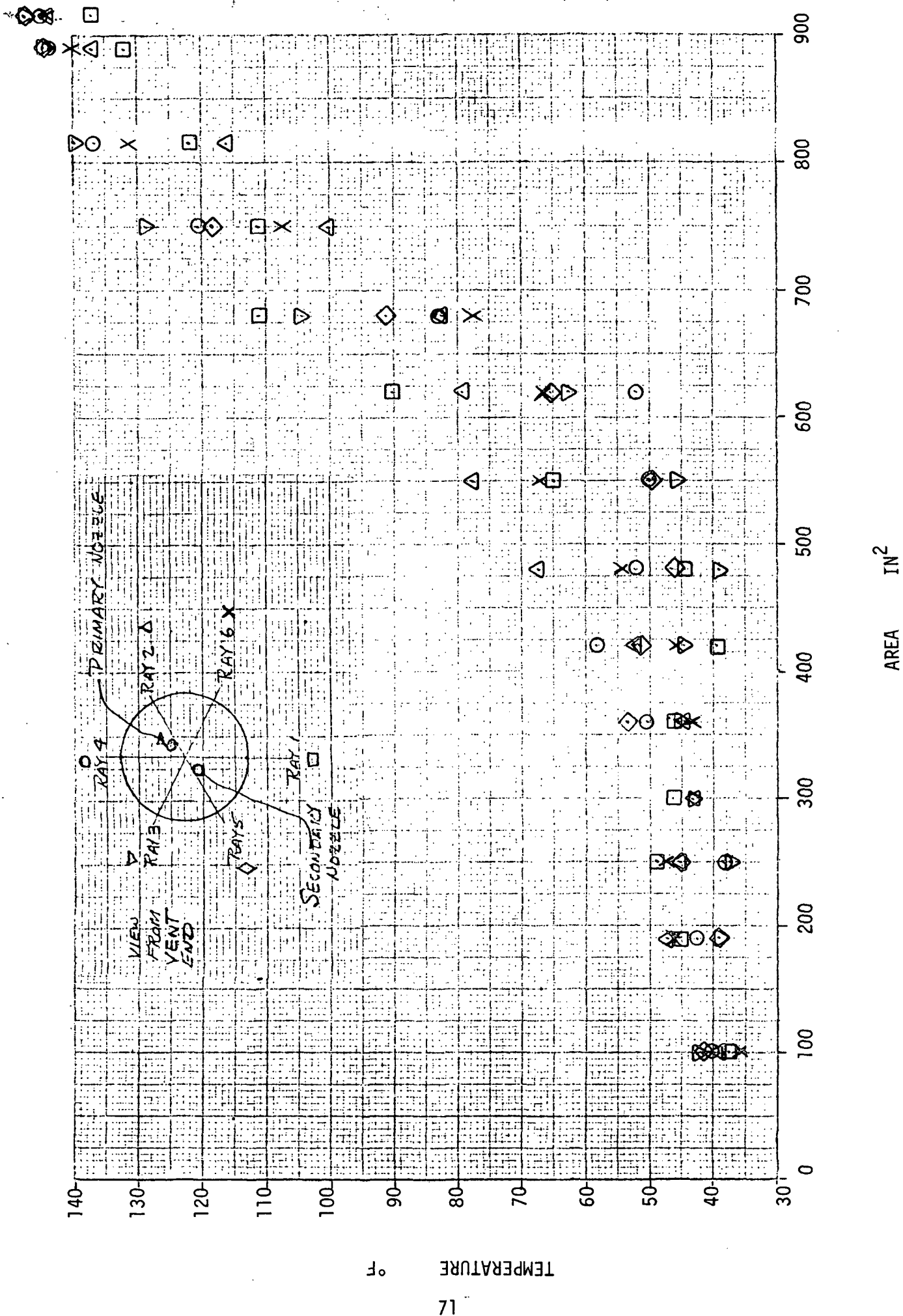


FIGURE 32 EVAPORATOR TEMPERATURE DISTRIBUTION, 0.032 x 0.041 NOZZLE SLOTS

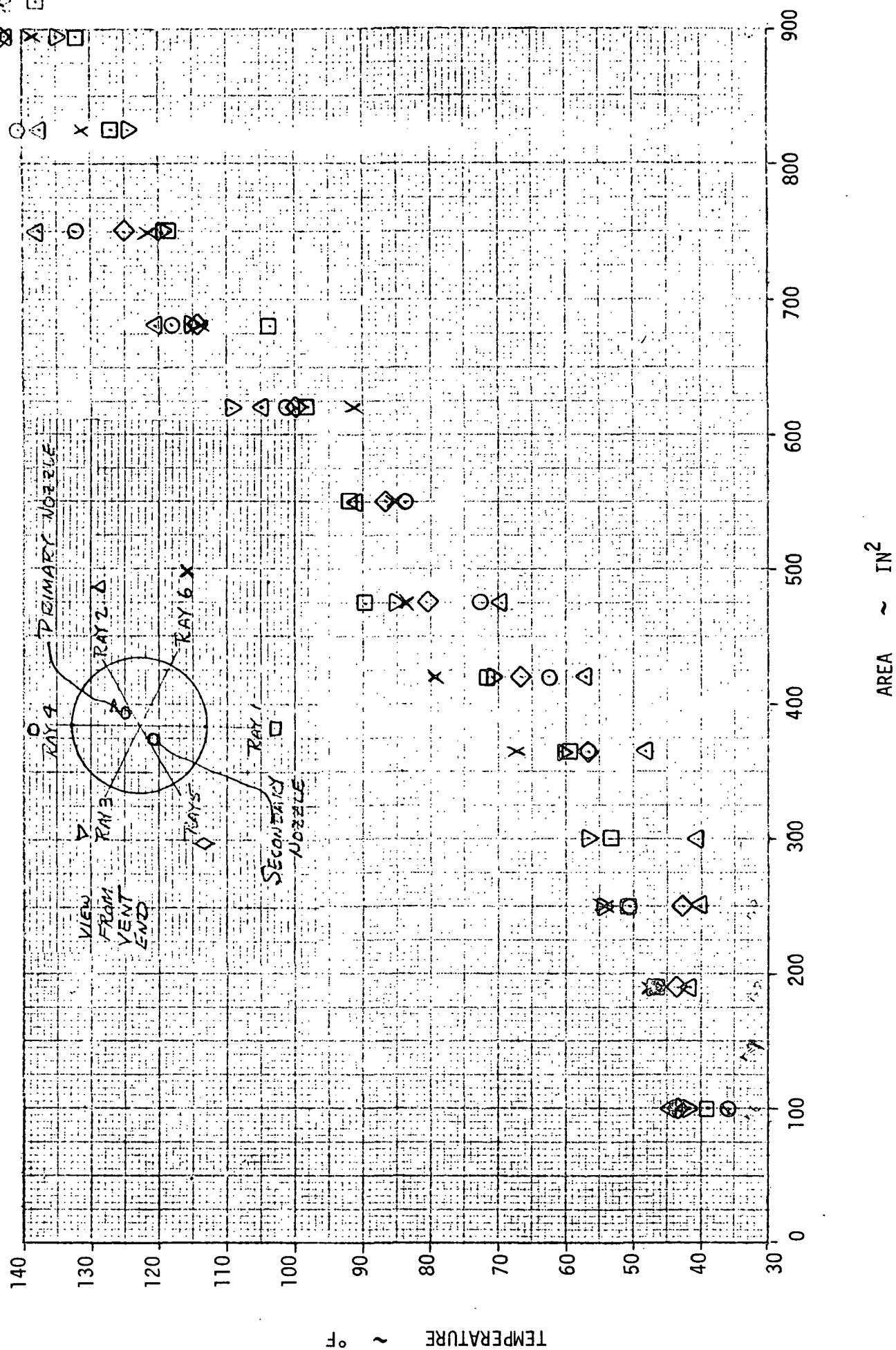


FIGURE 33 EVAPORATOR TEMPERATURE DISTRIBUTION, 0.032 x 0.044 NOZZLE SLOTS

In spite of the improvement in spray distribution, testing of the unit disclosed accumulations during operation. A plexiglas back (see Figure 34 ) was added to the unit through which the vaporization surface could be viewed. This revealed the presence of a band located approximately 45 degrees from the nozzle centerline at which frosting occurred. The frost covered approximately a width of one and one half inches spanning some 12 tubes, and was present on circumferentially spaced patches up to half of the evaporator girth in extent. The initial formation of frost had the appearance of a myriad of filaments joined end-wise to the surface and having a length of one-eighth inch. This fuzzy surface yielded to a more solid formation. This frost layer built until the joint temperature was raised to a level sufficient to generate vapor which cleaved the layer from the surface. The frost layer then fell to the bottom of the evaporator where it accumulated, and the process repeated.

The transport fluid temperature level was changed while maintaining constant heat rejection. The temperature which had frost accumulation had previously been at a level of 50 to 90°F (wall temperatures) and were raised 10°F with no apparent change in the frosting tendency. From this it was concluded that improvements in the transport side qualities could not be expected to aid the problem. Also, there were runs made at reduced load (120°F inlet, 40°F outlet) which had not shown any accumulation. (These runs were made before surface viewing was initiated). For this reason, it was concluded that the combination of droplet size and deposition rate were responsible for the accumulation. The simple theory of Reference 1 agrees with this conclusion. As shown in Figure 35 the relative difference between evaporation and supply time is much more sensitive to area (flow per unit area) and drop thickness than to surface temperature.

The feasibility test nozzle used (Spraying Systems N-4) was inserted into the evaporator to reproduce the earlier test conditions. It was positioned to cover an area of approximately 3 ft<sup>2</sup> and was flowed at 25 lb/hr as in previous testing. The evaporator vent area in this set up was double its previous value which was recognized to possibly permit droplet freezing-in-transient. The latter did not occur to a degree that inefficiency resulted. Also no frost occurred in the simulation of the earlier conditions. The evaporant flow was raised to 28 lb/hr at which condition frosting was observed from  $r=6$  to  $r=9$  on the circular face portion of the evaporator. Temperatures on the outside ranged from 35 to 50°F in this area. The transport fluid temperature level was raised 10°F while the frosting persisted showing again the insensitivity to surface temperature. The evaporant flow was returned to 25 lb/hr and the frosting ceased. The transport temperature was reduced 5°F from nominal with no effect (outlet temperature 35°F). As the transport fluid temperature was reduced another 10°F, frosting resumed and the outlet temperature dropped 8°F disclosing the reduced efficiency. During feasibility testing, loads to 43 lb/hr were achieved with the N-4 design with no evident accumulation. These runs were not sustained for long periods due to the inability of the smaller pumping capacity in the vacuum chamber at that time. It is possible that the accumulation was (1) not noted, (2) impeded by the higher chamber pressure,

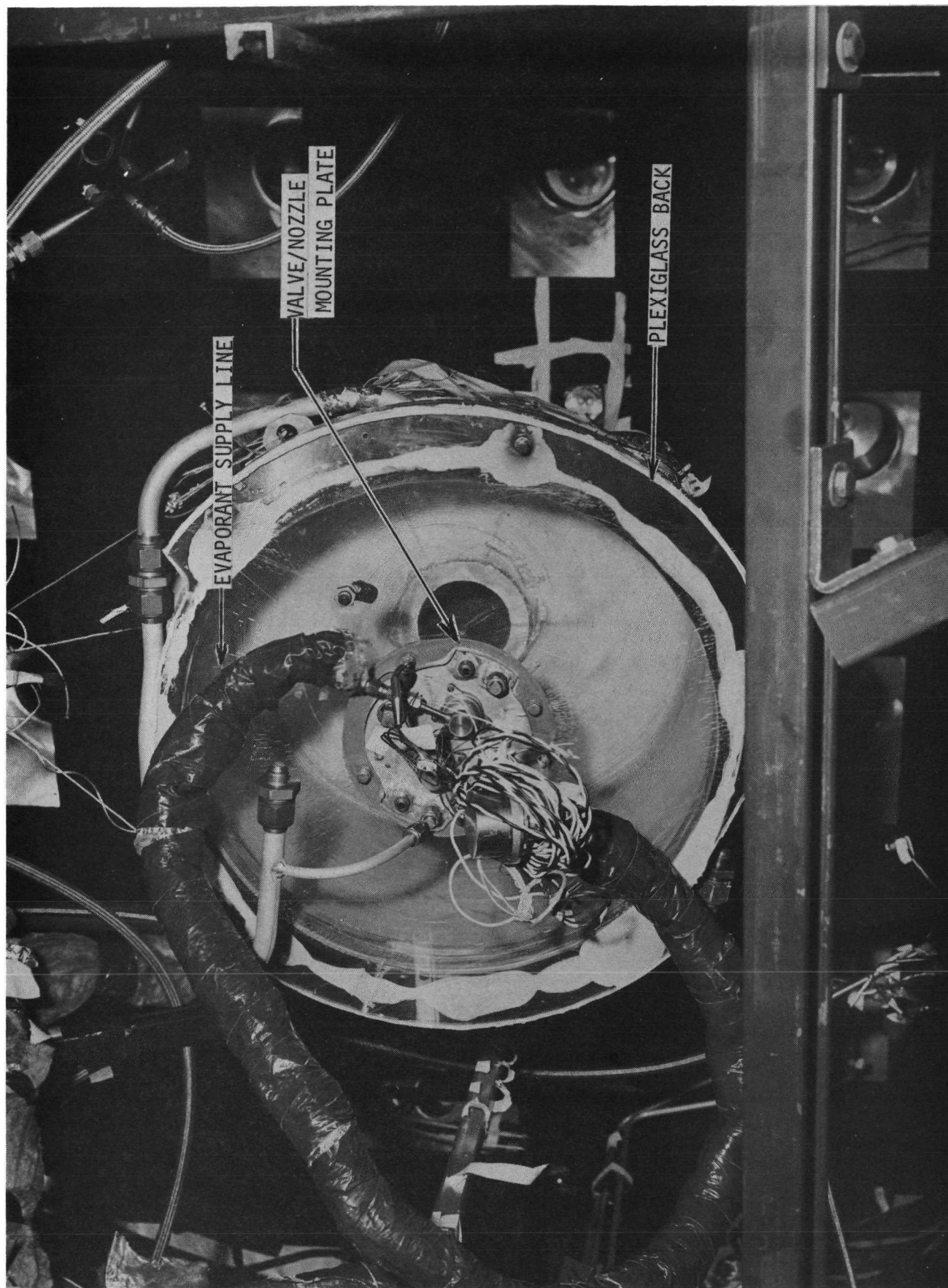


FIGURE 34 · EVAPORATOR WITH PLEXIGLASS BACK



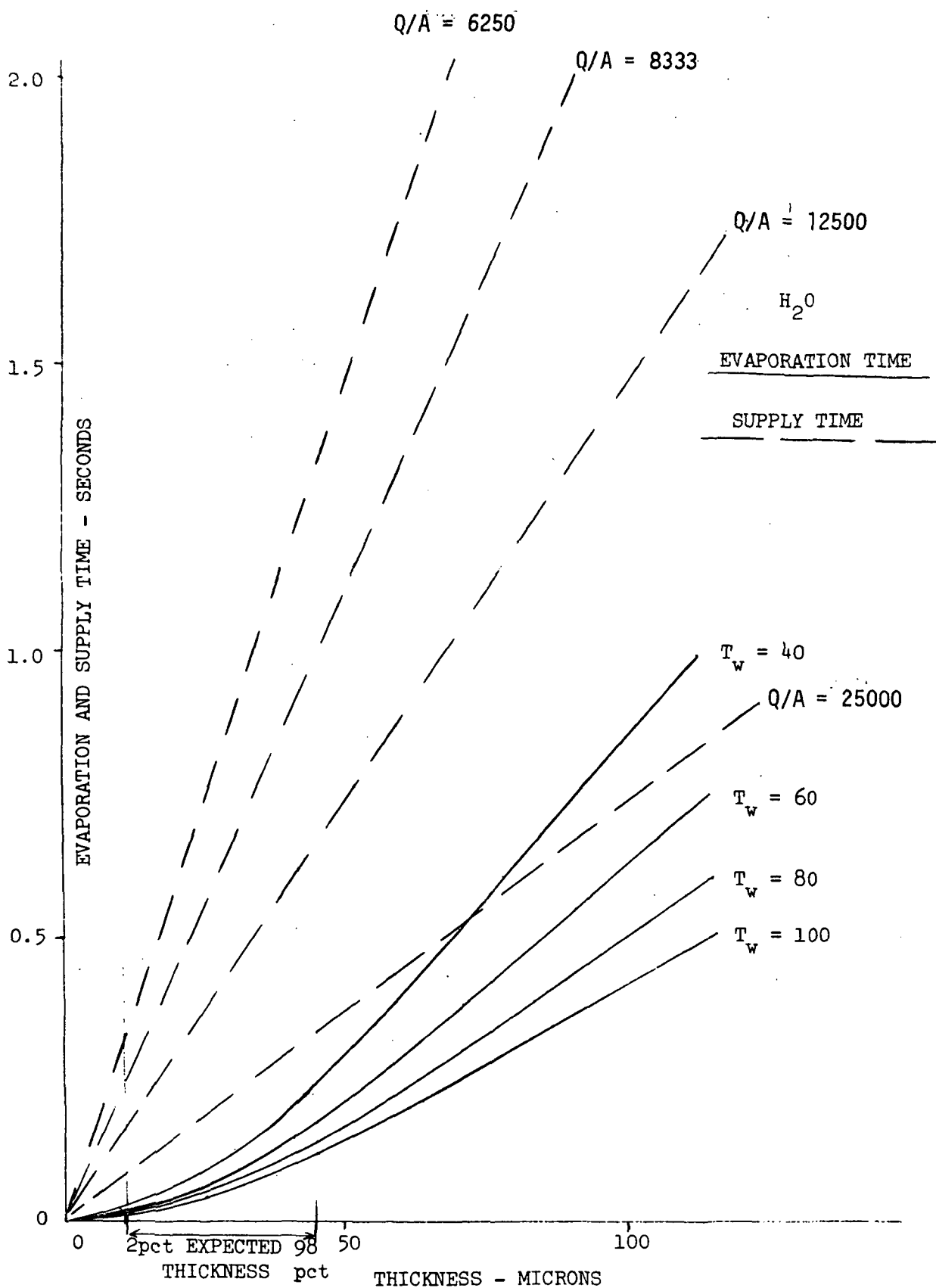


FIGURE 35 EVAPORATION AND SUPPLY TIMES FOR WATER

or (3) not present due to surface or geometrical differences from the prototype unit. Nevertheless it became apparent that an improved spray pattern was required to alleviate the frosting tendency.

In the course of nozzle trials several other variations of nozzle dimensions were tested. The following nozzles were installed and evaluated (see earlier sketch for dimensional definitions).

NOZZLE	NO. SLOTS	d	w	d <sub>0</sub>	DESIGNATION
1	2	.020	.031	.060	2 small slot
2	4	.020	.031	.060	4 slot
3	2	.020	.031	.042	N-4
4	6	.020	.028	.040	Delavan

The first two of these nozzles produced patterns which did not represent significant improvements. In neither of these cases did the spray cover the entire area, but frosting was observed in the cylindrical portion of the core. For this reason one would not expect that retracting the nozzle to cover more of the active surface would reduce frosting. The sprayed density at the critical location would be translated to a slightly larger radius due to the slight conical form of the "cylindrical" section. However this was not expected to result in more than a 10 percent reduction in spray density, and therefore was not employed. Nozzle 3 was the same as employed for the feasibility test and that used earlier at low load. It was repositioned so that the maximum spray density was located on the larger-radius cylindrical section and so that the spray coverage was a larger fraction of the total area. This arrangement similarly provided neither a superior spray distribution nor relief from the frosting tendency. Finally, the six slot design was employed which eliminated frost formation. This six slot nozzle was used in the remainder of the testing. Superficially, the spray distribution is inferior to the N-8 nozzle with deepened slots. However, the peak spray density is lower, less circumferential variation is present, and the droplet sizes are presumably smaller, due to the higher supply pressure (28 psi compared to 14 psi).

One problem incurred with the non-frosting nozzle which was not present with the frost-producing N-8 item is direct liquid carryover in the exhaust duct. This carryover is perhaps 8 percent of the total flow and presumably is due to the presence of smaller droplets which are swept out with the vapor. These particles were present in the feasibility test as evidenced by observation of frost on viewpoints located in the exhaust flow. Mirrors positioned for visualizing nozzles in upward and downward operation accumulated considerable amounts of ice during testing.

Another difficulty associated with the six-slot nozzle is the spray pattern effect on control. The control sensor in the "upstream" location has

been shown to exhibit superior response. The "upstream" position was presumed to be cooled at a representative rate so that the presence or absence of cooling on the surface could change the sensor temperature significantly (more than 1 or 2 degrees). However, in the search for such a position with the Delavan six-slot nozzle, the strong cooling extended over 90 percent of the cooling range, while the remaining 10 percent was relatively diffuse cooling, producing only perhaps one or two degrees of cooling of the sensor relative to the fluid. One then is faced with the  $\pm 5^\circ\text{F}$  swings associated with the "downstream" sensor positioning or load sensitivity. For

$$T_{\text{sensor}} = T_{\text{out}} + (\Delta T) \times L$$

Where L is the Load fraction

The nearest practical position of the sensor to the outlet was at an area  $250\text{ in}^2$  where the temperature is 8 degrees above the outlet at full load ( $\Delta T = 8$ ) as shown in Figure 36. This indicates that load sensitivity of the device would be approximately eight degrees over the load range. Turn "on" at low load ( $L \rightarrow 0$ ) at  $43^\circ\text{F}$  implies that at  $L \rightarrow 1$  the outlet could stabilize as low as  $35^\circ\text{F}$ . This approach was taken and the results are shown in Figure 37. As expected the outlet temperature sinks to  $35^\circ\text{F}$  at near full load before the evaporator achieves a true full load operation. Brief testing with the N-8 nozzles under control showed less load sensitivity ( $\Delta T \approx -4$ ) and could have been improved by better sensor location. The control runs (C-1 through C-4) are represented well by C-1 shown in Figure 38. Here the outlet temperature trace shows a small load bias until full "on" conditions are achieved where the outlet is a constant difference from the inlet temperature. In a progression of runs, the outlet temperature rise at maximum demand increased in proportion to the accumulation of frost in the evaporator. For, the evaporation rate from surfaces covered by frost is low compared to the non-accumulating surfaces. Thus any evaporant sprayed on the frost is "lost". As the accumulated frost pile increased in dimension, covering a larger fraction of the evaporator, the fraction of evaporant "lost" became greater. The tendency to supply more evaporant flow to offset this apparent deficiency in load capacity increases the flow per area and thus the rate of frost formation.

## 5.2 Results of Prototype Testing

The redundant channels were operated in each combination to evaluate the uniformity of flow channels and the effect of off-center nozzles. Figure 36 shows the outside wall temperature distribution produced for each evaporant position. Four runs were made with all combinations of primary and secondary flow circuits and the sensor position picked at a position of coincident temperature. The temperature distribution on the sensor ray is shown in Figure 39 for each evaporant/transport fluid circuit combination. The prospective sensor location is indicated in Figure 39. Differences in detailed temperature distribution using the alternate transport flow channels were small, as expected. Differences between supply circuits were greater,

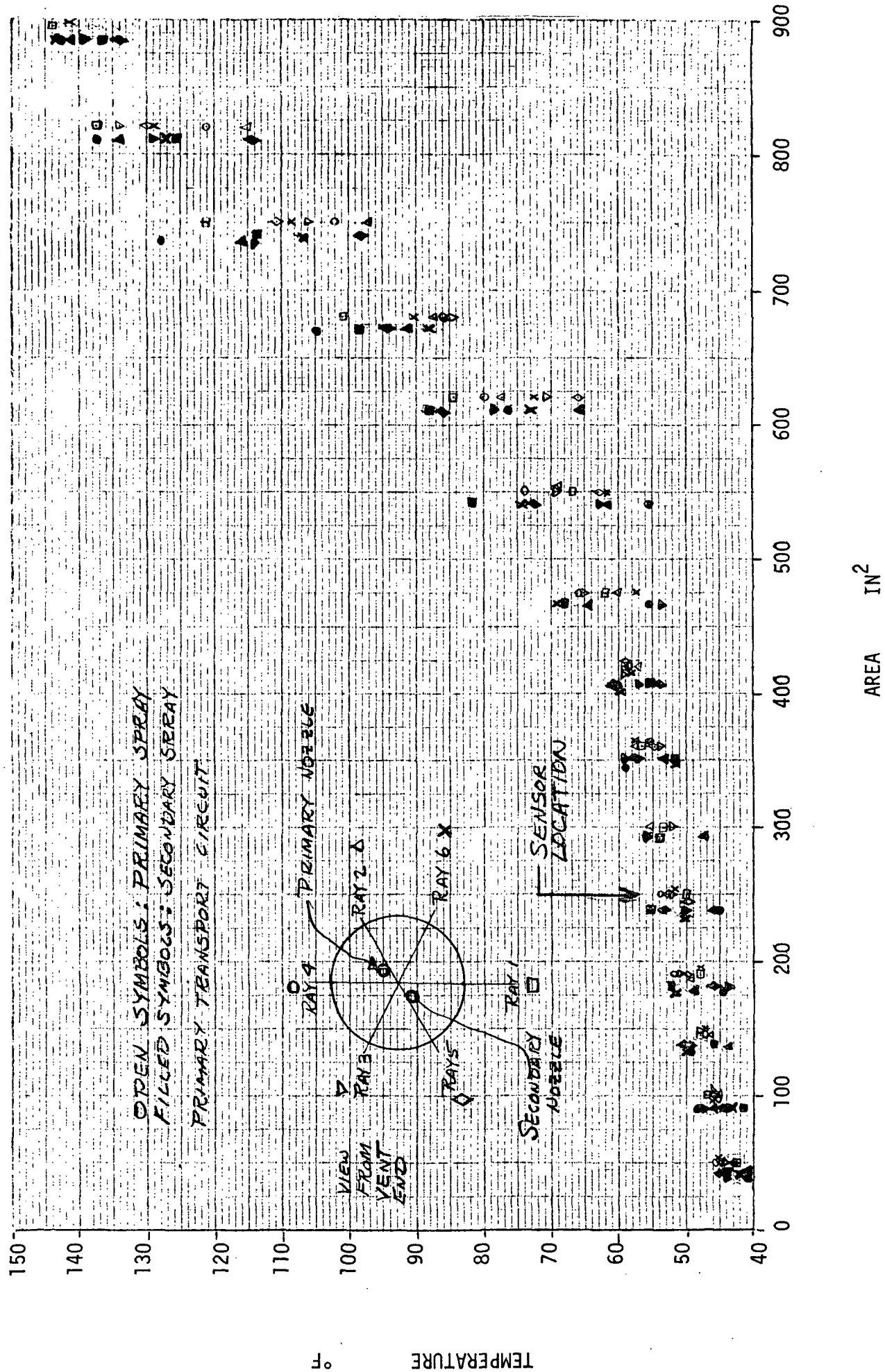


FIGURE 36 EVAPORATOR TEMPERATURE DISTRIBUTION, DELAVAN NOZZLE

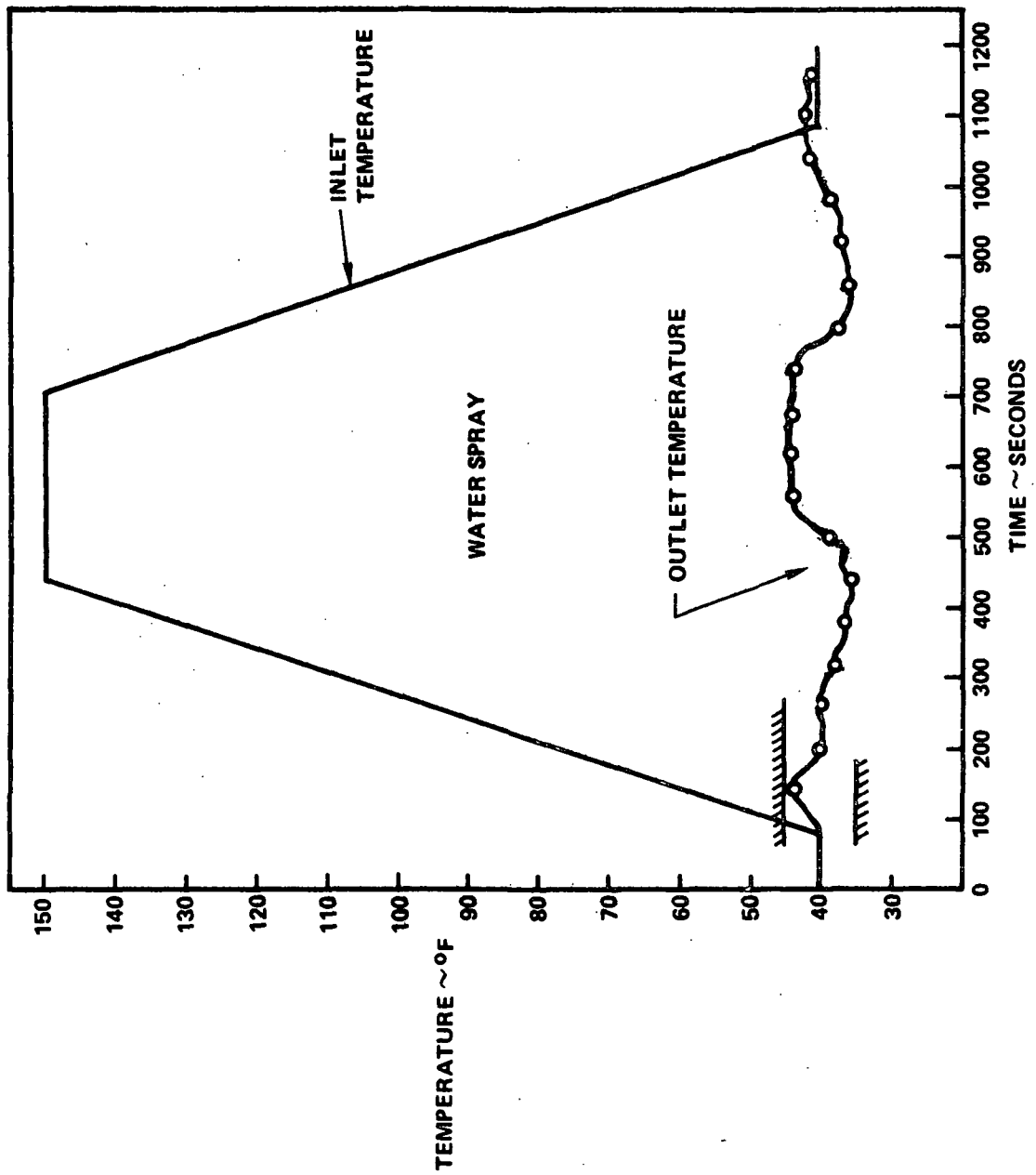


FIGURE 37 EVAPORATOR PERFORMANCE, DELAVAN NOZZLE

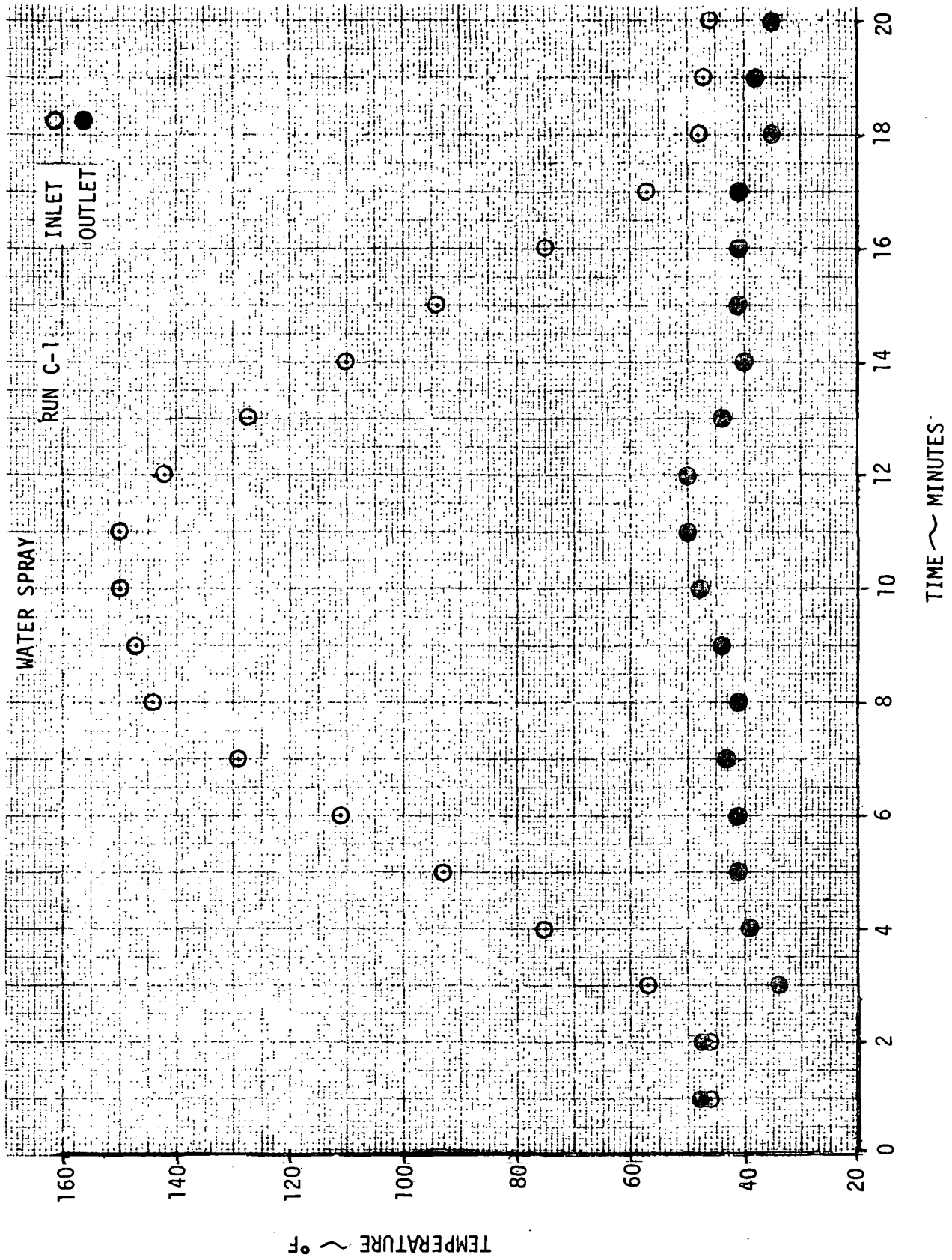


FIGURE 38 EVAPORATOR PERFORMANCE, N-8 NOZZLE

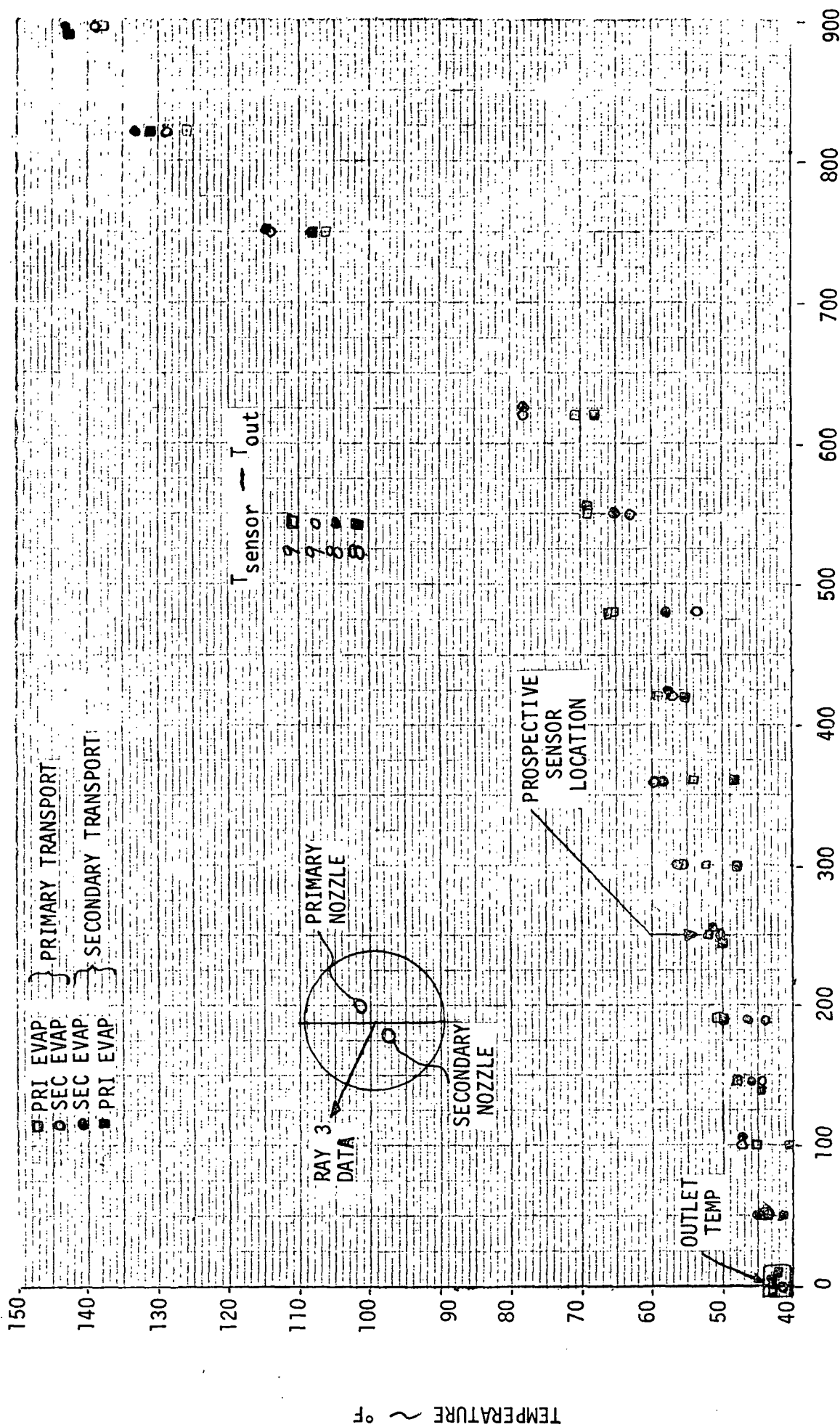


FIGURE 39 EVAPORATOR TEMPERATURE DISTRIBUTION FOR PRIMARY AND REDUNDANT COMBINATIONS

especially off the sensor ray, but showed a significant symmetrical relationship. In the horizontal position all four combinations were tested during the zero to maximum to zero heat load transient. Figure 40 shows the results which are extremely similar in character. The experience gained from this run sequence implies that the evaporator redundancy provisions can be engineered to be nearly equivalent in operating characteristics.

The effect of evaporator position during the simulated heat load profile is shown in Figure 41. In these runs the heat load bias during the increasing portion of the inlet temperature ramp appears to be slightly stronger for the spray down orientation. However this does not continue for the declining load portion of the run. Control in each position was to the  $40 \pm 5^\circ\text{F}$  required with the exception of a two minute period in the spray down position where the temperature was reduced as low as  $32^\circ\text{F}$ . Minor changes in liquid supply pressure account for the differences in the 500 to 800 second time period.

The effect of water supply temperature is more dramatic as shown in Figure 42. In both the hot and cold evaporant supply a greater portion of flow is apparently directed downstream of the sensor so that the heat load bias is increased. It is well known that viscosity affects the droplet size distribution and probably the spray spatial distribution. In addition, the balance of surface tension force and vapor pressure suggests an upper droplet size which lies within the expected droplet size range for the conditions anticipated. At the higher supply temperature the upper droplet limit is considerably smaller than at the normal ( $70^\circ\text{F}$ ) spray supply temperature. The smaller droplets are more susceptible to vapor drag which tends to collapse the spray pattern. Thus for both hot and cold supply temperatures the spray drop size and spatial distribution are subject to considerable variation.

The full "on" portion of operation (from 500 to 800 seconds) disclosed that the run with cold water never achieved a steady condition. No reason for this action has been determined. There was no measurable accumulation during the run and all inlet conditions were relatively stable. It is possible that some type of viscous instability could occur since the slot hydraulic diameter based Reynolds number approximates 1000. The heated supply water caused a leak to form in the nozzle seal which allowed a significant fraction of liquid to pass through the threads in the nozzle. This liquid was lost to evaporator function for all practical purposes. The amount of heat rejection was lowered by about 15% so that the outlet temperature achieved  $55^\circ\text{F}$  during maximum heat load. At the end of the run, about 1.6 lbs of the 11 lbs supplied had accumulated so that the 15% leak rate was present at the end of the run in solid form.

The effect of high and low evaporant flow rate is shown in Figure 43. At high (120% nominal) flowrate, full "on" operation is not achieved during the imposed load transient, and the heat load bias of outlet temperature is increased. Some 12 degrees of variation from low load to high load occurs yielding a minimum temperature of  $32^\circ\text{F}$ . At low (80% nominal) flow rate, the minimum outlet temperature remains above  $35^\circ\text{F}$ , but at maximum inlet temperature the outlet temperature rises to  $62^\circ\text{F}$  reflecting the diminished



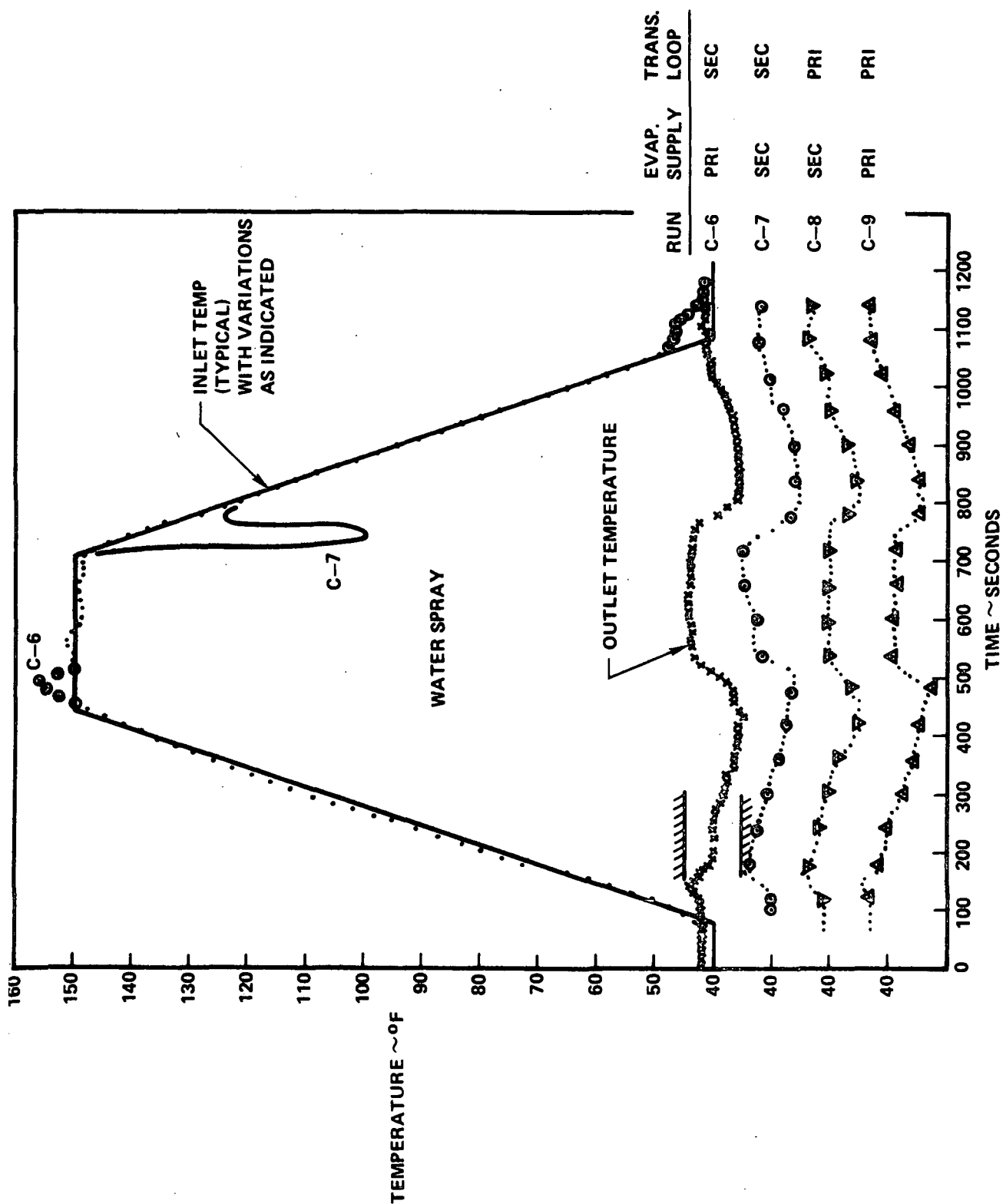


FIGURE 40 EVAPORATOR PERFORMANCE WITH VARIOUS REDUNDANCY COMBINATIONS

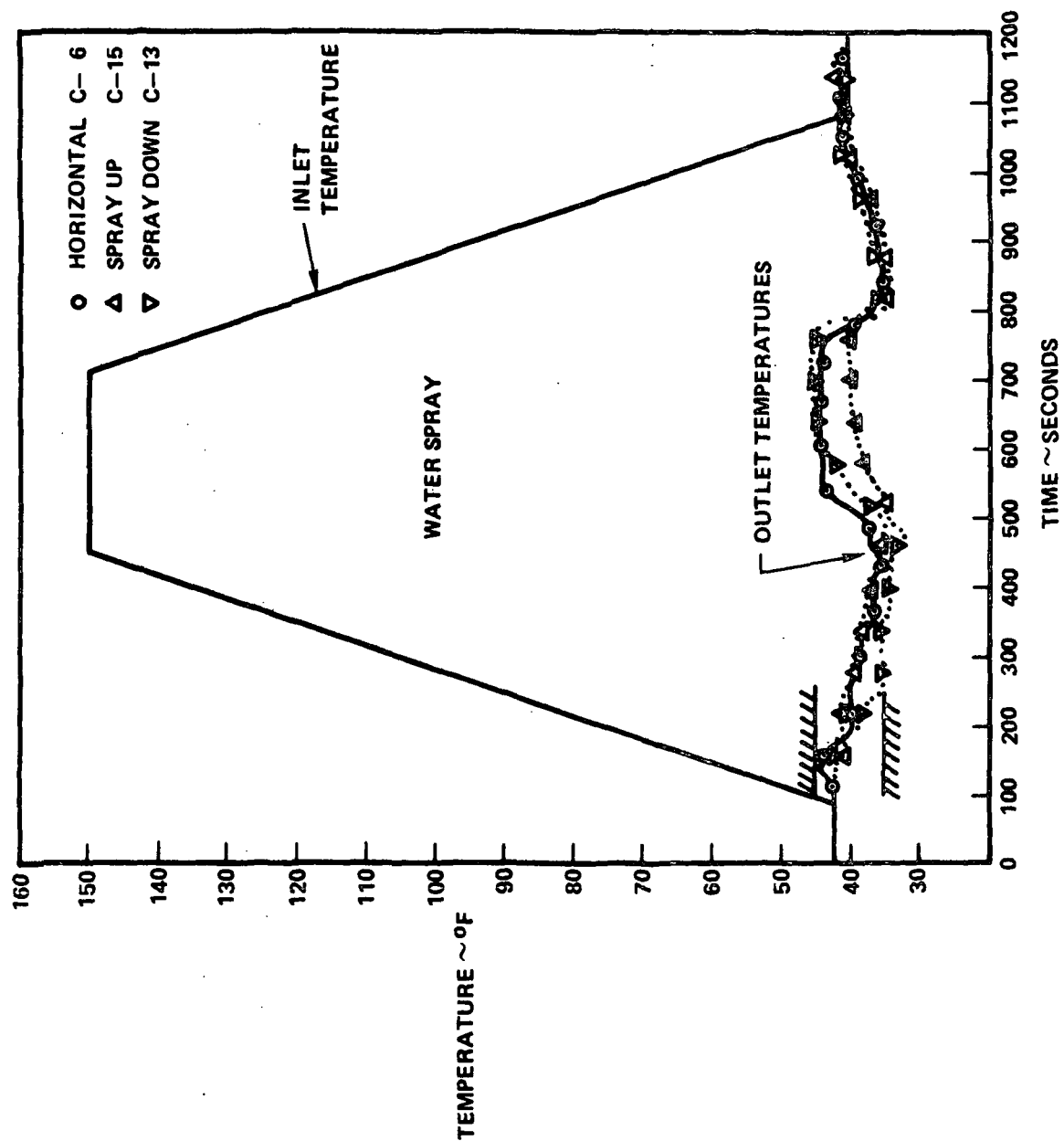


FIGURE 41 EFFECT OF EVAPORATOR ORIENTATION ON PERFORMANCE

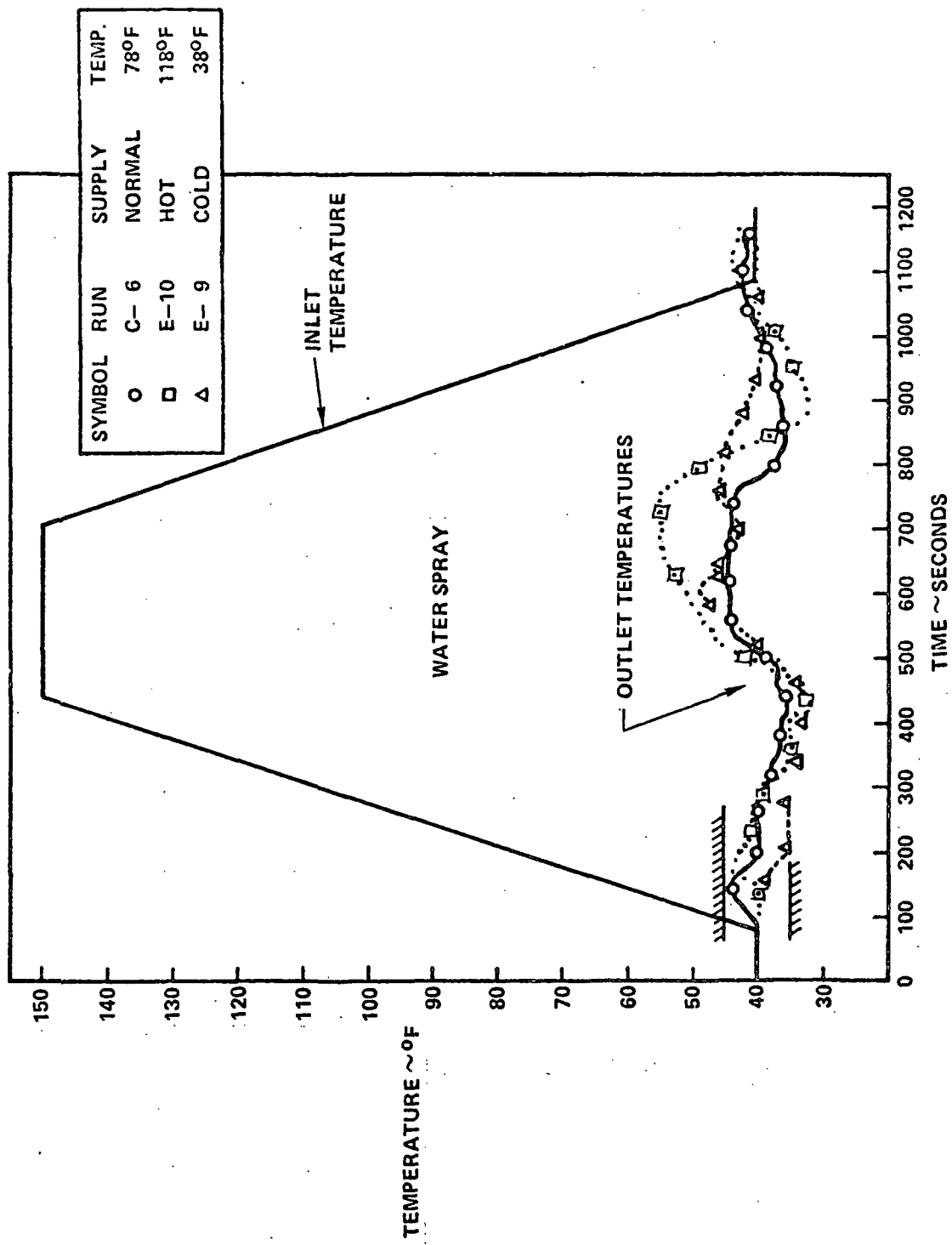


FIGURE 42 EFFECT OF WATER SUPPLY TEMPERATURE ON PERFORMANCE

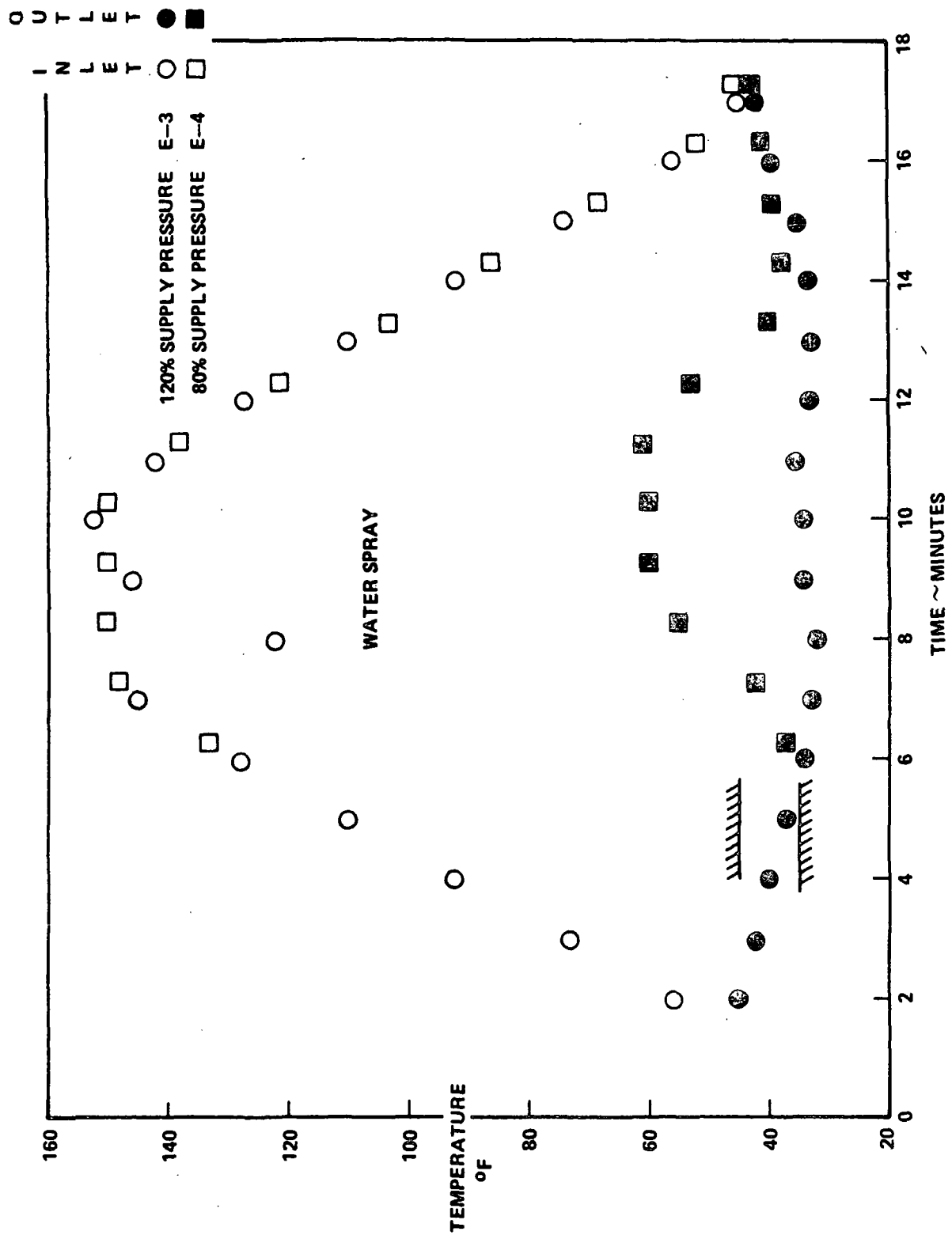


FIGURE 43 EFFECT OF WATER SUPPLY PRESSURE ON PERFORMANCE

evaporant flow. These runs are in line with expectations except that the heat load bias should not be dependent on the spray rate, only upon the change in spray distribution.

The effect of increased (2100 lb/hr) and decreased (1600 lb/hr) transport fluid flow is shown in Figure 44. In the high flow case, the inlet temperature was reduced to allow the maximum load level to attain 50,000 BTU/hr, while the inlet temperature was not raised proportionately for the low flow run. The controller was set inadvertently for the low flow run to  $-1^{\circ}\text{C}$  rather than  $+1^{\circ}\text{C}$  so that an offset of  $2^{\circ}\text{C}$  was built into the control function. The addition of  $3.6^{\circ}\text{F}$  to the outlet temperature raises the level to be nearly identical to the baseline case and the high flow rate case as well. No significant features are judged to characterize either of these runs.

The enthalpy of vaporization of water in the evaporator was calculated for each run. In the steady load conditions of the early set of nozzle runs, the data showed 1020 BTU/lb enthalpy change in situations where frost accumulation was not a factor. The change in nozzles to achieve margin from accumulation was, as already noted, accompanied by direct liquid carryover in the exhaust. As would be expected this carryover resulted in a lower value of vaporization enthalpy. The enthalpy change for these runs averaged 980 BTU/lb, which indicates approximately a four percent carryover. The random error in measurement and reduction of data is estimated at  $\pm 6$  percent, a band which covers the reduced data scatter. Two methods were used to achieve the enthalpy data: (1) heat rate per flow rate at maximum load and (2) integrated energy absorbed per evaporant weight consumed over the profile of inlet temperature. The heat rate data showed a definite tendency to exhibit lower enthalpy values of perhaps 30 BTU/lb. This tendency occurs even in the presence of a systematic error incurred by radiation which is estimated to amount to less than 4 percent at maximum load and less than 2 percent averaged over the load profile. Correcting for the radiation influence would reduce the enthalpy to about 960 BTU/lb, a value effectively equivalent to the 965 BTU/lb reported for the feasibility test result.

Results for Freon operation were not obtained in as many situations as were run with water. Some 3700 lbs. of Freon were expended which represents a significant cost of expendables. After moving the Freon spray location significantly off center, it was assumed that two nozzles side-by-side would operate identically. Thereby only a single evaporant position was operated. Other runs such as heated Freon spray and a detailed survey of orientation effects were not conducted.

Freon, sprayed axially from a nearly central location, forms a collapsed cone of mist which exerts its cooling strongly in a small area near the exhaust duct. Concomitant with this is that about 10-15% of the mist exits directly without being vaporized. Upon moving the Freon strongly away from the center and directing the spray at an acute angle toward the wall the direct carryover was reduced to nearly zero. The strong effect of cooling pattern on control with the type of control system utilized became an important

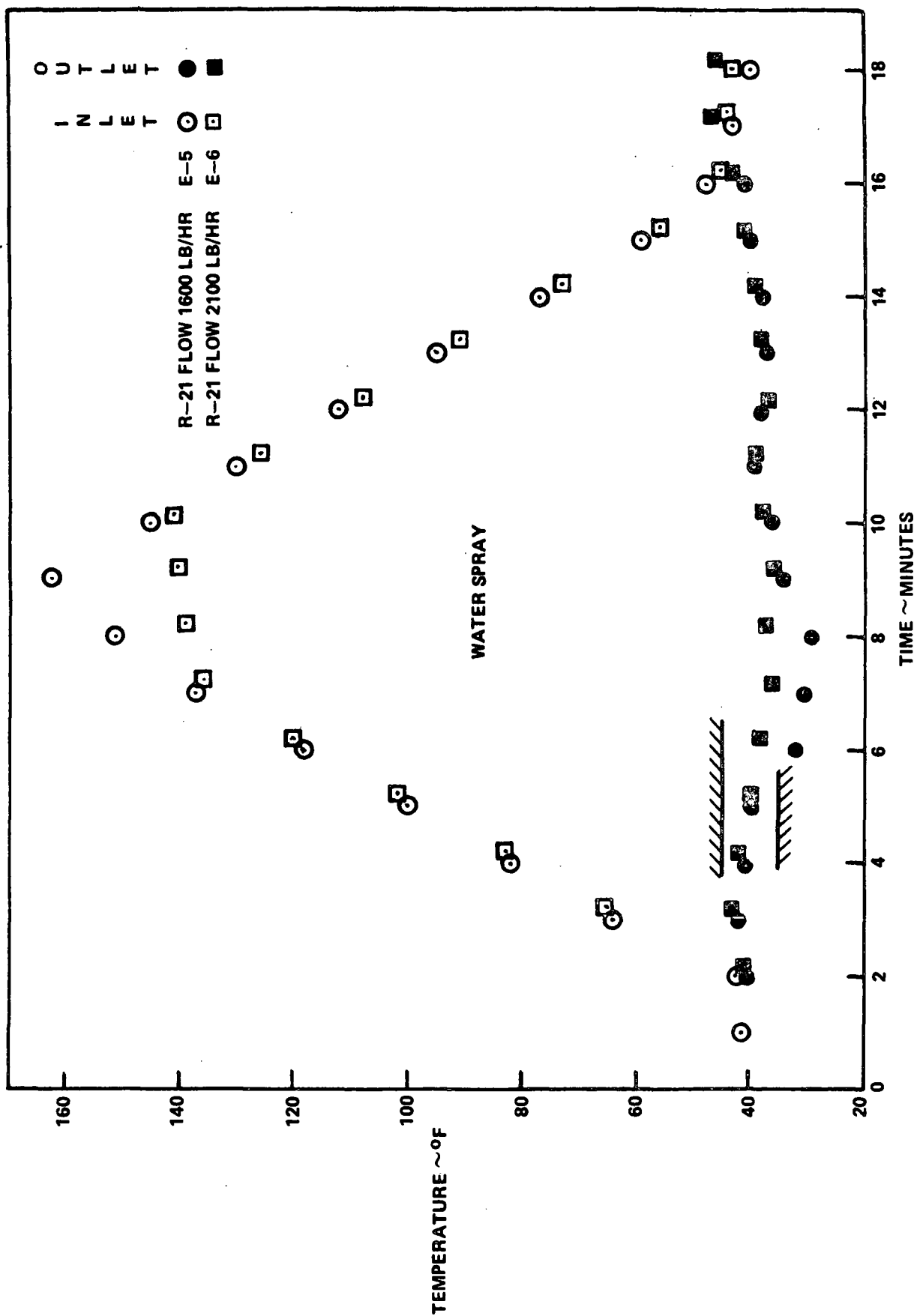


FIGURE 44 EFFECT OF TRANSPORT (R-21) FLOW RATE ON PERFORMANCE

evaluation to conduct. This control was shown to operate satisfactorily over the range of conditions expected for the shuttle. Two installations were made, indicating that there is not a unique position for which control may be obtained.

The primary operational difficulty experienced during operation of Freon was that of flow control. Several times it was observed that equal supply pressurization did not provide equal flow. The most probable explanation for this is that the valve used to meter Freon flow was not of adequate size so that a large pressure drop was obtained. At some conditions, the degree of supply subcooling was small so vaporization within the valve may have occurred. The existence of two phase flow in the valve-to-nozzle line could easily provide the sensitivity noted. Another source is that vaporization certainly occurs in the spray nozzle. Subfreezing temperatures in the nozzle and the Freon flow would lead to ice as the water contained in the Freon was cooled. This ice easily could change the passage dimensions and could persist for an uncertain duration. Such a constriction would radically affect the pressure drop. Further testing should be performed with a low pressure drop valve and consider incorporation of a dryer for removal of the 1% water contained in commercial R-22 to assure no ice can form in the nozzle.

The effect of evaporator orientation is illustrated in Figure 45 which compares horizontal and spray up conditions with an otherwise identical configuration. Only the down ramp portion of run C-11 is shown because the up ramp portion was run with the other sensor and was poorly controlled. No significant difference is disclosed due to the orientation, but the control was not optimum nor was the flow sufficient at the 1 psia condition. These runs were made with the aluminum back cone installed.

The remainder of Freon runs were performed after completion of the water operation. The Freon nozzle was reinstalled in the plexiglass back and its direction adjusted as follows. The spray was directed toward the evaporator surface upstream of the sensor. Its angle was then adjusted so that the sensor and outlet temperatures were equal. On successive runs C-19, C-20, and C-21 the R-22 flow was raised above the flow required at atmospheric conditions to reject 50,000 BTU/hr. This was done as a result of the experience that the flow increase at lower pressure ambient was not sufficient to offset the reduction in enthalpy of vaporization. Run C-22 demonstrated that a supply pressure reduction of 20 percent could be tolerated. Run C-23 demonstrated operation at 1 psia; C-24 at 3 psia; and E-7A, E-8A, and E-1 at 10 psia. Runs E-7A and E-8A also indicated the sensitivity to transport flow rate. E-8A had the supply pressure raised to allow for the increased load imposed, and the high pressure was used for run E-1 which followed.

Figure 46 shows the comparison between atmospheric, 1 psia, and 3 psia results. This comparison indicates that the control sensitivity decreases at low pressure operation.

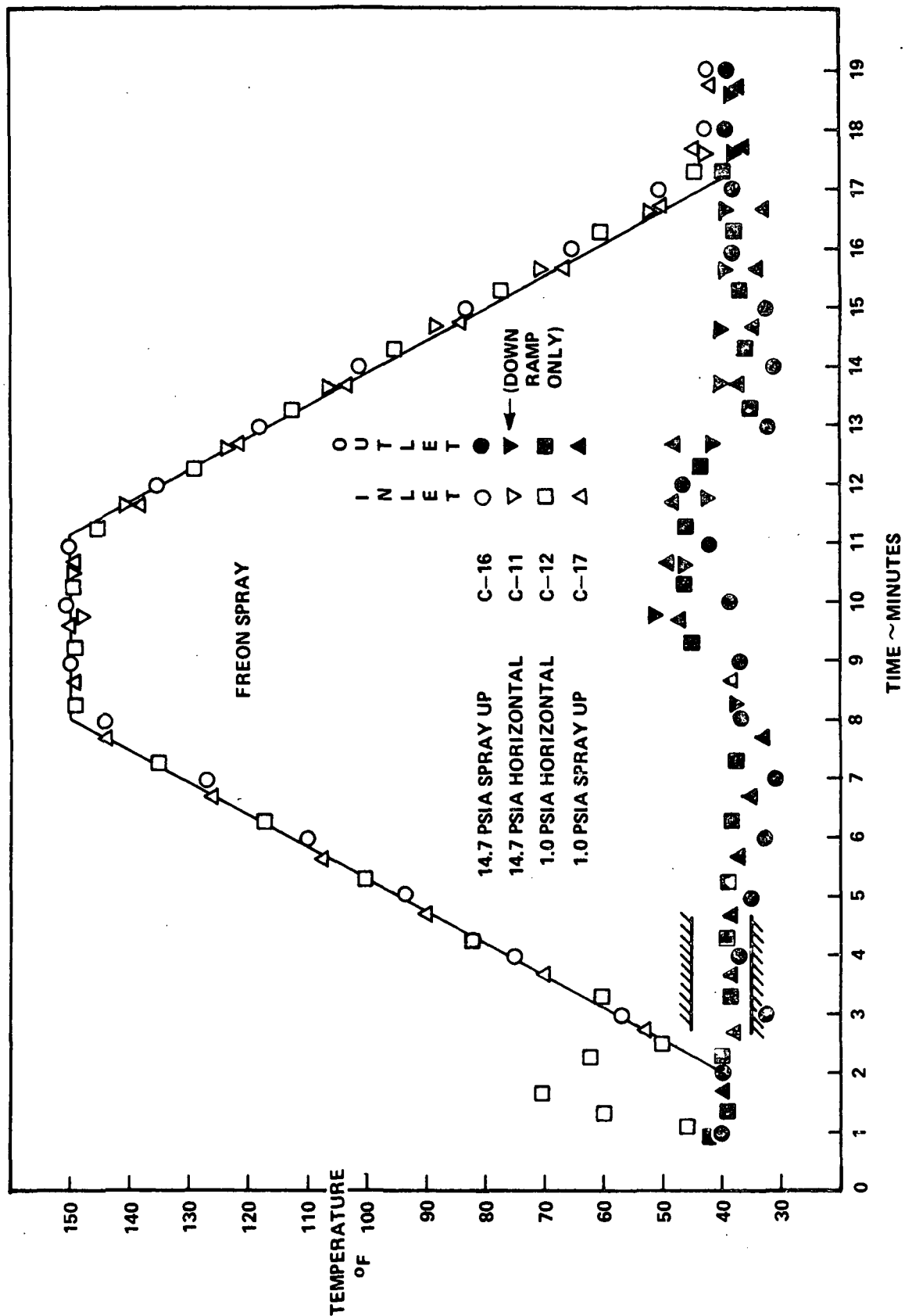


FIGURE 45 EFFECT OF EVAPORATOR ORIENTATION ON PERFORMANCE



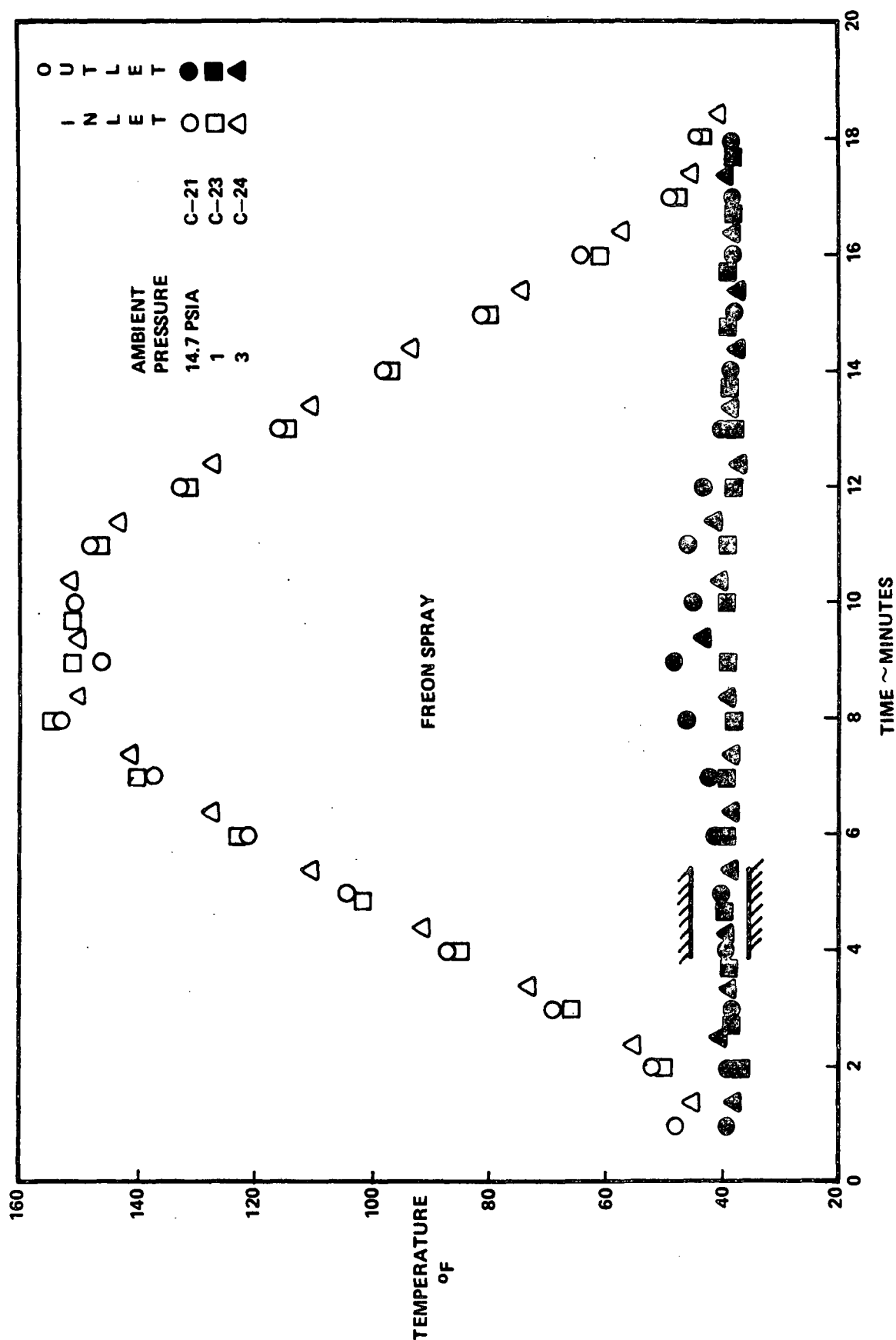


FIGURE 46 EFFECT OF AMBIENT PRESSURE ON PERFORMANCE

Figure 47 compares high supply pressure (120% nominal) with the low supply pressure (80% nominal). The low pressure supply run had atmospheric ambient pressure and the high supply pressure was conducted at 10 psia ambient conditions.

Figure 48 shows the results of variation in transport flow rate conditions at ambient pressure of 10 psia.

The above runs indicate that the Freon operation exhibits the expected sensitivity to the wide range of operating pressure environments. In each of the above runs the enthalpy of vaporization has been calculated as shown in Table 4. The runs reflecting efficiencies greater than unity can have resulted from instrumentation accuracy or from the fact that the vapor exit condition may be superheated.

Two switchover runs were conducted to simulate the boost and ascent conditions. A chamber pressure of 3 mm Hg was selected as a switching point. The transition from water to Freon is shown in Figure 49. At the switchover condition the outlet temperature had risen to about 37°F from the previous 35°F reflecting the rise in chamber pressure. The two records (12 seconds between records) following switchover to Freon reflected a slight decrease in temperature. This is probably due to the fluid within the evaporator being cooled by the Freon and still reflecting water vaporization. The next 15 records (3 minutes) show an abrupt rise to 80°F outlet decreasing to a steady condition at about 50°F outlet temperature. The Freon supply pressure was set to supply only 620 lb/hr initially and was increased after one minute to supply 720 lb/hr. This apparently was the cause for the temperature overshoot.

Switchover from Freon to water, shown in Figure 50, was done at an unknown pressure. The chamber pressure instrumentation was sensitive to gas composition and during Freon operation effectively was inoperative. (A pressure sensor specifically ordered for this test was not delivered). The Freon operation was started at full load and the outlet temperature rose to 60°F. The chamber pumps were full on and the liquid nitrogen cryopump was operative. Water flow was initiated and the outlet temperature rose quickly to 70°F (about 20 seconds), then rose slowly to 85°F and then decayed. After about seven minutes of water operation the outlet temperature was returned to 45°F. It is suspected that the transition to water was attempted at a pressure above the triple point and the achievement of 45°F outlet was restrained by the chamber pump down capability. One reason for the delay is that even though the Freon could be collected by the LN<sub>2</sub> cryopump, some liquid dripped on the chamber wall where it reevaporated. Only that fraction frozen was truly cryopumped and the remainder was pumped mechanically with a longer extinction time.

Incidental observations during the test included the runs wherein the nozzle temperature was monitored during repeated cycling. A typical temperature cycle is illustrated below for the thermocouple position sketched on page 98.

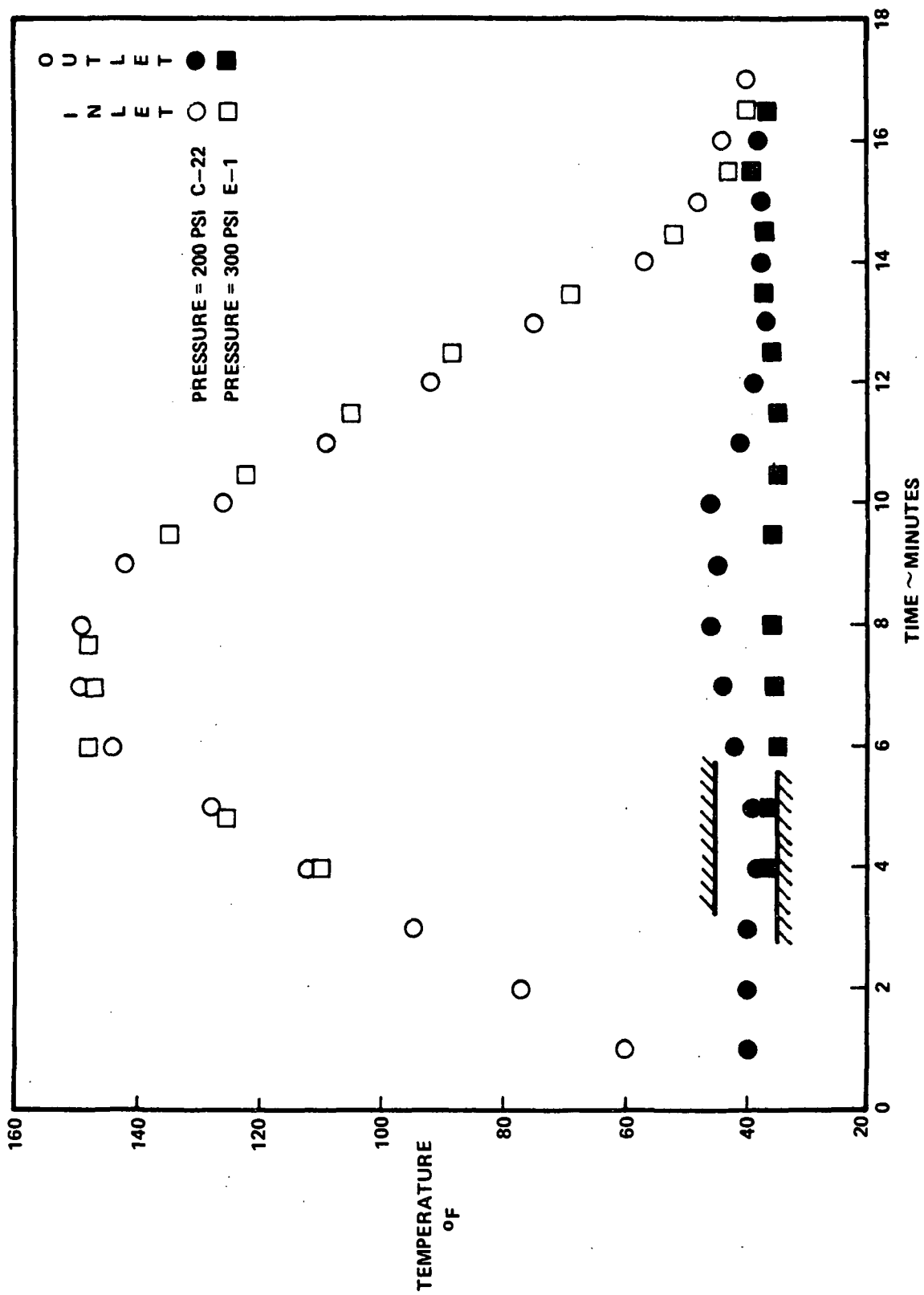


FIGURE 47 EFFECT OF FREON SUPPLY PRESSURE ON PERFORMANCE

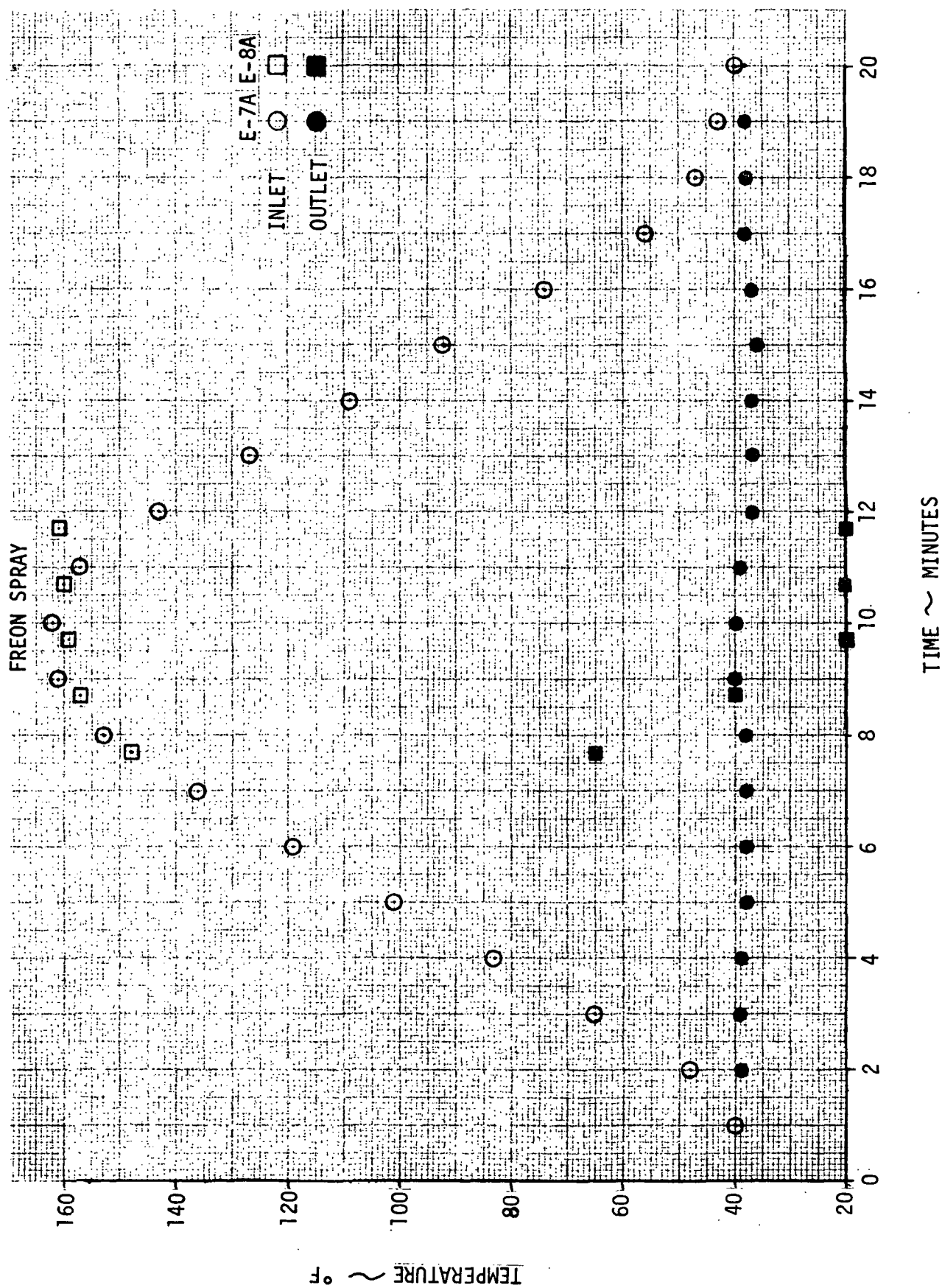


FIGURE 48 EFFECT OF TRANSPORT FLOW RATE ON PERFORMANCE

TABLE 4  
EVAPORATION ENTHALPY

RUN	P <sub>BACK</sub> psia	T <sub>SUPPLY</sub> °F	Δh THEO. BTU/lb	Δh MEASURED BTU/hr	EFF %
C-16	14.7	64	71.8	75.5	105
C-17	1	66	61.7	66.0	107
C-19	14.7	72.1	69.4	69.4	100
C-20	14.7	61	72.7	76.	104.5
C-21	14.7	65	71.5	74.7	100.5
C-22	14.7	65	71.5	70	98.
C-23	1	63	62.6	63	101
C-24	3	65	65.9	61	92.6
E 7A	10	63	68.3	65	95

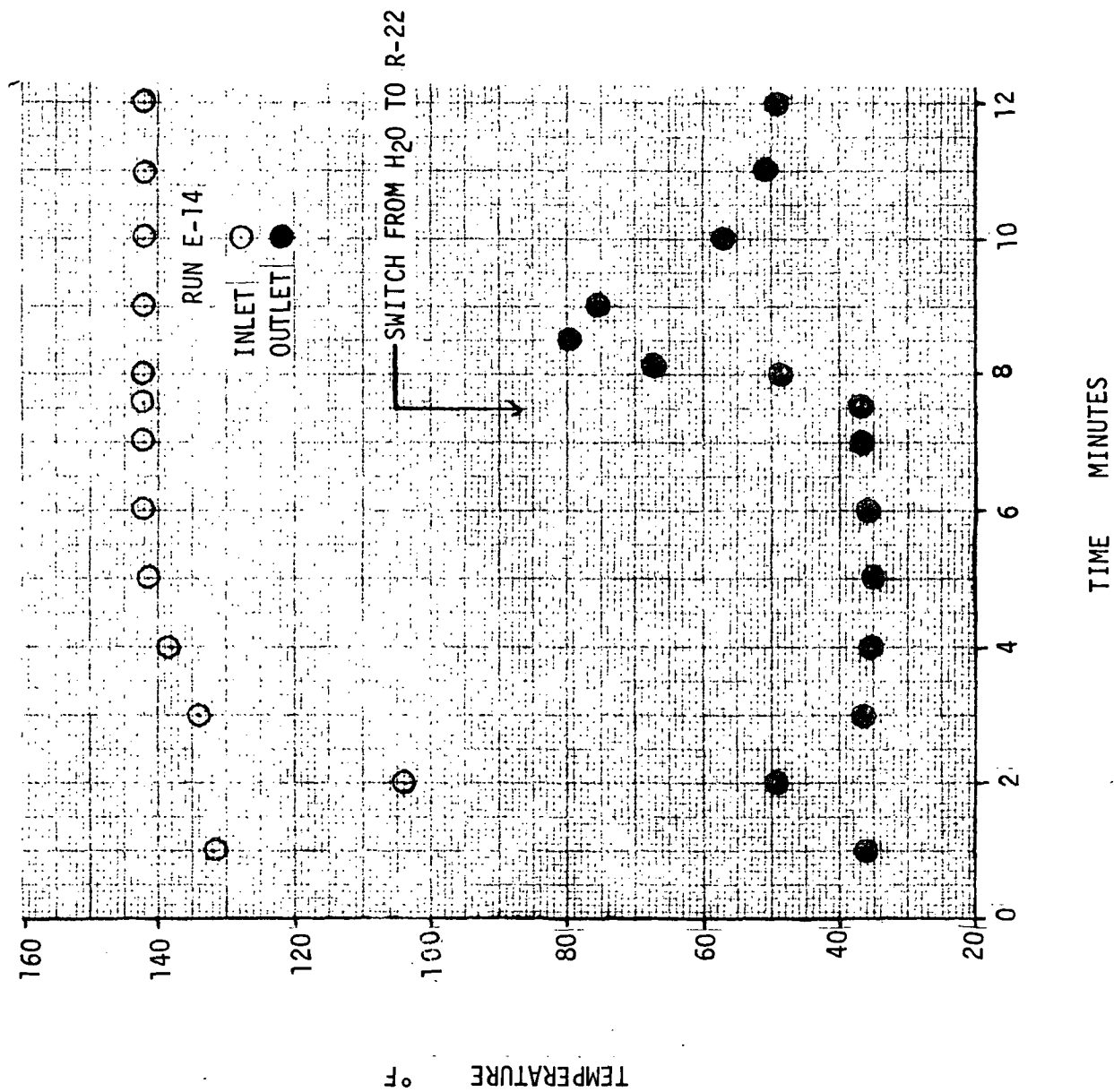


FIGURE 49 PERFORMANCE DURING H<sub>2</sub>O TO R-22 EVAPORANT SWITCHOVER

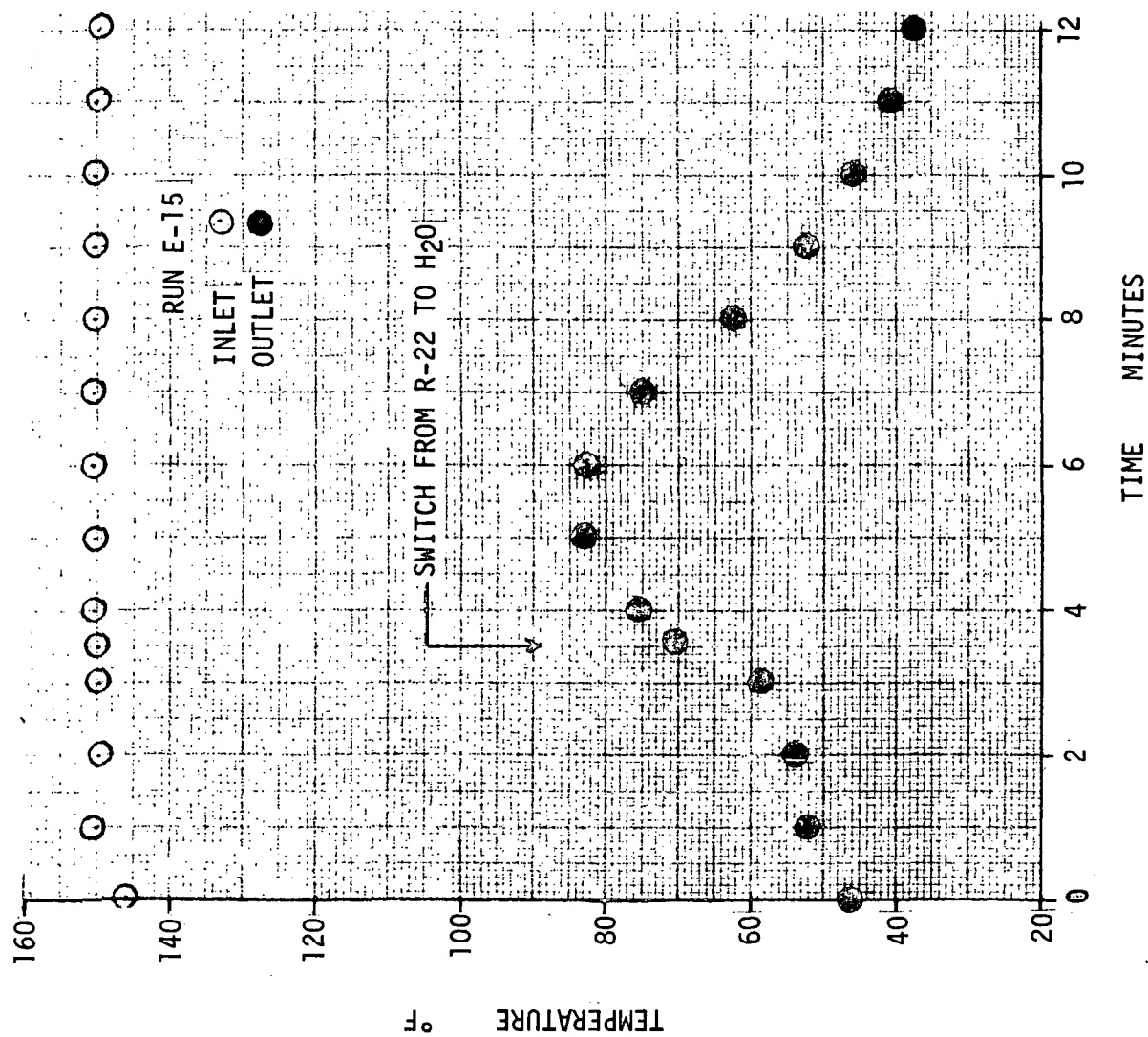
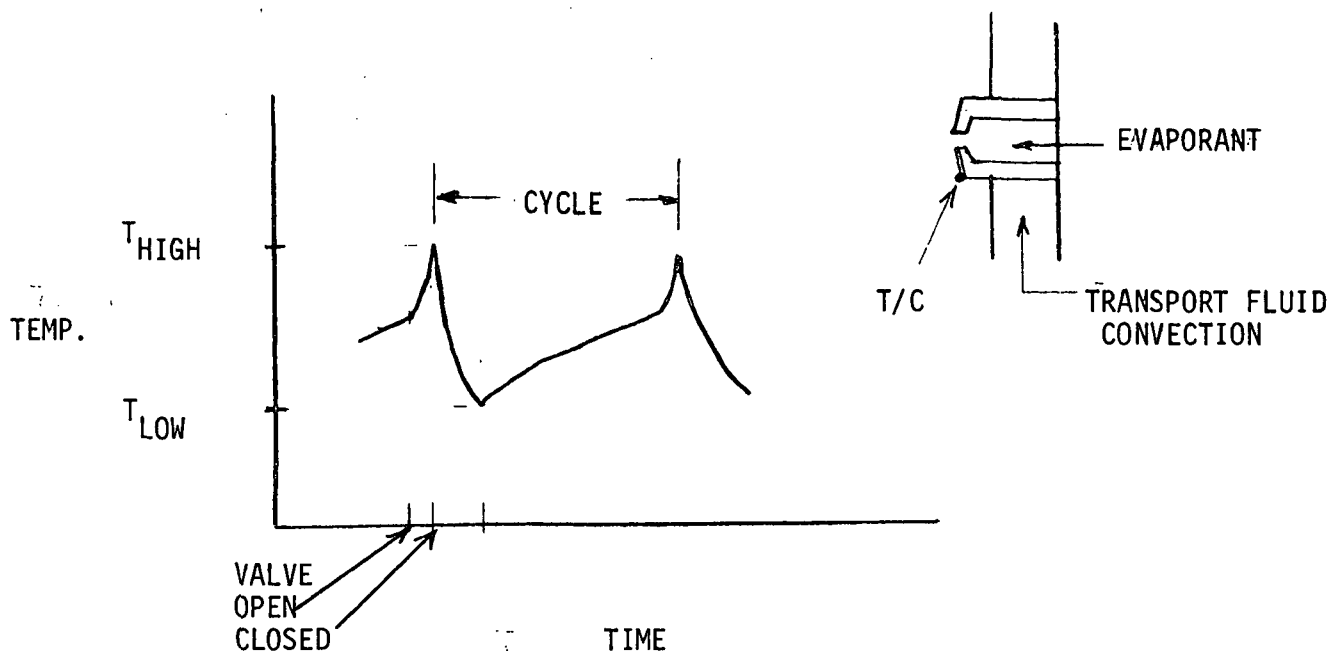


FIGURE 50 PERFORMANCE DURING R-22 TO H<sub>2</sub>O EVAPORANT SWITCHOVER



Several conditions were imposed on the nozzle by varying the cycle time and the transport fluid temperature. As the valve opens, the water inflow may warm or cool the nozzle. Upon shut-off of the nozzle, the liquid hold up is expelled and vaporized so that the nozzle is cooled. Then, the transport fluid begins to warm the nozzle by convection until the next valve opening. The actual values of  $T_{HIGH}$  and  $T_{LOW}$  achieved varied depending on the mode of liquid attachment to the nozzle. On some cycles, the liquid was observed to freeze covering a comparatively larger area which resulted in a lower value of  $T_{LOW}$  and also the following  $T_{HIGH}$ . The following table shows the results observed.

I. Transport Fluid Temperature 80°F, H<sub>2</sub>O Inlet 78°F

A. Cycle: 1 second on, 29 seconds off, 17 cycles

$T_{HIGH}$  average 73, low extreme 72

$T_{LOW}$  average 60, low extreme 58

B. Cycle: 1 second on, 19 seconds off, 36 cycles

$T_{HIGH}$  average 72, low extreme 70

$T_{LOW}$  average 58, low extreme 54



C. Cycle: 1 second on, 9 seconds off, 24 cycles

$T_{\text{HIGH}}$  average 70, low extreme 69

$T_{\text{LOW}}$  average 58, low extreme 55

D. Cycle: 1 second on, 4 seconds off, 5 cycles

$T_{\text{HIGH}}$  average 64, low extreme 63

$T_{\text{LOW}}$  average 59, low extreme 57

## II. Transport Fluid Temperature 65°F, H<sub>2</sub>O Inlet 78°F

A. Cycle: 1 second on, 19 seconds off, 12 cycles

$T_{\text{HIGH}}$  average 61, low extreme 60

$T_{\text{LOW}}$  average 58, low extreme 51

water supply line froze due to radiation. Insulate line.

B. Cycle: 1 second on, 19 seconds off, 22 cycles and formed ice tree

$T_{\text{HIGH}}$  average 59, low extreme 48

$T_{\text{LOW}}$  average 49, low extreme 41

C. Cycle: 1 second on, 19 seconds off, 36 cycles and formed ice tree

$T_{\text{HIGH}}$  average 57, low extreme 49

$T_{\text{LOW}}$  average 51, low extreme 44

D. Cycle: 1 second on, 19 seconds off, 39 cycles and formed ice tree

$T_{\text{HIGH}}$  average 57, low extreme 52

$T_{\text{LOW}}$  average 50, low extreme 47

## III. Transport Fluid Temperature 46°F, H<sub>2</sub>O Inlet 78°F

A. Cycle: 1 second on, 19 seconds off, 78 cycles and formed ice tree

$T_{\text{HIGH}}$  average 45, low extreme 43

$T_{\text{LOW}}$  average 41 low extreme 38

The ice tree formed on the thermocouple wire and was not judged to represent a freezing problem associated with the design. Of the four cases of ice formation, two were during visual observation and it is believed that the mode of freezing was the same for the other two. The amount of cooling reflected at the nozzle surface amounted generally to a 6 to 8°F drop, and

occasionally 10°F. The warming characteristics of the evaporant flow amounted to about a 2°F nozzle temperature rise with a 20°F potential in the one second flow duration. The heating is then expected to be of the form

$$T = T_a + (T_s - T_a)(1 - e^{-.1t})$$

Here  $T_a$  is the temperature approached just prior to nozzle pulsing,  $T_s$  is the supplied water temperature and  $T(t)$  is the nozzle temperature during water flow. The amount of heat supplied by the transport flow typically produced a rise from 49° F to 57°F in 19 seconds with the transport fluid at 65°F. The simple heating formula which results is

$$T = T_i + (T_t - T_i)(1 - e^{-.036t})$$

One can use these equations to estimate the lowest temperature which could be achieved for conditions other than those tested. For example, with water supplied at 40°F and a transport fluid temperature at 42°F, a one second pulse followed by a forty second off period will produce the following pattern.

$$T_H = T_a + (40 - T_a)(.1) \quad T_H = \text{highest temperature}$$

$$T_L = \text{lowest temperature} = T_H - 10^\circ\text{F}$$

$$T_a = T_L + (42 - T_L)(.764)$$

This set results in  $T_a = 38.9$  so that  $T_L$  is 29°F. The actual minimum value of  $T_L$  may be pursued readily knowing the relation of on and off time is related to the inlet temperature of Freon 21. Continuing this approach, one determines that the lowest temperature is achieved when the time for warming is least. The quickest total cycling observed was about six seconds. The difference in inlet Freon and nozzle temperature must be large enough that ten degrees of warming is produced in the six seconds, or about 50°F therefore the lowest temperature is not more than 50°F below the inlet temperature. From these observations, temperatures below about 25°F should not have occurred at any operating condition.

### 5.3 Recommended Design and Engineering Based On Test Outcome

1. No insulative materials should be used for the evaporator inner construction, particularly near the nozzles since such surfaces cause the formation of ice within the device.

2. The further reduction of nozzle holdup volume will increase the margin from freezing tendencies, and will increase the efficiency. Although no nozzle freezing was observed after the removal of insulating material or instrumentation wires, the holdup volume was observed to not vaporize completely. The ice chips formed are possible sites for frost growth and also represent a slight efficiency loss.

3. The formation of frost on active surfaces with some nozzles resulted from combinations of large droplets and locally dense spray patterns. The further investigation of this tendency should be explored by direct measurement of spray density and droplet size during the next development phase. Additionally, the nozzle spray pattern should be selected to eliminate liquid carryover in the exhaust flow which could result in possible freezing of the exhaust duct.

4. The on/off temperature switched method of evaporant control has proven to be sensitive to the spray pattern. The position chosen for the sensor was about 8 to 10°F above the temperature of the ideal location. Also, particularly for Freon operation, slight directional variations can produce large variations in outlet temperature.

5. The margin on the evaporative side was shown to be larger than previously demonstrated. During feasibility testing outlet temperatures to 34°F were produced, while in the prototype testing, the outlet temperature was brought deliberately as low as 30°F before any inefficiency was realized. This fact implies that (1) a greater value of  $T_w - T_{fluid}$  (or less heat transfer coefficient) could be adopted permitting lower pressure drop, (2) a lower control point can be adopted with no penalty.

## 6.0 REFERENCES

1. J. L. Gaddis, "Feasibility Demonstration of a Spraying Flash Evaporator", NASA CR114913, 7 May 1971.



**VOUGHT MISSILES  
AND SPACE COMPANY**  
TEXAS DIVISION